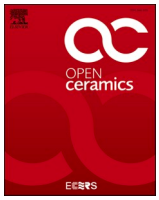
Open Ceramics 23 (2025) 100803



Contents lists available at ScienceDirect

Open Ceramics

journal homepage: www.sciencedirect.com/journal/open-ceramics



Review



Porous polymer-derived ceramics for environmental applications: Sorption, filtration, and catalysis

Oyku Icin [a], Damla Zeydanlı [c], Mattia Biesuz [d], Gian Domenico Sorarù [d], Cekdar Vakifahmetoglu [a,b,*]

[a] Department of Materials Science and Engineering, İzmir Institute of Technology, İzmir, 35430, Turkey
[b] Faculty III Process Sciences, Institute of Material Science and Technology, Chair of Advanced Ceramic Materials, Technische Universität Berlin, Berlin, 10623, Germany
[c] Vocational School of Health Services, Laboratory Technology, Istanbul Gelisim University, Istanbul, 34310, Turkiye
[d] Department of Industrial Engineering, University of Trento, Via Sommarive 9, Trento, 38123, Italy

ARTICLE INFO

Keywords:
Polymer-derived ceramics
Preceramic polymers
Environmental applications
Ecology
Sustainability

ABSTRACT

Polymer-derived ceramics (PDCs), obtained from preceramic polymers, have emerged as promising materials for environmental applications due to their high thermal and chemical stability, tunable nano-microstrucure and porosity, and versatile surface functionalities. This review focuses on the recent advances in porous PDCs and their use in key environmental fields such as sorption, filtration, and catalysis. A comparative analysis of precursor chemistry, synthesis strategies, and resulting structural properties is presented, emphasizing how these factors influence performance in environmental remediation tasks. By consolidating findings across specific application areas, the work aims to clarify the functional potential of PDCs and identify current research gaps and opportunities for future development in environmental material science.

1. Introduction

The 21st century may be designated *the Century of the Environment*. Concerns about increasing ecological threats, biodiversity preservation, and the sustainability of natural resources are becoming increasingly important in environmental studies. As is known, the mentioned ecological issues are receiving a lot of political and scientific attention due to the growing global population and agricultural and industrial activities.

While industrialization offered significant economic and social development, it caused substantial environmental hazards due to its release of various toxic chemicals, gases, solid waste, and microorganisms into our surrounding ecosystem, affecting land, air, and water, besides leading to massive consumption of natural resources. Thus, scientific research aims to reduce existing damage, such as water and air purification, and sustainably utilize more eco-friendly natural resources and green energy. We can briefly recall that, while connected, we currently face two significant global challenges: environmental pollution and energy shortage [1,2]. Broadly speaking, environmental pollution can be categorized into various types: water/soil, air, solid

Abbreviations: AC, activated carbon; AF, acid funcsin; Al_2O_3, alumina; APTE, 3-aminopropyltriethoxysilane; Ar, argon; BET, Brunauer-Emmett-Teller; Bi_2WO_6, bismuth tungstate; CeO_2, ceria; CF_4, carbon tetrafluoride; CH_4, methane; CH_3OH, methanol; CH_3NH_2, methylamine; C_2H_4, ethylene; C_2H_6O, ethanol; C_3H_8, propane; C_3H_6O, acetone; C_6H_6, benzene; CO, carbon monoxide; CO_2, carbon dioxide; CV, crystal violet; DPF, diesel particulate filters; DRM, dry reforming of methane; DVB, divinylbenzene; D_4Vi, tetramethyltetravinylcycletetra; GO, graphene oxide; HC, hydrocarbon; HEPA, high-efficiency particulate air; HER, hydrogen evolution reaction; IPA, isopropyl alcohol; LMH, liters per square meter per hour; MB, methylene blue; MOF, metal-organic framework; N_2, nitrogen; NA, not available; PAA, polyacrylic acid; PAN, polyacrylonitrile; PC, polycarbonate; PCS, polycarbosilane; PDC, polymer derived ceramic; PDMS, polydimethylsiloxane; PE, polyethylene; PEN, polyethylene naphthalate; PET, polyethylene terephthalate; PHMS, polyhydrodimethylsiloxane; PLA, polylactic acid; PMS, polymethyl-silsesquioxane; PMPS, poly-methyl-phenyl-silsesquioxane; PP, polypropylene; PPM, parts per million; PS, polystyrene; PSD, pore size distribution; PU, polyurethane; PVA, polyvinyl alcohol, PVDF, polyvinylidene fluoride; PVP, polyvinylpyrrolidone; PVS, poly(vinyl)silazane; RB, rhodamine B; SEM, scanning electron microscopy; SF_6, sulfur hexafluoride; SiBCN, silicoboron carbonitride; SiC, silicon carbide; SiCN, silicon carbonitride; Si_3N_4, silicon nitride; SiO_2, silica; SiOC, silicon oxycarbide; SSA, specific surface area; TEM, transmission electron microscopy; TiO_2, titania; UV, ultraviolet; ZnO, zinc oxide; ZrO_2, zirconia.

* Corresponding author at: Faculty III Process Sciences, Institute of Material Science and Technology, Chair of Advanced Ceramic Materials, Technische Universität Berlin, Berlin, 10623, Germany.
E-mail address: ahmetoglu@tu-berlin.de (C. Vakifahmetoglu).

https://doi.org/10.1016/j.oceram.2025.100803
Received 28 March 2025; Accepted 26 May 2025
Available online 29 May 2025
2666-5395/© 2025 The Authors. Published by Elsevier Ltd on behalf of European Ceramic Society. This is an open access article under the CC BY license (http://creativecommons.org/licenses/by/4.0/).

waste, food, noise, thermal, and radiation pollution [3]. Addressing these challenges and promoting environmental sustainability involves scientific research exploring innovative materials through new designs, syntheses, and modifications to enhance their performance in various applications.

Water is a fundamental requirement for pH; e.g., all environmental, industrial, and metabolic functions rely on water. When water quality is diminished due to contamination, causing the water to be unsuitable for its intended purpose, it is considered polluted. Contamination of water sources poses a significant risk to both humans and aquatic ecosystems. The typical water pollutants are natural organic matter, heavy metals, dyes, oils, disinfection byproducts, pesticides, fertilizers, pharmaceuticals, personal care products, and microorganisms [4,5].

Air pollution, a significant global issue, can be caused by indoor (cooking, smoking, heating, ventilation systems, and various materials emitting combustion byproducts and volatile organic compounds) and outdoor sources (power plants, industries, and vehicles) [6]. A variety of gaseous (volatile oxides of nonmetallic elements such as sulfur, nitrogen, and carbon) and particulate matter (solid particles, liquid droplets, or mixtures thereof, including aerosols containing viruses, bacteria, and spores) can cause air pollution [7]. As a result of air pollution, detrimental impacts emerge on the environment that may manifest in acid rain, ozone depletion, and climate change, notably global warming due to increased emissions of greenhouse gases.

In recent years, different material groups have been tested in applications related to environmental sustainability. Because of their high catalytic efficacy, metal nanoparticles (Ag, Au, Fe, Pd, etc.) are studied in environmental remediation, including hydrogen peroxide catalysis, soil decontamination, and wastewater treatment [8]. Besides, Ag, Fe, Cu, Zn, and Ni-based systems have been used to make antibacterial components such as the ones in water-filtering membranes [9,10] and air filters [11–13]. Over the past decades, metal-organic frameworks (MOFs) with uniform pore size (<2 nm) and high SSA (reaching even to 3500 $m^2.g^{-1}$) [14] serving copious active sites, have been explored for purifying water from various contaminants, including heavy metal ions, non-metal inorganics, organic dyes, and pharmaceuticals [15]. Furthermore, high SSA (10-100 $m^2.g^{-1}$) and micro-mesoporous (<50 nm) metal-based materials have garnered attention in applications like supercapacitors (Pt film, Pt-Au alloy, etc.), batteries (Si, Ge, Sn, Cu, and Al-Ge alloy), and electro/photocatalysis (Pt-Cu, Pt-Ni alloys, and Ag nanoparticles) due to their high power rate and prolonged cycle lifetime. They facilitate the oxidation of small organic molecules [methanol (CH_3OH), ethanol (C_2H_6O), and formic acid] and play a crucial role in oxygen reduction reactions, making them pivotal electrode reactions in fuel cells. Although it has a high cost, Pt still stands out as one of the most efficient electrocatalysts [16].

A significant number of synthetic polymers [e.g., polyethylene (PE), polypropylene (PP), polystyrene (PS), polyurethane (PU), etc.] have been used, directly or as a substrate in environmental remediation applications (water/soil treatment [17–19], air filtration [7,17,20,21], soil stabilization [22,23], energy storage, etc.). Polymeric air filters are used to purify air within vehicles, clean rooms, warehouses, and laboratories, and as personal protective equipment (surgical or face mask). They are also employed in gas turbines, compressors, and engines as air filters [24,25]. The predominant material types used to form air filters are synthetic polymers. Typically, polymers are transformed into fibers using spinning methodologies at moderate temperatures to obtain systems with relatively high SSA, good permeability to gases, and high flexibility. Different air filter materials have been recently examined, focusing on diverse manufacturing techniques and their effectiveness [7]. Numerous polymer types (PU [26], PE [27], PP [28], PS [28], polyacrylonitrile (PAN) [29], polyvinylpyrrolidone (PVP) [30], polyvinyl alcohol (PVA) [31], polyacrylic acid (PAA) [32], polyethylene terephthalate (PET) [33], Polyvinylidene fluoride (PVDF) [34], polylactic acid (PLA) [35], Nylon-6 [36], cellulose acetate [37], aramid [38], etc.) were processed via different techniques such as electrospinning, melt-spun, melt-blown, blow spun, and needle punching for polymeric filter production and tested against different pollutants (cigarette, sandalwood, and incense smoke, NaCl/KCl, aerosol particles, paraffin mist, Escherichia coli, Staphylococcus Aureus, Di-Ethyl-Hexyl-Sebacat oil). Apart from filtration/purification, various polymers were used in other applications, such as energy storage [39], thermal insulation [40,41], and vibration/sound insulation [42].

Natural materials such as silk, wool, starch, cellulose, chitin/chitosan, fungi, algae, etc., offer high potential for capturing airborne or water contaminants, albeit with limited chemical and thermal stability. For instance, silk was used to produce facial masks designed for air filtration [43,44]. Wool has been employed as an adsorbent and membrane for extracting heavy metal pollutants [45], virus reduction during water filtration [46], and filtering and absorbing harmful gases from the air [47]. Similarly, algae [48] and fungi [49] and plant seeds [50] (okra, pumpkin, grape, and squash) derived natural sorbents are widely used for the removal of metal ions (Cu, Pb, Zn, mercury, etc.) and organic pollutants (e.g., anionic and cationic dyes) from aqueous solution [51].

Minerals play crucial roles in environmental applications, ranging from water treatment and soil remediation to carbon capture. Silica (SiO_2) [52], dolomite [53], wollastonite [54,55], zeolite [56], clays (bentonite and kaolinite) [57], and coal-based adsorbents [58] are used in water/soil treatment processes (removal of heavy metals, microbes, and chemicals). Magnesium oxide and olivine are being explored for carbon capture and storage [59,60]. These minerals can chemically react with carbon dioxide (CO_2), forming stable carbonates through a process known as mineral carbonation, thereby sequestering CO_2 [61]. Additionally, they are used in waste management practices, including landfill liners and covers. Bentonite and kaolinite are employed in landfill liners to prevent leachate migration and groundwater contamination [62]. Natural materials can also be used in composite systems, e.g., chitosan combined with clays was extensively used for the retention/immobilization of heavy metals in polluted systems to remove Hg, Ni, Pb, and Cr from water and contaminated soil environments [63].

Inorganic solids (ceramics and glasses) are suitable for many environmental applications [64–67] due to their superb chemical and thermal stability, even under harsh conditions [67,68]. For example, alumina (Al_2O_3), zirconia (ZrO_2), titania (TiO_2), silicon carbide (SiC), zeolites, etc.) have been used for wastewater and desalination treatments [69–71]. Alternatively, various forms of carbon e.g., activated carbon (AC), fullerenes, carbon nanotubes, graphene, and graphene oxide (GO) have excellent water treatment and purification potential [72]. Both powdered and granular forms of AC are among the most efficient and extensively utilized adsorbents on an industrial scale for the removal of air/water pollutants, purifying of water, and refining drinking water quality due to their remarkably high SSA (up to 1500 $m^2.g^{-1}$), microporosity, and surface functional groups. To date, AC has been derived from non-renewable sources (such as coal, lignite, and peat) as well as agricultural residues (biomass wastes like rice&coffee husk, peanut&coconut shell, banana peel, etc.) by following pre-treatment, carbonization, and activation steps [73]. AC has been explored not only as adsorbents but also as catalysts and catalyst supports for removing heavy metals, pharmaceuticals, pesticides, organic matter, toxic chemicals (e.g., cyanide), synthetic textile dyes, and microplastics [74–76].

Ceramic filters and membranes are utilized for particulate filtration in various applications (e.g., ash filtration from hot gases, diesel exhaust gases, and air purification) [77]. Dust-containing hot flue gas is an intermediate product in industries where electricity generation (coal--fired), glass and cement production, waste burning, catalyst manufacturing, and biomass feedstock pyrolysis. Capturing and recovery of dust can lower intermediate energy usage and diminish the release of pollutants. In this regard, the ceramic candle filters (Mullite, Al_2O_3, and SiC) [65,78] have been used as hot gas filters. Among these, silicate-bonded SiC candle filters have been predominantly selected due to their low thermal expansion coefficient, high resistance to thermal

shock, abrasion, and erosion, inertness, and high mechanical strength, even at elevated temperatures [79–82].

Although recent regulations aim to restrict their utilization in automobiles [83], diesel engines are widely utilized in various vehicles. Such engines emit critical pollutants such as particulate matter and nitrogen oxides. Particulate matter has to be filtered, so filters have been integrated into passenger cars since 2000 [84]. Cordierite (MgAl-silicate), aluminum titanate, FeCrN, Mullite, silicon nitride (Si_3N_4), and SiC are candidates for honeycomb-shaped wall-flow diesel particulate filters (DPF) [84,85].

In air purification systems, ceramic filters (Al_2O_3 fiber [86], ZrO_2 fibrous membrane [87], SiC foam [88], etc.) have been developed and evaluated for their usage as high-efficiency particulate air (HEPA) filters [88–90]. HEPA filters, with efficiencies of 99.95 % to 99.995 %, are designed to prevent airborne pathogen and allergen spread in medical facilities and protect sensitive products from contamination in industries like cosmetics, pharmaceuticals, food, optics, and microelectronics. They are also increasingly used in residential and commercial air purifiers to improve indoor air quality [91]. HEPA filters consist of a pleated mat of randomly arranged fibers that capture particles through three main mechanisms: diffusion for small sized particles (such as smoke and fine dust <0.1 μm) collide with air molecules and flow a random, irregular path, increasing their probability of being captured by fibers, interception, where particles similar in size to the spacing between fibers are trapped as they flow the airstream; and impaction, which occurs when larger particles (>0.3 μm) deviate from the airflow and directly collide with the filter fibers [88].

Ceramic systems are used for gas filtering, separation, and sequestration processes. CO_2 emissions can be managed through carbon sequestration, which involves capturing and securely storing the CO_2 released from fossil-fuel-fired plants. Notably, ceramic membranes such as microporous glasses, Al_2O_3, SiO_2, Si_3N_4, SiC, zeolites, and various metal oxides have gained significant attention for their capability to separate different gases under conditions that demand high abrasion, chemical, and thermal resistance. These ceramic membranes surpass traditional polymeric membranes, having high perm selectivities and low fluxes and becoming plasticized at high CO_2 pressure [92]. Different types of ceramics, including lithium and sodium zirconates, silicates, aluminates, and metal oxides [93,94], have already been suggested and tested to capture CO_2 through physical adsorption and chemisorption [95].

The rising global energy demand, driven by population growth and industrial expansion, has increased attention towards nuclear energy as a viable alternative to finite fossil fuels and limited renewable sources. However, the establishment of new nuclear power plants has resulted in the generation of significant radioactive waste, posing a severe threat to the environment and human health [96–98]. For this purpose, glasses (borosilicates and phosphates) or ceramics were used as a host for immobilizing radioactive waste via vitrification technology due to the high chemical, physical, and mechanical stabilities for many years [99–108].

Energy storage and conservation are other issues for modern civilization due to the increasing energy consumption and environmental aspects. Ceramic materials have already been used in energy storage technologies (dielectric capacitors and batteries) [109–113] and insulation applications (sound/thermal insulators and electromagnetic wave absorbers) [114–122].

Noise arises from various sources, such as traffic, industrial activities, and architectural structures. Noise pollution and other hazards are a significant environmental concern in the 21st century. Mitigating the adverse effects of noise exposure necessitates reducing noise levels to acceptable standards [123]. Sound-absorbing materials find extensive use across diverse applications, including acoustic liners in aircraft and automotive mufflers, combustion chambers in gas turbines, components of air conditioning systems, pump chambers, motor insulation, and construction projects [124,125]. Sound absorption applications may necessitate the absorbent material to withstand corrosion and high temperatures. In such scenarios, using ceramic material for sound control offers potential advantages over other material options [126]. Porous ceramics, particularly those with open pores, favor sound absorption [127]. The conventional inorganic sound-absorbing materials include glass wool [125], rock wool [125], glass/ceramic fibers [128,129], foam glass [130], ceramic sponges [123], porous zeolite [125], ceramic tiles [131], ceramic aerogels [132].

The concept of a "low-carbon economy" is currently of great significance. It entails several sectors, such as energy, transportation, industry, and agriculture, to reduce their carbon footprint. Increasing emphasis on energy efficiency across many areas—buildings, transportation, and manufacturing processes—involves adopting new technologies, improving insulation, and optimizing energy use to lower overall consumption. One potential way to decrease energy consumption is to minimize the heat losses. While organic materials have primarily dominated the market for building insulation, inorganic products offer distinct advantages such as high-temperature stability, fireproof performance, resistance to chemical degradation, and non-toxicity [133]. Foam glass/ceramics [133,134], ceramic tiles [135,136], silica aerogel (glazing, blankets or in panels, evacuated solar collectors, mortar, bricks, cement composites) [137–139] are used to improve the building thermal insulation. In addition, a range of ceramic coatings (such as Al_2O_3, TiO_2, ZrO_2, yttria-stabilized ZrO_2, mullite, cerium oxide, lanthanum zirconate/aluminate, etc.) has been evaluated as thermal barrier coatings for thermal management and protection due to their superior properties such as low thermal conductivity, high corrosion, and thermal shock resistance, etc [140].

While the risks are not yet certain, prolonged use of electronic devices (mobile phones, tablets, Wi-Fi routers, powerlines, cell towers, etc.) that generate electromagnetic fields may have potential health implications [141]. Considerable efforts have been directed toward developing advanced materials capable of effectively absorbing or shielding against these high-frequency (GHz) electromagnetic waves [142]. Carbon nanotubes, graphene, oxide (e.g., zinc oxide (ZnO)) & nitride [e.g., Si_3N_4 and silicoboron carbonitride (SiBCN)] ceramics, and SiC are among the extensively studied electromagnetic wave absorbers [143,144].

PDC method has been employed to produce inorganic solids in the Si-O-C-N-B family, such as SiC, Si_3N_4, SiBCN, silicon oxycarbide (SiOC), silicon carbonitride (SiCN), and many others [145]. In a straightforward definition, manufacturing involves the initial shaping of the polymer/-oligomers and its cross-linking. Subsequently, pyrolysis of the cross-linked thermoset at temperatures typically exceeding 800°C, where organic components are eliminated, yields an inorganic material [146,147]. Interestingly, PDC can be used to obtain porous structures, crucial in environmental applications such as support for catalytic reactions or filters. Examples include the replica method by PDC technologies of a thermoplastic preform that could be a simple PU foam or a 3D-printed complex lattice. Furthermore, the crosslinking of pre-ceramic resin within a solution causes its gelation, and the subsequent removal of the solvent in controlled conditions (supercritical drying, freeze-drying) paves the way to porous PDCs with outstanding SSA.

Compared to conventional ceramics produced by powder processing, the PDC route offers several advantages, including composition control, the possibility of complex geometric shapes, and low processing temperatures [148–150]. Despite the numerous advantages of PDCs in reducing environmental pollution and saving energy, their processing still presents challenges. During the pyrolysis, various gas species such as ethylene (C_2H_4), benzene (C_6H_6), methane (CH_4), silanes, methylamine (CH_3NH_2), and hydrogen (H_2) are released, typically within the temperature range of 400 °C to 1000 °C [151,152].

For nearly half a century, the production of PDCs has focused on tailoring the microstructure, chemical, and physical structure of the formed ceramics. Apart from many research papers, there have been comprehensive book chapters and reviews on the processing and

properties of PDCs. The application areas of these advanced materials follow technological developments in an ever-expanding window in many places, from sensors to bioengineering and environmental to energy storage. There has been significant recent hype on exploring the potential and capabilities, especially their utilization for ecological challenges.

PDCs find various field utilization in areas such as water purification (removing dyes, heavy metals, oils, etc.) [153–156], gas separation [157,158], and energy-related applications (insulation [159–164], batteries [165–169], and dielectrics [170,171]).

Comprehensive reviews [17,19,172,173] and books [174–176] have been published on environmental applications of various materials, including metals, polymers, ceramics, natural materials, and nanomaterials. However, these publications have not thoroughly addressed the environmental applications of PDCs obtained from preceramic polymers. As seen in Fig. 1A, the number of published works has been increasing exponentially, highlighting the importance of PDCs as a remedy for different environmental problems. Accordingly, this topical review aims to analyze these works to emphasize the high versatility and potential value of PDCs in environmental sustainability research.

2. Application methods

PDCs can be used in applications such as adsorption, filtration, catalysis, and energy conversion and storage [177–179]. Most PDCs used in these applications are porous, and structural properties such as pore size distribution (PSD), specific surface area (SSA), open, closed, aligned, or gradient porosity, which can vary depending on the production process, play an essential role defining the capability for a particular application type [180].

2.1. Adsorption

The adsorption technique is widely studied among available approaches utilized in environmental studies, such as water treatment and gas capture/separation applications, due to its simple applicability, versatility, rapid kinetics, and cost-effectiveness [181–185].

In water treatment, adsorption involves bonding impurities and pollutants onto the surface of an adsorbent material. This technique enables the efficient and economical treatment of large volumes of water. On the other hand, gas adsorption is employed to capture and separate gases from mixtures or to store gases in porous materials. One of the prospective advantages of adsorption is the ability to regenerate and reuse the adsorbent. In adsorption, the adsorbate and adsorbent are attracted to each other through weak physical forces (physisorption) or stronger chemical forces (chemisorption) [186]. This interaction occurs when the adsorbate first adsorbs to the surface and then penetrates the pores and active sites of the adsorbent [187].

Natural clays [188,189], zeolites [190], and AC [183], can be counted as classic representative of adsorbents for pollutant removal. All of these have pros and cons in the context of purification processes, but AC is the most commonly used [191,192].

The preference for PDCs as adsorbents in water and wastewater treatment [153], as well as gas adsorption, stems from their alterable composition, surface functionality, high SSA, and total porosity, which can be deliberately controlled through adjustments in pyrolysis conditions and polymer composition. They have been primarily utilized in the adsorption of common pollutants such as metal ions, dyes [177,193], oils, and pesticides [194].

2.1.1. Water/wastewater treatment

Industrialization and urbanization caused severe water pollution, particularly from non-biodegradable and toxic substances (heavy metals, dyes, oils, pesticides, fertilizers, etc.) [195]. Numerous studies and review articles have investigated various types of adsorbents (AC, Al_2O_3, clay minerals, SiO_2 gel, zeolites, biomaterials, industrial byproducts, agricultural solid wastes, magnetic, etc.) for water treatment [196–200].

A wide variety of works have already demonstrated the utilization and properties of several PDCs to eliminate different adsorbates (dyes, oils, herbicides, antibiotics, and metal ions), as detailed in Table 1. Among all the compositions in the table, SiOC is the most widely researched one as an adsorbent for water treatment. This is primarily because the precursors to obtain SiOC are economic and can be easily handled and processed in ambient atmospheric conditions. SiOC ceramics can be produced via either sol-gel or organosilicon preceramic polymers, namely polyorganosiloxanes $–[SiR^1R^2–O]_n–$. Following the preceramic polymer route, crosslinking, and pyrolysis (typically around 1000 °C or higher) in an inert atmosphere, it is possible to obtain an amorphous SiOC structure noted as $SiO_xC_{1-x/2}$, where $0 \leq x \leq 2$, characterized by simultaneous bonding of Si atoms with O and C atoms. A free carbon phase also comprises sp^2-hybridized carbon layers arranged to form amorphous carbon, turbostratic, or nanocrystalline graphite [148]. The resulting polymer-derived SiOC ceramic systems have unique properties, including *(i)* amorphous or nanocrystalline structure depending on the composition and processing conditions, *(ii)* tailored composition by adjusting the precursor chemistry, *(iii)* various forms (foams, membranes, aerogels, beads, etc.), *(iv)* high-temperature

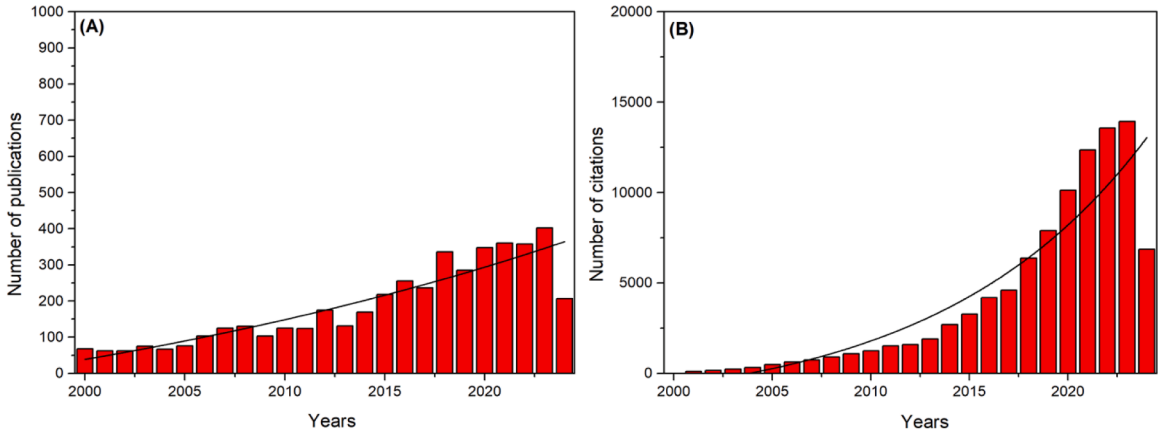


Fig. 1. Trends in the number of publications/citations per year related to the use of PDCs and related materials in environmental applications. **(A)** The number of publications resulting from a web of science search with the keywords "Polymer derived ceramics", "Preceramic polymer", "Polysiloxane", "Polysilane", "Polysilazane", "Siliconoxycarbide", "Siliconcarbonnitride", "SiOC", and "SiCN" combined with terms such as "enviromental", "water treatment", "water purification", "wastewater", "purification", "adsorption", "photocatalyst", "photocatalytic", "photocatalytic", "membrane", "hot gas filtration", "absorption", and "insulation". **(B)** The number of citations. Both data were extracted from 2000 up to now, and the line represents an exponential growth function fit.

Table 1
Polymer derived ceramic adsorbents and utilization for wastewater treatment.

Adsorbent	*SSA* ($m^2.g^{-1}$)	*Adsorbate type*	*Adsorbate conc. (ppm)*	*Contact time (h)*	*Adsorption Capacity* ($mg.g^{-1}$)	*Refs.*
		Dyes				
SiOC	120-660	MB, RB and CV	25	24	50-186	[155]
SiOC	88	RB	5	2	N.A.	[215]
SiOC	60-398	MB	~10	2	N.A.	[177]
SiOC/wood	91-463		20	2	69-147	[153]
SiOC nanobeads	23		5	2-24	4 – 8	[154]
SiOC /TiO_2 nanobeads	36		5	4	4	[154]
SiOC/ZnO	153-260		~10	2	N.A.	[177]
SiOC/TiO_2	129		~10	3	15	[202]
SiOC/TiO_2	212-382		~10	2	N.A.	[203]
SiOC/N-doped TiO_2	129-254		~10	2	N.A.	[203]
N-doped TiO_2/SiOCN	186		~20-40	12	N.A.	[216]
Ni/SiOC(H)	253-344	AF	200	2	124–130	[204]
SiCN	252	AF & MB	200-300	24	1084-1328	[193]
SiOC aerogel	163	MB & RB	1-1000	1-172	0.16-45	[205]
SiOC aerogel	163		100-800	48-172	14.8-44.2	[206]
SiC aerogel	102		1	48	N.A.	[206]
		Others				
SiOC ambi/aerogel	274-318	Sesame & engine (oil)	NA.	1.5	980-1390	[163]
SiC/C aerogel	215	Glyphosate (herbicide)	2	48	0.6	[194]
SiOC	480-766	Ciprofloxacin (antibiotic)	10	1.5	85-148	[210]
SiC Foam	0.13-0.31	Non-steroidal anti-inflammatory drugs	0.002-0.01	24-72	0.0002-0.0042	[214]
SiOC aerogel	207	Cr(III)/(VI) ions	5-200	1	30	[208]
SiCN aerogel	388		5-200	1	20	[208]
SiOC	120-660	Cr (III), Pb (III), and Cd (II) ions	1	2	2-6	[155]

N.A. = Not available, and CV = crystal violet

stability and oxidation resistance, resulting in significant potential in many applications [201].

Pan et al. [153]. developed porous SiOC composites by mixing polysiloxane precursor and wood powder, which was cured and pyrolyzed under argon (Ar) at different temperatures (1000-1300 °C). SiOC composite (SSA: 91 $m^2.g^{-1}$) produced by pyrolyzing the system at 1000 °C exhibited a Methylene Blue (MB) adsorption capacity of 69.17 $mg.g^{-1}$ with a 60 % removal rate at the end of 2 h. Instead, samples prepared at 1200°C (SSA: 290 $m^2.g^{-1}$) and 1300°C (463 $m^2.g^{-1}$) demonstrated higher adsorption capacities with 111.58 $mg.g^{-1}$ and 146.77 $mg.g^{-1}$, respectively. The trend was attributed to increased BET (Brunauer--Emmett-Teller) SSA, which offers accessible and potent adsorption sites.

In another study, emulsion-derived SiOC nanobeads were produced using commercial polymethyl-silsesquioxane (PMS) precursor via pyrolysis at 600 and 1200 °C. Additionally, samples were mixed with Titanium(IV) n-butoxide/C_2H_6O solution to prepare TiO_2 coated-SiOC nanobeads [154]. Adsorption performance was evaluated for MB removal from aqueous solutions as a function of pyrolysis temperature and TiO_2 coating. Neat SiOC nanobeads (pyrolyzed at 1200 °C, SSA: 23 $m^2.g^{-1}$) showed a maximum adsorption capacity of ~8.20 $mg.g^{-1}$ and an 82 % removal rate, instead ceramer SiOC nanobeads (pyrolyzed at 600 °C, SSA: 370 $m^2.g^{-1}$) had lower adsorption capacity of 0.6 $mg.g^{-1}$ and 5 % removal rate by the end of the 24 h period. Despite the high SSA, the relatively poor adsorption efficiency of the samples pyrolyzed at 600 °C was ascribed to factors such as hydrophobic nature, absence of free carbon deposition, and surface silanol groups. After the TiO_2-coating of SiOC nanobeads (pyrolyzed at 1200 °C), the adsorption capacity was tested for only 4 h, giving a maximum adsorption capacity of ~3 $mg.g^{-1}$.

Mesoporous TiO_2/SiOC samples were formed following two steps: *(i)* mixing of polyhydrodimethylsiloxane (PHMS) and mesoporous carbon and then pyrolyzing at 1000 °C, and *(ii)* coating mesoporous SiOC-C with titanium n-tetrabutoxide and heat treating at 500 °C (in the air) to fabricate TiO_2/SiOC nanocomposites. The process yielded two different types of PDC adsorbers. The mesoporous composite (SSA:129 $m^2.g^{-1}$) displayed a significantly greater adsorption capacity of 15.20 $mg.g^{-1}$, with complete MB (10 parts per million; ppm) adsorption in 10 min. In contrast, macroporous composite (SSA: <1 $m^2.g^{-1}$) had a 0.16 $mg.g^{-1}$ capacity, for which the difference was explained by the higher SSA present in the mesoporous samples [202].

Hojamberdiev et al. [203] investigated the effect of pyrolysis temperature (700-900 °C) and TiO_2 (0-20 wt.%) addition in SiOC ceramic for MB adsorption. Results indicated that the sample pyrolyzed at 700 °C with greater SSA values (up to 400 $m^2.g^{-1}$) and increased mesoporosity yielded higher adsorption capacity than microporous SiOC ceramic.

In a different fashion, magnetic Ni-modified SiOC(H) ceramic nanocomposites were synthesized by pyrolysis of the crosslinked polycarbosilane (PCS) and Nickel (II) acetylacetonate. The samples were then investigated for their adsorption capacity towards Acid Funcsin (AF) dye [204]. Notably, this type of material offers the advantage of convenient recyclability from the reaction system by applying an external magnetic field. Mesoporous ceramic nanocomposites with high SSA in the range of 253–344 $m^2.g^{-1}$ yielded an adsorption capacity reaching 85.80 $mg.g^{-1}$ in the first 10 min and 129.80 $mg.g^{-1}$ in 2h.

Polysilazane (PSZ) -polydivinylbenzene (DVB) derived macro/micro-porous SiCN hybrid ceramics were produced through the pyrolysis between 600-1100 °C and examined for MB and AF adsorption. The adsorption mechanism of the porous Si–C–N hybrid material was due to Van der Waals forces between the sp^2 carbon in the adsorbent and the triphenyl structure of the dye. Quantum modeling confirmed that the distance between the sp^2 carbon and MB was within the Van der Waals range. Additionally, electrostatic interactions between Si–NH–Si sites in the material and the amino groups of the dyes further enhanced the adsorption process. It was shown in Fig. 2A, that while the maximum adsorption capacity reached 1328 $mg.g^{-1}$ for MB, it was 1085 $mg.g^{-1}$ for AF. Q_e (mg/g) represents the amount of adsorbate retained per unit mass of adsorbent at equilibrium, while C_e (mg/L) denotes the equilibrium concentration of the dyes remaining in the solution. Such samples revealed superior adsorption capacities compared to other adsorbents tested, such as magnetic chitosan grafted with GO, organo-bentonite-modified cellulose, and carbon nanotube-graphene hybrid aerogel. Furthermore, the samples were regenerated at 400 °C for 2 h (in a nitrogen (N_2) atmosphere) to eliminate the adsorbed dye, resulting in a recycling performance with a removal efficiency of 93.56 % even after the 5th cycle (Fig. 2B) [193].

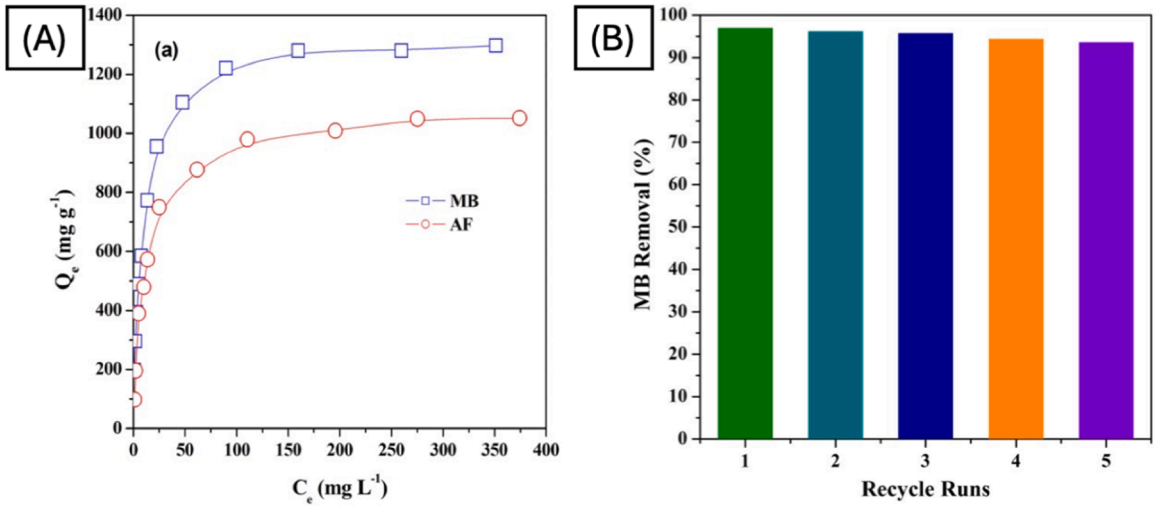


Fig. 2. **(A)** Adsorption isotherms of two dyes for SiCN hybrid material, and **(B)** Removal percentages of MB in five recycle runs using regenerated SiCN hybrid material (initial concentration: 200mg.L^{-1}). (Reproduced from [193], with permission Springer Nature, Copyright 2015).

Aerogels were also tested in this manner, e.g., polymer-derived [liquid PHMS/PCS with DVB] SiOC and SiC ceramic aerogels were produced by crosslinking and followed by CO_2 supercritical drying and pyrolysis (at 900 °C). The aerogel samples were then investigated as sorbents for the removal of MB and Rhodamine B (RB) [205,206]. Adsorption experiments were conducted to assess the removal efficiency at a high dye concentration (100 ppm), closely resembling the textile wastewater levels. The impact of the initial dye concentration on the removal capacity was discussed, revealing a capacity of 16.70 mg.g^{-1} for 100 ppm MB and 45.00 mg.g^{-1} for 547 ppm MB concentration after 172 h. These aerogels, which had a total porosity around 70 vol% and a SSA ranging from 100 to 160 m^2.g^{-1}, manifested a higher removal capacity compared with granular AC [207] (SSA: 747 m^2.g^{-1}) and mesoporous silica SBA-15 [206] (SSA: 490 m^2.g^{-1}), displaying a lower capacity of 21.50 and 41.20 mg.g^{-1}, respectively. The increased capacity of the PDC aerogels was ascribed to the presence of the sp^2-free carbon, interacting with the aromatic structured organic dye through Van der Waals forces, along with the inorganic SiOC nanostructured silica and carbon network [205,206].

SiOC adsorbents were also tested for oil, antibiotic, and metal ion sorption from contaminated water. Commercial PMS-derived polymeric, hybrid, and SiOC ceramic ambi/aerogels were recently synthesized using an ambient pressure/CO_2 supercritical drying route followed by pyrolysis at temperatures ranging from 600 to 1000 °C [163]. All ambi/aerogel ceramics were evaluated for their potential to adsorb both sesame and engine oil. Hydrophobic polymeric ambi/aerogels (with SSA:690–780 m^2.g^{-1} and total porosity: 80 vol%) presented a similar capacity of ~3.15 g.g^{-1}. After pyrolysis at moderate temperatures (600–800 °C), the oil sorption capacities of hybrid ambi/aerogels were found to be 1.78-2.51 g.g^{-1}. Hydrophilic SiOC ceramic ambi/aerogels, featuring SSA of 274-318 m^2.g^{-1} and total porosity of 80 vol%, showed oil absorption capacity of 0.98-1.39 g.g^{-1}. According to the results, pyrolysis temperature altered the wetting behavior of samples, with the highest oil sorption performance achieved by structures with high SSA and predominantly hydrophobic characteristics. The regeneration process was also employed, resulting in only a 28 % decrease in oil sorption performance after the second cycle.

PDC aerogels such as SiOC and SiCN were examined for their ability to adsorb Cr(VI) and Cr(III) ions from aqueous solutions [208]. To produce preceramic aerogels, polysiloxane and PSZ were separately combined with a DVB crosslinker, followed by gelation and pyrolysis, forming SiOC and SiCN, respectively. These ceramic aerogels were produced through varying pyrolysis atmospheres (N_2, NH_3, and CO_2) and temperatures (900 and 1300 °C). The highest adsorption capacity for Cr(VI) ions was observed to be 30 mg.g^{-1} for SiOC aerogel pyrolyzed in an N_2 atmosphere (SSA: 207 m^2.g^{-1}) and 20 mg.g^{-1} for SiCN aerogel pyrolyzed in an NH^3 atmosphere (SSA: 388 m^2.g^{-1}) after 1 h. All aerogels exhibited lower adsorption capacities for Cr(III). This underlines the intricate nature of metal ion adsorption onto porous materials influenced by various factors like SSA, surface functionalities, net surface charge, etc.

Polymer-derived SiOC and hydrofluoric acid (HF)-etched SiOC components have been tested for adsorption of Cd(II), Pb(II), and Cr(III) [155]. Fig. 3A gives a scanning electron microscopy (SEM) image of HF-treated SiOC displaying a rough and porous surface, with the transmission electron microscopy (TEM) image showing both macro and mesopores. The HF-treated high SSA SiOC samples yielded slightly higher adsorption affinity. The highest metal ion sorption (see Fig. 3B) occurred at pH 6, and the adsorption capacities for metal ions ranged from 2.7 to 5.6 mg.g^{-1} for Cd(II), 3.4 to 5.6 mg.g^{-1} for Pb(II), and 3.7 to 4.0 mg.g^{-1} for Cr(III) (Fig. 3C). HF etching of the SiOC material altered the surface chemistry and pore morphology by primarily targeting Si-O bonds. The increased SSA and an enhanced surface charge negativity create additional cation adsorption sites. Comparative studies in the literature on the metal ion adsorption behavior of SiOC are limited; nonetheless, the maximum adsorption capacity values for Cd(II), Pb(II), and Cr(III) are clearly lower than those of AC, which has maximum adsorption capacities of 60 mg.g^{-1} for Cd(II) and 90 mg.g^{-1} for Pb(II) [209].

The risk of environmental contamination from pharmaceuticals is considered high and near-term. Pharmaceuticals (such as antibiotics, painkillers, hormones, etc.) can be found in insufficiently treated wastewater from cities, hospitals, drug factories, and animal farms, and are potential sources of pharmaceutical pollution in rivers, lakes, and groundwater. To eliminate antibiotic (ciprofloxacin) from contaminated water, hierarchically porous SiOC composites [210], synthesized from silicone resin and rice husk via pyrolysis at temperatures ranging from 1000 to 1200 °C were tested. The porous SiOC sample (with SSA: 766 m^2.g^{-1}), produced using a 1:1.5 silicon resin to rice husk ratio and pyrolyzed at 1100 °C, shows evidence of high adsorption capacity (148 mg.g^{-1}) for ciprofloxacin removal from wastewater after 90 min at a pH of 6.8. Compared to other common adsorbents such as carbon xerogel (120 mg.g^{-1}) [211], magnetic mesoporous carbon (75 mg.g^{-1}) [212], and herb biochar (43 mg.g^{-1}) [213], it is clear that the porous SiOC adsorbent confirmed better capacity. Moreover, regeneration studies displayed superior reusability after five cycles, with no significant

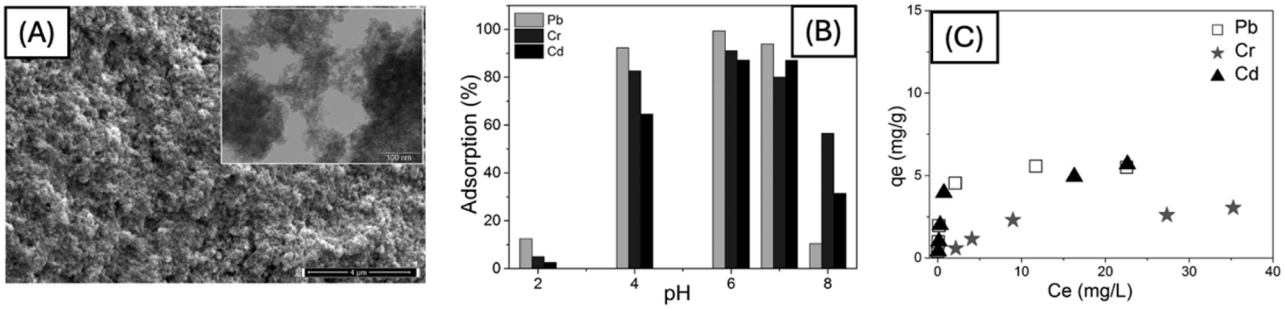


Fig. 3. **(A)** SEM image showing HF etched SiOC component (inset: TEM image), **(B)** The effect of pH for metal ion sorption, and **(C)** Adsorption data for metal ions HF etched SiOC component. (Reproduced from [155], with permission John Wiley and Sons, Copyright 2018).

reduction and ~90 % of its initial adsorption capacity retained.

Foams can be directly used as an adsorbent without a scaffold or filter. Regenerating a foam is straightforward and efficient, unlike powder or granular form adsorbents, without material loss. Polymer-derived SiC foams were from PCS preceramic polymer upon pyrolysis at 1200 °C with a 2 h dwell time. The adsorption capacity of SiC foams towards non-steroidal anti-inflammatory drugs (ibuprofen, fenbufen, flurbiprofen, naproxen, etc.) was evaluated after different contact times (24, 48, and 72 h) [214]. Approximately 0.0042 mg of ibuprofen could be adsorbed by 1 g of SiC foam (SSA: 0.31 $m^2.g^{-1}$) in 72 h. The findings indicate that adsorption capacity improved as contact time increased for all target compounds, with the process being governed by slow kinetics.

Porous SiC-C aerogels were assessed as a potential sorbent for the glyphosate herbicide [194]. The PDC aerogel was synthesized using PCS, DVB, and cyclohexane, followed by gelation (150°C, 5 h), supercritical drying, and pyrolysis at either 1000°C or 1500°C to compare the glyphosate retention capabilities of amorphous and crystalline SiC. While aerogel formed at 1000 °C showed deficient removal performance (13.0 %) due to Si-OH formation and its lower SSA (102 $m^2.g^{-1}$), one treated at 1500 °C had a higher SSA (215 $m^2.g^{-1}$), adsorption capacity (0.6 $mg.g^{-1}$), and removal efficiency (> 90 %) after 48 h.

2.1.1.1. Panel: sorption. The sorption mechanisms for contaminants, such as heavy metals, organics, etc., on inorganic non-metallic adsorbents vary based on the distinct nature of metal ions and organic molecules, with the surface charge and functional properties of the adsorbents playing a critical role. For metallic ions, adsorption generally involves ionic and chemical bonding, forming covalent or ionic bonds with surface functional groups, as well as electrostatic interaction. In contrast, dye molecules have complex chemical structures that influence their sorption, with mechanisms including electrostatic attraction (depending on the charge interaction between the dye and ceramic), hydrophobic interactions with nonpolar dye regions, hydrogen bonding through dye functional groups (like –OH or $–NH_2$) with ceramic hydroxyl groups, π–π interactions between aromatic rings in the dyes and π-electrons on the ceramic, and Van der Waals forces aiding neutral or nonpolar dye adsorption. Specific surface modifications are often needed for oils, herbicides, and pharmaceuticals; hydrophobicity benefits oil adsorption, while mixed polarity and diverse functional groups improve the adsorption of herbicides and drugs.

The sorption capability of sorbents may depend on different variables such as SSA, time, surface functionality, pH, etc [217]. In simple terms, when the concentration of the solute remains constant, equilibrium conditions are set [199]. The equilibrium sorption isotherms, which may vary (refer to Fig. 4A), are used to evaluate these experimental conditions. From these isotherms, constants and coefficients are usually determined to comment on the results. Although the linear isotherm does not indicate selectivity, it is sometimes favored because it simplifies the modeling, particularly when equilibrium data is incorporated into dynamic conditions. Sorbents with isotherms that exhibit an upward convex curvature are referred to as favorable, as typically modeled by Langmuir and Freundlich models, details on such models can be obtained from published books [218].

Inorganic non-metallic solids offer stability across a range of pH levels, temperatures, and chemical conditions, allowing for repeated use and cost efficiency in water treatment applications. Diverse interactions contribute to the effectiveness of PDC adsorbents. Surface functional groups like Si-OH, sp^2 carbon, and magnetic responsiveness provide unique adsorption mechanisms. For example, micro-mesoporous SiOC components with SSA ranging between 120-660 $m^2.g^{-1}$ were investigated for cleaning cationic dyes [155]. These materials verified dye sorption capacities between 50-186 $mg.g^{-1}$. The increased SSA and altered SiOC pore structure provided additional sorption sites.

Similarly, Pan et al. [153] reported the production of SiOC composites revealing SSA ranging from 90 to 465 $m^2.g^{-1}$, a pore volume between 0.06-0.31 $cm^3.g^{-1}$, and an average pore size of 2.8 nm. The composite with an SSA of 91 $m^2.g^{-1}$ displayed a relatively low adsorption capacity for MB (C_{max}: 70 $mg.g^{-1}$). In contrast, samples with higher SSA values (290 and 465 $m^2.g^{-1}$) yielded higher adsorption capacities (C_{max}:112 and 147 $mg.g^{-1}$). Therefore, the increased dye adsorption was

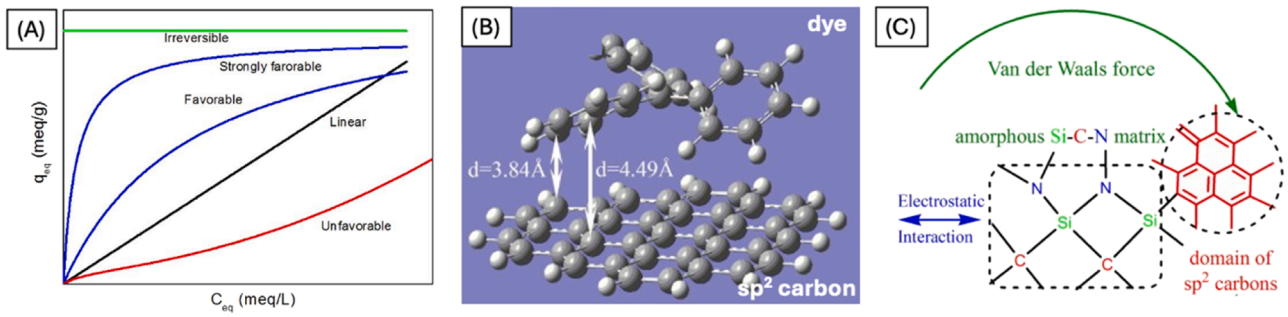


Fig. 4. **(A)** The arithmetic graph between concentration vs adsorbent loading presents different adsorption isotherms (Reprinted from [219], Licensee IntechOpen 2013), **(B)** The interaction between the sp^2 carbon domain and triphenyl structure of MB, and **(C)** suggested selective adsorption mechanism of dyes for porous Si–C–N hybrid material. (Reproduced from [193], with permission Springer Nature, Copyright 2015).

credited to the high SSA, offering numerous accessible and strong adsorption sites.

Magnetic porous Ni-modified SiOC ceramic nanocomposites were synthesized via a template-free PDC approach and evaluated for their efficiency in adsorbing acid fuchsin dye [204]. These nanocomposites, predominantly mesoporous, with a SSA of 250–345 $m^2.g^{-1}$ and a pore volume ranging from 0.13 to 0.18 $cm^3.g^{-1}$, achieve adsorption capacities of 124 $mg.g^{-1}$ and 130 $mg.g^{-1}$, respectively. The authors recognized the superior adsorption performance toward AF dye molecules due to their mesoporous structure and high SSA, with the Ni-based phase enhancing chemisorption.

Porous SiOC samples with an SSA of 480–766 $m^2.g^{-1}$ and a pore volume of 0.43–0.84 $cm^3.g^{-1}$ were assessed for their ciprofloxacin adsorption capacity from wastewater [210]. The adsorption capacity increased from 85 to 110 $mg.g^{-1}$ as the SSA nearly doubled. This enhanced adsorption capacity for ciprofloxacin was largely due to the higher SSA and greater pore volume. Additionally, TiO_2/SiOC nanocomposites with mesoporosity (SSA: 129 $m^2.g^{-1}$) had rapid and almost complete MB dye adsorption within 10 min, while macroporous samples (SSA <1 $m^2.g^{-1}$) displayed limited adsorption [202].

SiOC ceramic ambi/aerogels [163], with an SSA of 274–318 $m^2.g^{-1}$, a pore volume of 1.4 $cm^3.g^{-1}$, and a total porosity of 80 vol%, yielded oil absorption capacities ranging from 0.98 to 1.39 $g.g^{-1}$. PDC-SiOC aerogels, with SSA values between 120 and 660 $m^2.g^{-1}$, had promising adsorption capacities reaching 6 $mg.g^{-1}$. In comparison, SiCN aerogels with an SSA of 390 $m^2.g^{-1}$ showed an adsorption capacity of 20 $mg.g^{-1}$ for metal ions such as Cr(VI), Cd(II), and Pb(II) [155,208].

These findings highlight that while a higher SSA generally improves adsorption capacity across most PDC materials, optimal adsorption is not solely governed by SSA. Other factors, such as surface functionalities, facilitate bonding and enhance adsorption performance. While surface characteristics, particularly surface Si-OH groups, are critical for metal ion sorption, a combination of Van der Waals forces and π-π interactions between the aromatic structures of the dyes and the sp^2 carbon domains within PDCs becomes important for dye molecules. Electrostatic interactions also contribute significantly, mainly when amino groups on dye molecules interact with Si–NH–Si sites [193].

Quantum chemical modeling, depicted in Fig. 4B, confirmed that the atomic distance between the sp^2 carbon clusters and MB lay within the Van der Waals range. Fig. 4C illustrates the adsorption mechanism of the porous Si–C–N hybrid material by Van der Waals forces between the sp^2-hybridized carbon domains in the adsorbent and the triphenyl structure of the dye.

To summarize, the adsorption mechanism of polymer-derived ceramics is governed by a combination of physical and chemical interactions imposed by the structural and surface properties (overviewed in Fig. 5). By tailoring these, PDCs may selectively adsorb specific molecules or ions for different applications. Studies reveal that while physisorption is affected by high porosity/SSA, chemisorption is predominantly determined by the type and presence of surface functional groups. For instance, SiOC and SiCN commonly present –NH, –C=O, and –Si–OH functional groups, facilitating specific chemical interactions with adsorbates. The adsorption of dyes onto such surfaces can be facilitated through van der Waals interactions between the aromatic structure of the dyes and the sp^2-free carbon phase, a common feature of the Si-based PDCs [205], or through electrostatic interactions involving carbon-oxygen complexes (C–O/C–OH) or surface Si-OH moieties [206]. Van der Waals interactions are particularly notable for the aromatic structure of dyes such as methylene blue and Rhodamine B, interacting with the segregated carbon phase in SiOC [205]. In contrast, phase pure silica relies solely on ionic adsorbate-adsorbent interactions. Beyond dyes, polysiloxane-derived SiOC micro- and mesoporous hybrid ceramics (ceramers) demonstrate suitability for adsorbing n-heptane and oil with minimal water adsorption due to their hydrophobic surface [163,220].

2.2. Filtration

Air pollution, originating from natural and human activities, consists of gaseous and particulate substances that can cause significant harm to human and environmental health. Most commonly, air pollutants can be categorized as gaseous and particulate pollutants. Pollutants [sulfur, nitrogen, carbon oxides, and particulate matter (PM)] are released into the atmosphere. Gaseous pollutants comprise volatile oxides and volatile organic compounds, while particulate pollutants encompass solid particles and liquid droplets [221]. These particulates are further categorized by size, with classifications including coarse (PM_{10}), fine ($PM_{2.5}$), and ultrafine ($PM_{0.1}$), denoted as PM_x, where x represents the maximum particle diameter in micrometers (μm) [222].

Air pollution is a significant risk for noncommunicable diseases, affecting respiratory health, with conditions such as asthma and lung cancer linked to pollutants like nitrogen dioxide and sulfur dioxide. Cardiovascular diseases are also aggravated by fine and ultrafine particulate matter. PM can affect systemic inflammation, oxidative stress, and direct vascular damage [223]. Air pollution harms not only human health but also the environment. Environmental impacts of air pollution include acid rain, haze, ozone layer depletion, and climate change [224]. To mitigate these effects, stronger pollution controls and methods are necessary.

Ceramic filters are employed in a wide range of industries and

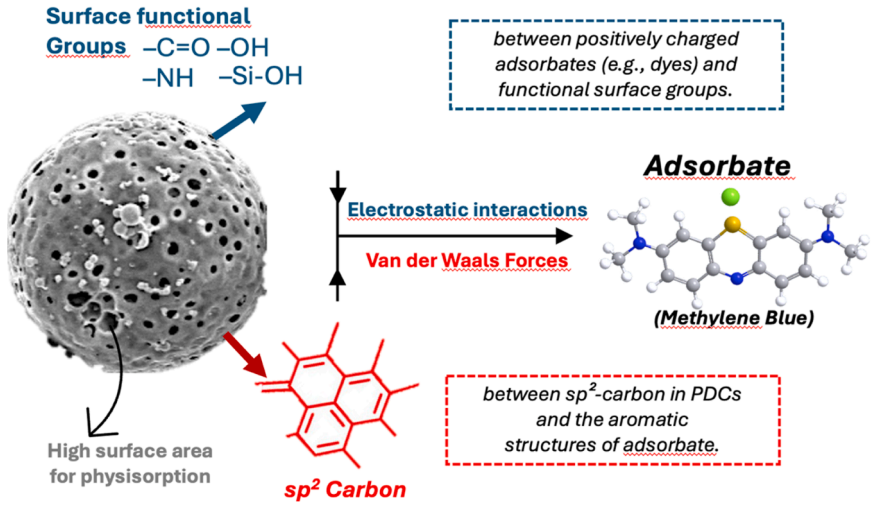


Fig. 5. Visualization of the adsorption mechanism of porous PDCs.

environments (including water treatment, hot gas purification, diesel exhaust particulate control, air filtration, metal processing, and more, as given in Fig. 6) due to their remarkable ability to endure high temperatures, resist chemical corrosion, and maintain structural integrity under extreme conditions [90,225–228].

Hot gas filtration purifies industrial gases in power plants, chemical processing, and waste incineration, effectively removing particulates and contaminants even at elevated temperatures. In particular cases, such as in metal casting, ceramic filters are employed to purify molten metals, removing impurities and enhancing the quality of the final cast products. They are also highly effective in water filtration, efficiently removing contaminants like bacteria, sediment, and microorganisms to ensure clean and safe drinking water. Their robust construction and long-lasting durability make them appropriate for household and industrial use, where reliable filtration performance is essential [229]. The utilization of ceramic air filters is a reliable solution for maintaining air quality and an environmentally sustainable choice. Their ability to be regenerated through cleaning processes such as counter pressure or high-temperature treatment extends their lifespan and reduces waste [89].

2.2.1. *Hot gas filtration*

Hot gas filtration is defined as filtration conducted above 260 °C (up to 900 °C, at pressures up to 8 MPa, in both oxidizing and reducing atmospheres) according to the VDI (Verein Deutscher Ingenieure, Association of German Engineers) guidelines 3677-3. For more details, the interested reader is referred to reviews on the detailed processing of hot gas filtration [230,231]. The filter medium has to be stable against temperature, pressure, and chemical composition of gas (such as H_2S, HCl, NH_3, Cl_2, and H_2O) and dust [230]. Hot gas filters must be reliable for over 10,000 h, efficiently removing particulates while withstanding mechanical and thermal stresses.

Rigid, self-supporting ceramic and metal filter elements are suitable for high temperatures. Ceramic or metal candles are among the most promising hot gas cleanup material types outlined in Fig. 7A-**B**. They offer a cleaning efficiency higher than 99 %, successfully removing particulates and contaminants [231]. Ceramic hot gas filters, e.g., candle filters, have been widely used in advanced coal-fired power generation systems and have been beneficial in biomass-fired systems for decades [232]. Among the others, SiC ceramic candles boast high particulate collection efficiency. They are frequently employed in industrial power generation facilities because of their high-temperature stability, thermal shock resistance, low thermal expansion, high fracture toughness, and high-temperature creep resistance [232,233].

Ceramic filter elements, preferred for hot gas filtration, come in various shapes, including candle forms and honeycomb monolith structures [230]. The honeycomb monolith (in Fig. 7C-**D**) comprises numerous cells arranged in parallel. Gas flow enters the open cells on the upstream side, traverses through the walls, and exits through the open cells on the downstream side. Particles are trapped along the walls of the upstream cells. Studies have illustrated that ceramic foams can provide more efficient heat transfer than particle beds and honeycombs [234]. In other words, foams offer a superior mass transfer-to-pressure drop ratio, benefiting from radial mixing, which is particularly well-suited for gas filtration applications [225,235].

Although porous PDCs are ideal for hot gas filtration due to their high thermal stability, chemical resistance, and oxidation resistance, only one study [225] has explored the hot air permeability of polymer-derived SiOC reticulated foams produced using the PU foam replica technique. The microstructural characteristics of SiOC foams were adjusted by modifying processing parameters such as the type of PU foam (cell size and open or partially closed cells), cross-linking conditions (temperature range: 80-220 °C and time), and the nature of the cross-linking polymeric blend (PHMS, polydimethylsiloxane; PDMS, and tetramethyltetravinyl-cyclotetrasiloxane; TMTVS). Preceramic solutions impregnated PU foams were cured and pyrolyzed (at 1000 °C) to obtain SiOC foams. Hot gas permeability tests proved that SiOC foams, with a total porosity of 95 %, remained stable up to 700 °C without any loss of functionality.

Inorganic non-metallic solid filters play a vital role in DPF in the automotive industry, significantly reducing soot emissions and helping vehicles meet strict environmental regulations. Porous ceramics are excellent candidates for DPF; however, few studies have explored PDCs for DPFs. In this study [237], SiC and SiOC membranes were formed to

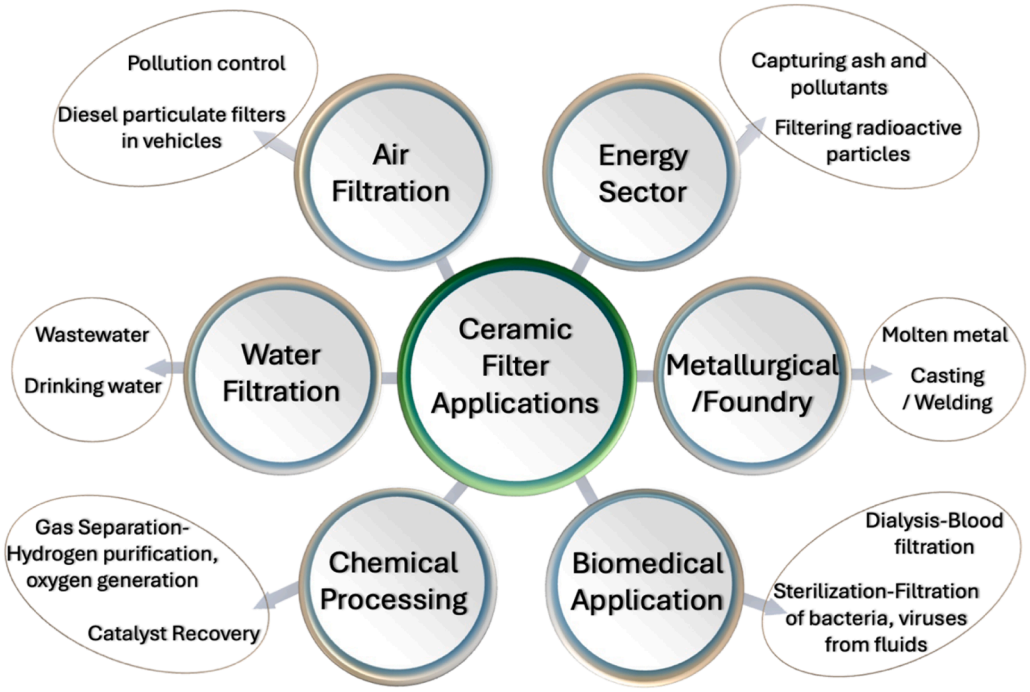


Fig. 6. Inorganic non-metallic solid filters are used in various sectors, including air filtration, energy, metallurgy/foundry, biomedical applications, chemical processing, water filtration, and more.

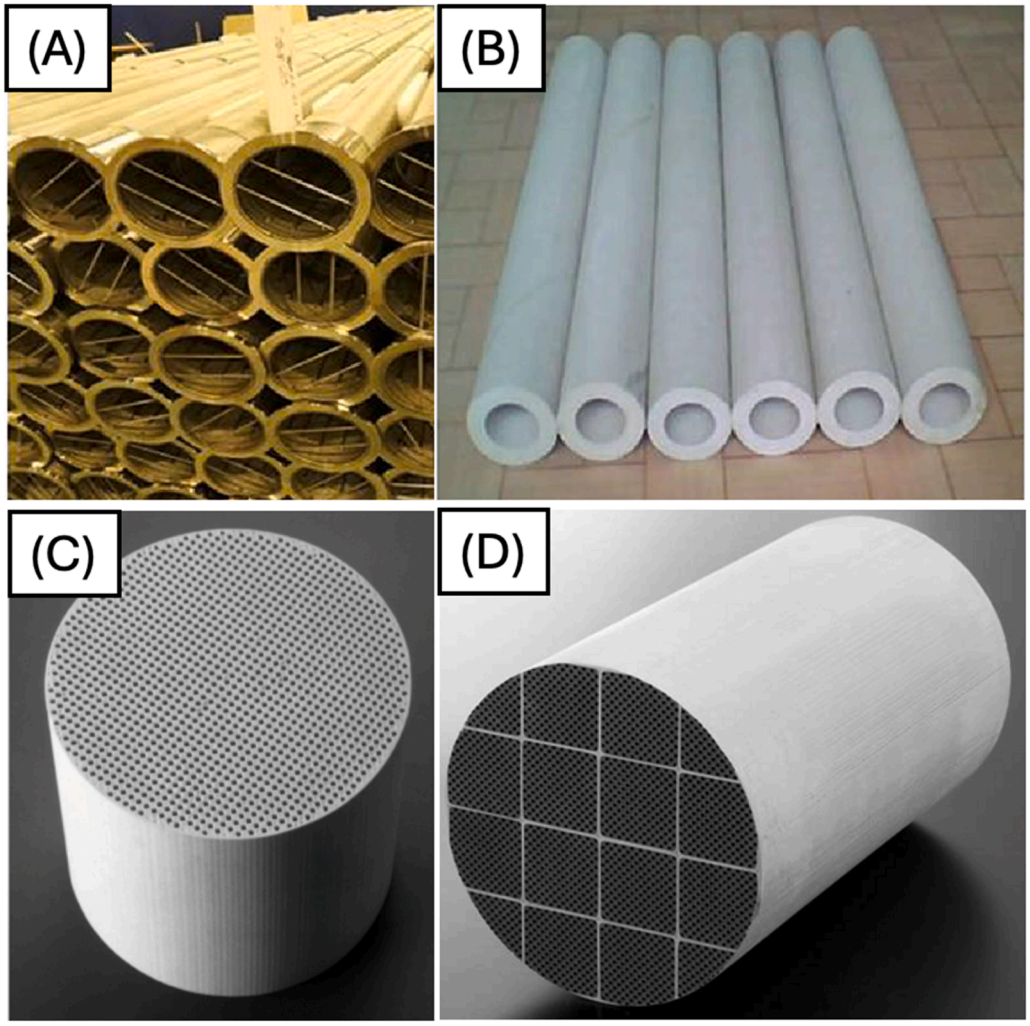


Fig. 7. Pictures of the typical ceramic filter elements; candle filters for hot gas filtration **(A)** ceramic filter, **(B)** metallic filter (Reproduced from [236], with permission Elsevier, Copyright 2022), and commercial ceramic te DPFs **(C)** monolith cordierite filter, **(D)** Segmented SiC filter. (Reproduced from [84], with permission John Wiley and Sons, Copyright 2005).

filter soot particles, with a schematic overview in Fig. 8 of the fabrication process. Briefly, using commercial preceramic polymers (SMP-10 and SPR-036), the DPFs were dip-coated to reduce pore size and improve filtration, with polymer concentrations used in dip-coating ranging from 10-40 vol%. After pyrolysis at 1000 °C for 2 h under Ar flow, coatings reduced DPF porosity from 43 % to 40 % and pore size from 22 to 18 μm without increasing back pressure. The membranes enhanced durability, and catalytically active Ce–O–Fe–Pt/SiC coatings improved CO/HC oxidation and soot combustion, with soot burning occurring at 30 °C below the SiC baseline. While PDCs have higher initial costs than traditional ceramics, they offer durability, confinement of catalysts, and reusability.

2.2.2. *Membrane filtration*

Membrane-based separation technologies (simple operation, easy to scale up, energy-conserving, and high efficiency) have become prevalent in water treatment, food processing, pharmaceuticals, and gas separation [238–241]. This method involves using a semi-permeable membrane to separate components in a fluid, selectively allowing certain particles or molecules to pass through based on size, charge, or chemical properties.

Membranes can be designed as 'porous' or 'dense' based on the intended applications. The separation mechanism for porous membranes in liquid separation is primarily due to pore-sieving, whereas for dense membranes in gas separation, it is mainly driven by solution-diffusion phenomena [69]. Various material systems (zeolite, Al_2O_3, ZrO_2, TiO_2, SiC, SiO_2, carbon, GO, several polymers, etc.) have been employed in developing membranes [71,242,243].

Polymeric membranes are widely used in water treatment and desalination, yet their inadequate long-term chemical and mechanical stability, as well as susceptibility to fouling and compaction, restrict their application. Similarly, carbon-based membranes suffer from structural collapse at high temperatures in gas separation. Instead, metal-based membranes are susceptible to hydrogen embrittlement during H_2 separation. Despite their promise, mixed-matrix membranes encounter hurdles, including the high cost of fillers and the necessity for further scaling-up studies. In contrast, ceramic membranes have distinctive advantages: high mechanical strength, superior chemical and thermal resistance, fouling resistance, ease of cleaning, regeneration/decontamination at high temperatures, and extended operational lifespan [71,240,241,243]. Ceramic membranes can endure backwashing pressures and resist damage from cleaning agents and oxidants. Methods like chemically enhanced backwashing and cleaning in place, using high concentrations of sodium hypochlorite, sodium hydroxide, or ozone, have effectively restored ceramic membranes in water and wastewater treatment [244]. Most ceramic membranes are inherently hydrophilic, possessing a lower fouling tendency.

Reviews [69,71,244] classify ceramic-based membranes on pore size

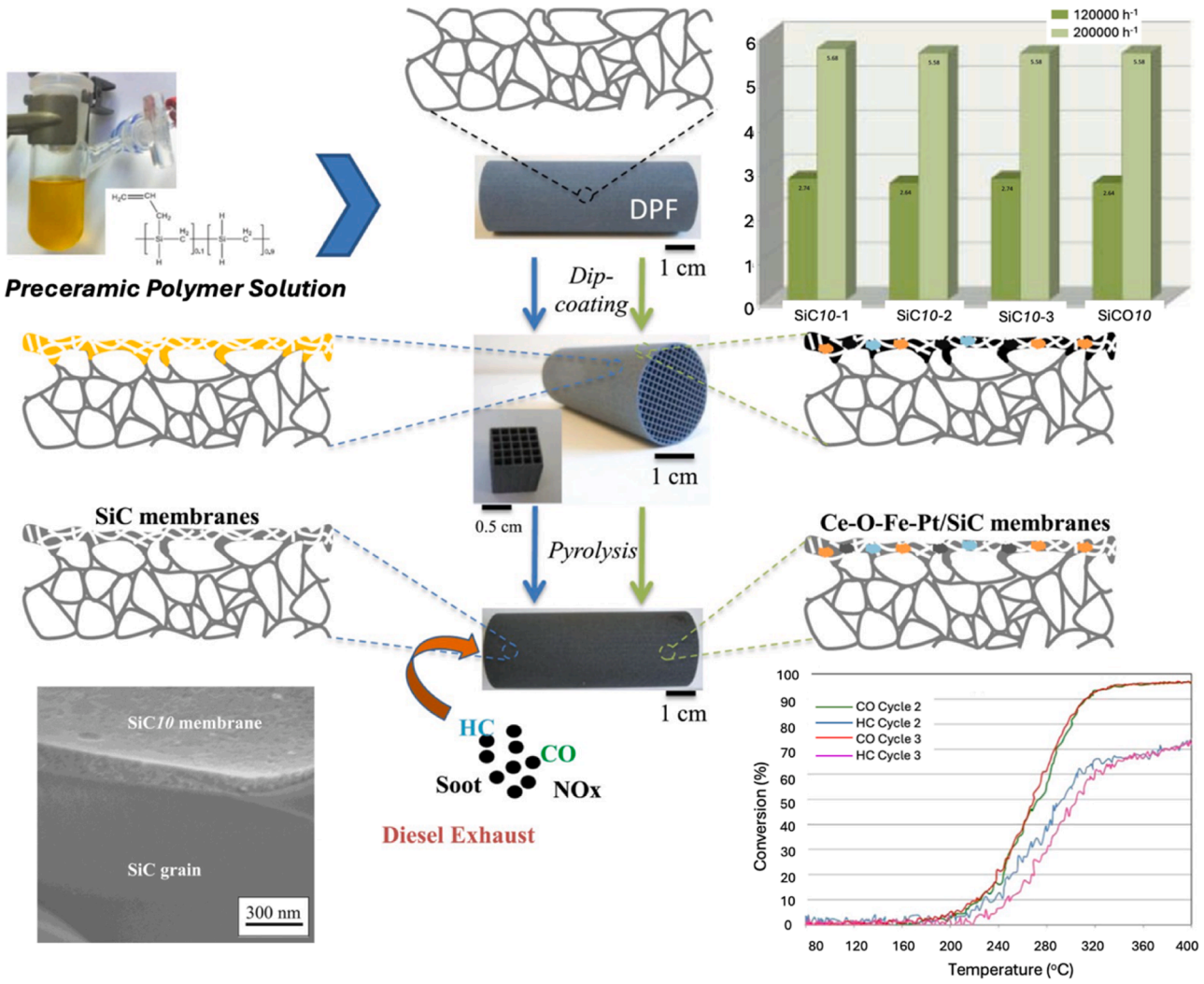


Fig. 8. Process flow for developing SiC and Ce-O-Fe-Pt/SiC membranes from preceramic polymer precursors. (Reproduced from [237], with permission Elsevier, Copyright 2016).

(macro, meso, and micro), surface character (hydrophobic or hydrophilic), and applications (pressure and thermally-driven). They typically feature a multi-layered structure comprising a substrate offering mechanical support, an intermediate layer for customized pore size, volume, and an active top layer for separation purposes. Ceramic membranes, such as Al_2O_3, TiO_2, and ZrO_2, reveal distinct advantages and drawbacks. Al_2O_3, particularly α-Al_2O_3 (corundum), stands out as a commonly used material due to its price-to-performance ratio, ease of processing, and inherent properties like high strength, chemical resistance, and thermal stability. It serves multiple roles in ceramic membranes, functioning as a substrate, intermediate, and active membrane layer. Typical processing methods for Al_2O_3 membranes include sol-gel, dip coating, and sintering. Commercially available Al_2O_3 membranes vary in shape, pore size, and module configurations, although achieving precise control over smaller pore sizes remains challenging [245].

TiO_2 is recognized for its effectiveness in separation and photocatalysis. Yet, it faces challenges in water treatment due to its, in general terms, lower SSA and the instability of its anatase structure at high temperatures. Silica membranes suffer from structural instability when exposed to water due to their high affinity, necessitating improvements in hydro-stability. Zeolite membranes encounter difficulties in achieving defect-free structures with desired thicknesses.

PDC membranes have gained significant attention as alternatives to traditional polymeric and inorganic membranes due to their superior thermal and chemical resistance, tunable porosity, and processability. Specifically, here, the proceeding section provides an overview of fabrication strategies, structure-property-performance relationships, and the emerging applications of PDC membranes in environmental remediation, particularly in water treatment, dye removal, salt rejection, oil-water separation, and gas filtration.

Polymer-derived SiOC, SiCN, and SiC membranes are proven to be highly effective in separating gases and liquids at high temperatures, are resistant to chemical cleaning, and are employed in fluid separation processes. Preceramic polymers offer an efficient way to produce these membranes, known for simplicity and processing flexibility, and are suitable for both batch and continuous production. PDC membranes, monolithic or as coatings, with pore sizes ranging from nano to micron size, were synthesized using polysiloxane, PSZ, and PCS precursors, followed by pyrolysis. Published studies showed that these membranes have significant potential for water [156,195,241,242,246–248] and gas separation [157,239,240,243,249–251]

As known, different fabrication methods, such as dip-coating, electrospinning, phase inversion, and selective laser printing, can facilitate control over pore size, surface chemistry, and membrane architecture. PDC membrane production can be done by casting/self-sacrificial methods, coating/spraying on substrates, and spinning or 3D printing, see Table 2.

SiOC membrane was developed via a reactive self-sacrificing method

Table 2
PDCs filters and applications.

Filter Element	*Preceramic Precursor*	*Processing Method*	*Pyrolysis*	*Other Properties*	*Application*	*Refs.*
SiOC Foam	Polysiloxane	PU template (65-80 PPI) Replica	1000 °C 2h /Ar	SSA: 1- 80 $m^2.g^{-1}$ Pore size: 141-886 μm Porosity: 93-97 vol% σ_c=0.208–0.244 MPa	Hot gas	[225]
SiOC Foam	Polysiloxane	PU template (10 PPI) Replica	1000 °C 2h /Ar	Pore size: 2042 μm Porosity: 98 vol% σ_c=0.079 MPa	Molten Metal	[265]
SiOC(N) Foam	Polysilazane	PU template (10 PPI) & 3D-printed PU template Replica	1200 °C 2h /N_2	Pore size: 2179 μm Porosity: 61-98 vol% σ_c=0.027-27 MPa	Molten Metal	[265]
SiOC Membrane	Polysiloxane	Self-sacrificed template	1000 °C 2h /N_2	SSA: 8- 28 $m^2.g^{-1}$ Pore size: 6-10 nm Porosity: 27-45 % Permeability:140Flux@ 2.5 bar	Water Purification	[195]
SiOC Composite Nanofiltration Membrane	Polycarbosilane	Dip Coating on ceramic substrate	700 °C/N_2	Thickness: 1-2.4 μm σ_c=28-31 MPa Flux: 3.37-22.6 $m^{-2}h^{-1}bar^{-1}$ Dye rejection rate: 96 %	Water Purification	[242]
SiOC Membrane	Polysiloxane	Preceramic Liquid Casting	1100-1400 °C 3h /Ar	Pore size: 0.59-0.95 μm Porosity: 30-65 % N_2 permeation: 6.4 × 10^5 -3.9 × 10^6 LMH/bar Water permeation: 9.8 × 10^2-3.3 × 10^3 LMH/ bar Oil rejection rate: 94.6 % Salt rejection rate: 99.9 %	Oil-in-water emulsion filtration & membrane distillation	[156]
SiOC Membrane	Polysiloxane	Tape casting	600-1000 °C/N_2	SSA: 4-473 $m^2.g^{-1}$ Pore size: 1-10 μm Porosity: 33-47 % σ_f=20-48 MPa Water permeation: 1-23 LMH @1 bar 6–55 LMH @3 bar	Water filtration	[246]
SiOC Membrane	Polysiloxane	Coating onto Yttria Stabilized ZrO_2 hollow fiber membrane	800 °C 1h /Ar	Thickness: 15 μm Pore size: 50 nm-2 μm Porosity: 34-41 % Water permeation: 1549 LMH @0.1 MPa	Water filtration	[247]
SiOC Membrane	Polycarbosilane	Electrospinning	1100 °C/Ar	σ_f=6.5 MPa Modulus=302 MPa.	Water/Oil separation	[248]
SiOC/SiC/TiO_2 Membrane	Polysiloxane	Tape casting	600-1000 °C/N_2	SSA: 10-200 $m^2.g^{-1}$ Pore size: 0.3 -1.4 μm Porosity: 30-40 % σ_f=15-35 MPa Water permeation: 2.5-370 LMH@2 bar Oil rejection rate: 81–98 %	Water/Oil separation	[241]
SiOC Membrane	Polysiloxane	Coating on γ-Al_2O_3 & ZrO_2 substrates	700-800 °C/ inert	H_2 permeance: 0.56-49.8 LMH @25-300 °C Permselectivity: H_2/CO_2: 0.9-9.1 H_2/C_3H_8: 3.7-92.8 H_2/SF_6: 7.1-320	Gas separation	[157]
SiOC Membrane	Polysiloxane	Top coating γ-Al_2O_3 coated -Al_2O_3 substrate	700°C 1h/Ar	Thickness: 300 nm Permselectivity: H_2/CO_2: 10 H_2/CH_4: 23 H_2/SF_6:320 @300 °C	Gas separation	[240]
SiOC Membrane	Silane & Siloxane	Coating on α-Al_2O_3-SiO_2-ZrO_2 substrate	500-800°C 0.5h/N_2	SSA: ~50-350 $m^2.g^{-1}$ Pore size: 1-5 nm Permselectivity: @50-500 °C H_2/CF_4: 240-640 H_2/SF_6: 1400-2900	Gas separation	[249]

(*continued on next page*)

Table 2 (*continued*)

Filter Element	*Preceramic Precursor*	*Processing Method*	*Pyrolysis*	*Other Properties*	*Application*	*Refs.*
				N_2/CF_4: 98 H_2/N_2: 5.9-62		
SiOC Membrane	Silane & Siloxane	Deposited onto α-Al_2O_3 substrate	500-700°C 0.5h/N_2	SSA: 315-393 $m^2.g^{-1}$ Permselectivity: @200 °C H_2/CH_4: 15-19 H_2/SF_6: 1000-1400	Gas separation	[250]
SiOC Membrane	Polysiloxane Phenolic resin	Selective Laser Printing & precursor impregnation	1000-1600 °C/Ar	σ_f = 18.9–27.3 MPa Pore size: 0.1-30 μm Porosity: 35–42 % Gas permeation flux: 2759 LMH Water permeation flux: 24 LHM	Gas & water treatment	[239]
SiOC Membrane	Polysiloxane	Sprayed onto a Si_3N_4 membrane	500-1000 °C 3h/Ar	Thickness: ~1.8 μm H_2 permeance: 3.26 × 10^{-8} mol.m^{-2}.Pa^{-1}.s^{-1} Permselectivity: @25 °C H_2/CO_2: 20	Gas separation	[243]
SiCN Membrane	Polysilazane	Coating on ZrO_2 substrate	600-900 °C/ inert	Permeance @25-300 °C H_2: 25.6-11.2 LMH Permselectivity: H_2/CO_2: 1.5-4.6 H_2/C_3H_8: 1.8-29.7 H_2/SF_6: 8.1-103	Gas separation	[157]
SiC Membrane	Polycarbosilane	Dip-Coating on γ-Al_2O_3 coated α-Al_2O_3 substrate	800 °C 1h /Ar	Thickness: ~380 nm Permeance @600 °C He: 2.43 × 10^{-7} -1.06 × 10^{-6} H_2: 1.31 - 8.1 × 10^{-7} CO_2: 6.2 × 10^{-8}- 1.28 × 10^{-7} Ar: 1.31 - 6.33 × 10^{-8} N_2: 1.55 - 7.01 × 10^{-8} mol.s^{-1}.m^{-2}.Pa^{-1} Permselectivity: @300-800 °C H_2/CO_2: 5-13 He/CO_2: 5-19	Gas separation	[251]
SiC Membrane	Polycarbosilane	Dip-Coating on α-Al_2O_3 substrate	400-800 °C 2h /Ar	Thickness: ~1-2 μm Permeance @100 °C He: 62-84 × 10^{-10} H_2: 18-63 × 10^{-10} CO: 0.16-3 × 10^{-10} N_2: 0.13-2.6 × 10^{-10} mol.s^{-1}.m^{-2}.Pa^{-1} Permselectivity: @100 °C H_2/CO: 22-114	Gas separation	[258]
SiC Membrane	Polycarbosilane	Coating on α-Al_2O_3 substrate	300-800 °C 0.5h /N_2	Thickness: ~200 nm Permeance @200 °C H_2: 0.2-5 × 10^{-6} mol.s^{-1}.m^{-2}.Pa^{-1} Permselectivity: 200@ °C H_2/N_2: 12-56 H_2/SF_6: > 10,000 N_2/SF_6: > 800	Gas separation	[259]
SiC-based membrane	Polycarbosilane Polyvinylsilane	Spin-coating on γ- Al_2O_3	850 °C 0.5h /Ar	Thickness: ~1.25 μm SSA: 1.25-2.09 $m^2.g^{-1}$ H_2 permeance: 10^{-10}-10^{-8} mol.s^{-1}.m^{-2}.Pa^{-1} Permselectivity: 250@ °C H_2/N_2: 3.7-254	Gas separation	[260]
SiC-based membrane	Polycarbosilane	Coating on α-Al_2O_3 substrate	350-750 °C 0.5h /N_2	Pore size: 0.4-0.6 nm H_2 permeance: 5.87 × 10^{-7} - 1.95 × 10^{-6} mol.s^{-1}.m^{-2}.Pa^{-1} Permselectivity: R.T to 200@ °C	Gas & pervaporation separation	[261]

(*continued on next page*)

Table 2 (*continued*)

Filter Element	*Preceramic Precursor*	*Processing Method*	*Pyrolysis*	*Other Properties*	*Application*	*Refs.*
				H_2/N_2: 4.2-9.5 He/H_2: 0.6-0.8 N_2/SF_6: 12-761 N_2/CF_4: 4.3-76 N_2/CH_4: 0.8-1.9		
Ti/SiC-based Membrane	Polytitanocarbosilane	Coating on α-Al_2O_3 substrate	750 °C 0.5h /N_2	Permeance H_2:10.7×10^{-7} N_2:1.3×10^{-7} $mol.s^{-1}.m^{-2}.Pa^{-1}$ Permselectivity: 200@ °C H_2/C_3H_8: 34 H_2/CF_4: 404 N_2/SF_6: 2,110 H_2/SF_6: 16,600	Gas & pervaporation separation	[262]
Pd-doped SiOC membrane	Polycarbosilane	Electrospinning	1100 °C 1h / Ar	Thickness: ~50 μm Pore size: 11.2-18.1 nm SSA: 29-52 $m^2.g^{-1}$ σ_T=0.5-33 MPa $E_{modulus}$= 290-620 MPa $F_{modulus}$= 2-8 kPa	Air filtration	[274]

[195]. The cyclosiloxane hybrid polymer was synthesized through the polymerization of 2,4,6,8-tetramethylcyclotetrasiloxane and 2,4,6,8-tetramethyl-2,4,6,8-tetravinylcyclotetrasiloxane in a 1:1 mass ratio. PDMS served as the sacrificial template. The prepared viscous mixture was transferred to Teflon molds and degassed in a desiccator before being cured in an oven at 80-150 °C. Following curing, the samples were pyrolyzed in flowing N_2 at 1000 °C for 2 h. During pyrolysis, the PDMS template thermally decomposed, forming membrane pores facilitating water transportation. The pore size and porosity were tunable by varying the amount and type of PDMS (vinyl and trimethyl terminated) with molecular weights ranging from 25,000 to 139,000 $g.mol^{-1}$ used in the fabrication process. As the PDMS content increased, both linear shrinkage and porosity of the membrane increased while the apparent density decreased. The SiOC membranes attested hydrophilic surfaces, the water flux increased linearly with pressure across all membranes, and water permeability was closely related to PSD and membrane porosity. Water permeability and rejection performance were tested using a homemade dead-end membrane filtration system. Various pressures, ranging from 0 to 2.5 bar, were applied to assess pure water permeability. The SiOC membrane, prepared with trimethyl-terminated PDMS (M_w = 63,000 $g.mol^{-1}$, 30 wt%), had high water permeability (60 $L.m^{-2}.h^{-1}$ (LMH)@1 bar to 140 LMH@2.5 bar) and a 95 % removal rate of RB, showcasing its potential applications in water treatment.

Porous SiOC ceramic membranes were fabricated from liquid polymer (PHMS to tetramethyltetravinylcycletetra (D_4Vi) mass ratio of 1:1) and PDMS (30-60 wt%) as a pore-forming agent [156]. The mixture was cast into glass molds and, after gelation, subjected to pyrolysis at 1100-1400 °C in a flowing Ar atmosphere for 3 h. PDMS was also employed for surface modification, resulting in a super-hydrophobic surface. The mean pore size ranged from 0.59 to 0.95 μm, and porosity varied from 30 % to 65 %, increasing with higher PDMS content (30-60 wt%). This increase in porosity led to decreased bending strength and density due to increased total porosity. N_2 (6.4×10^5 LMH/bar to 3.9×10^6 LMH/bar) and water permeation rates (9.8×10^2 LMH/bar to 3.3×10^3 LMH/bar) also increased with larger pore sizes and higher porosity. Membranes with an average pore size of 0.59 μm effectively separated an oil-in-water emulsion with an average oil droplet diameter of 0.83 μm, achieving a 95 % rejection rate. A high salt rejection rate of 99.9 % was achieved with NaCl solutions (4-16 wt%) at various temperatures (55-85 °C). The membranes manifested stable performance for over 100 h, using 4 wt% NaCl in the feed at 75 °C.

Porous SiOC membranes were produced using a PDC route adapted to the phase inversion tape casting technique, with commercial methyl polysiloxane as the ceramic precursor [246]. The process involved mixing the preceramic polymer with C_2H_6O, imidazole as the catalyst, pre-heat treated preceramic particles, and PVP, followed by casting the slurry and pyrolyzing. The membranes' characteristics were tailored by adjusting pyrolysis temperatures (600 and 1000 °C), PVP, and preceramic particle loading. The resulting membranes had porosity of 33–47 %, SSA of 4–473 $m^2.g^{-1}$, and pore sizes of 1–10 μm. Incorporating particles improved slurry processability, mechanical flexural resistance (20–48 MPa), and reduced average pore size. The membranes possessed hydrophobic surfaces at 600 °C, with water contact angles of 128°, and hydrophilic surfaces at 1000 °C pyrolysis. In PDCs, particularly derived silicon-based precursors such as siloxanes, carbosilanes, and silazanes, a lower pyrolysis temperature often results in a very high SSA due to transient microporosity. However, the surface tends to be hydrophobic due to residual hydrogen. The pyrolysis temperature not only tailors the microstructure but also influences water affinity and surface chemistry. It is important to note why some PDCs are hydrophilic while others are hydrophobic. The porosity and the amount of residual hydrogen from the organic precursor play a key role in defining these properties. A lower pyrolysis temperature can lead to transient microporosity and a higher residual hydrogen content, making the surface more hydrophobic. In contrast, higher pyrolysis temperatures tend to reduce hydrogen content and modify the surface chemistry, potentially increasing hydrophilicity [252,253].

Water flux performance, evaluated under different pressures (1–3 bars), directly correlated with pore size and porosity, with 6 to 55 LMH fluxes. Compared to commercial borosilicate glass (8 LMH at 3 bar), mullite (7–40 LMH at 3 bar), and Al_2O_3 membranes (23 and 37 LMH at 2 bar), the polysiloxane-based membranes performed better. PDC-based membranes offer lower production costs and the ability to tailor surface characteristics through single-step pyrolysis.

For microfiltration applications [241], Fontão et al. developed porous ceramer and SiOC composites using a 1:1 mixture of commercial methyl/phenylmethyl polysiloxanes as the preceramic precursor, combined with xylene as a solvent, imidazole as a crosslinking agent, micron-sized SiC, and nanofillers TiO_2. Azodicarbonamide served as the pore former. The resulting slurry was cast onto a PET carrier film, and a doctor blade was applied. The cured tapes were then pyrolyzed at temperatures between 600-1000 °C under a N_2 atmosphere for 4 h. Sponge-like structured membranes with spheroidal pores had an average pore size ranging from 0.3 to 1.4 μm, and porosities between 30-40 %. High SSA of up to 200 $m^2.g^{-1}$ was achieved for tapes pyrolyzed at 600 °C, but these values decreased to as low as 10 $m^2.g^{-1}$ at higher

temperature thermal treatment. The pore size and maximum strength (σ_{max}) increased from 15 ± 5 MPa to 35 ± 5 MPa with higher pyrolysis temperatures. Water permeation and oil-in-water emulsion filtration performance were tested using a homemade dead-end setup. A linear relationship was observed between water flux and applied pressure, with higher pressures resulting in higher permeation fluxes. Larger pore sizes led to lower mass transfer resistances and higher permeation rates, with pure water fluxes ranging from 2.5 to 370 LMH at 2 bar. Lower flux values for samples pyrolyzed at 600 °C were assigned to their more hydrophobic nature. Oil removal efficiencies ranging from 81 to 98 % were achieved at an initial oil concentration of 1000 mg.L^{-1}, evidencing the potential of these PDC membranes for treating oily wastewater. Incorporating TiO_2 could impart self-cleaning properties to the membranes under appropriate light conditions, potentially reducing membrane fouling, a significant challenge in membrane applications.

A multi-scale porous SiCN-based ceramic membrane was developed by integrating shaping and coating techniques with a single preceramic poly(vinyl)silazane (PVS), followed by pyrolytic transformation, summarized in Fig. 9A [254]. The fabrication involved three primary stages: (*i) A sacrificial filler approach produced a macroporous support formation planar-disc configuration*. Poly(vinyl)silazane was blended with polyethylene particles, then cast, cross-linked, and pyrolyzed at 800 °C for 4 h, resulting in discs with a diameter of 13.5 mm and thickness of 2.5 mm. (*ii) Intermediate layer deposition;* an intermediate layer was applied via dip-coating using a slurry composed of uncured PVS, pyrolyzed PVS-derived particles, and tolüene as solvent in weight ratio of 8:32:60. After coating, samples underwent another pyrolysis at 800 °C, and (*iii) Microporous Selective Layer Formation;* a selective layer with average pore sizes of 0.8 nm was dip-coated onto the intermediate layer and pyrolyzed at 600 °C to induce microporosity. The membrane's performance for gas separation was tested by measuring single-gas permeance at temperatures up to 500 °C for a variety of gases (He, N_2, Ar, C_2H_6, and CO_2). At 500 °C, the membrane established He/N_2 and He/CO_2 selectivities of 3.1 and 4.1, respectively, with He permeance reaching 3 × 10^{-8} mol.m^{-2}.Pa^{-1}.s^{-1} (can be seen in Fig. 9B).

The dip coating process enhances wetting and ensures an even spread of the precursor solution across the substrate. This controlled method enables the formation of uniform and continuous ceramic membranes, minimizing defects and irregularities. The support structure plays a critical role in the performance and efficiency of composite membrane separation layers. Choosing a suitable support material is essential as it significantly affects the membrane's functionality and separation properties. The support provides a stable foundation for the active separation layer, with its mechanical properties impacting the composite membrane's integrity and durability. On the other hand, the design of the intermediate layer is crucial in preventing the penetration of the coating solution into the support layer, thereby enhancing the separation layer's quality [255].

SiOC ceramic composite nanofiltration membranes [242] were synthesized using a dip-coating approach. The synthesis involved preparing a PCS solution to form the coating suspension for the separation layer and preparing a ZrO_2 to SiO_2 intermediate layer. The substrate (α-Al_2O_3/TiO_2/black talc with 62 vol% porosity and an average pore size of 6.3 μm) was dip-coated with the suspension. The samples were then dried and subjected to pyrolysis (at 700 °C, under N_2 atmosphere), resulting in SiOC separation layers with a 1.05-2.38 μm thickness. The SiOC ceramic composite membranes exposed compressive strength of approximately 30 MPa and water contact angles between 78° and 88°. Hydrophilicity significantly influences membrane flux, with weaker hydrophilicity potentially reducing flux. Notably, the SiOC membrane with a contact angle of 78° achieved a flux of ~22 LMH/bar and a dye rejection rate of 90 %. In comparison, a less hydrophilic SiOC membrane (contact angle of 88°) indicated the highest flux of ~3 LMH/bar and high dye rejection rate of 96 %. These membranes maintained stable water flux for at least 24 h, indicating good long-term stability during cross-flow filtration.

Guo et al. [247] fabricated SiOC film ceramic membranes with tunable pore structures by dip-coating polysiloxanes onto yttria-stabilized ZrO_2 (YSZ) hollow fiber substrates, followed by cross-linking and pyrolysis at 800 °C for 1 h in an Ar. The precursors used were PHMS and D_4Vi siloxane, while linear methyl-terminated PDMS and silicone S184 served as sacrificial fillers (in weight ratios of 1:2, 2:2, and 3:2, and 30-50 wt% relative to the precursors). The resulting SiOC film, approximately 15 μm thick, had a pore size range of 50 nm to 2 μm and a porosity of 35–40 %, achieved by varying the pore-forming agents. The corrosion resistance properties of the SiOC layers were also investigated. The SiOC-coated fiber membranes manifested a high corrosion resistance, with only a 0.07 wt% weight loss in a 20 wt% H_2SO_4 solution. This exceptional resistance to chemical corrosion is due to the unique SiOC micro-lattice structures, which provide significant chemical durability. Compared to Al_2O_3 hollow fiber substrates (1.25 wt%) [256] and cordierite membranes (17.0 wt%) [257], the SiOC film-coated YSZ membranes had significantly lower weight loss during the chemical corrosion test.

Hydrophilic SiOC and hydrophobic SiOC-palladium ceramic nanofiber membranes were fabricated using electrospinning [248]. PCS and PS were used for the spin solution, stabilized by curing at 210 °C, and pyrolyzed at 1100 °C in Ar. The hydrophobicity was achieved by incorporating trace amounts (0.2-0.5 wt%) of palladium. The resulting SiOC-palladium membranes revealed high hydrophobicity with a water contact angle reaching 137°, whereas the neat SiOC membrane was hydrophilic. Chemical resistance tests revealed that the fibrous structure remained intact and flexible after immersion in basic (KOH) and acidic (H_2SO_4) solutions at 80 °C for 36 h. Moreover, the SiOC-palladium membranes retained their hydrophobicity across the entire pH spectrum. The fibrous membranes possessed robust mechanical properties, with a tensile strength of 6.5 ± 1.0 MPa and a modulus of 302 ± 43 MPa. Flexural property tests involving repeated specimen bending (300 times) confirmed excellent flexural behavior (see Fig. 10).

Amorphous SiOC and SiCN membranes [157] were deposited as thin

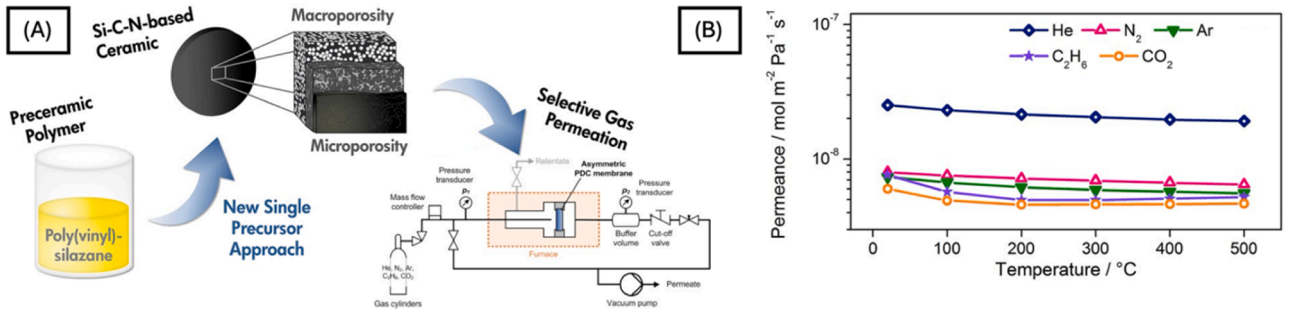


Fig. 9. **(A)** Schematic of the asymmetric poly(vinyl)silazane-derived ceramic membrane design & experimental setup for single-gas permeance testing up to 500 °C, using the constant-volume variable-pressure technique, and **(B)** Gas permeance characteristics of the asymmetric poly(vinyl)silazane-derived ceramic membrane as a function of test gas. (Reproduced from [254], with permission Elsevier, Copyright 2016).

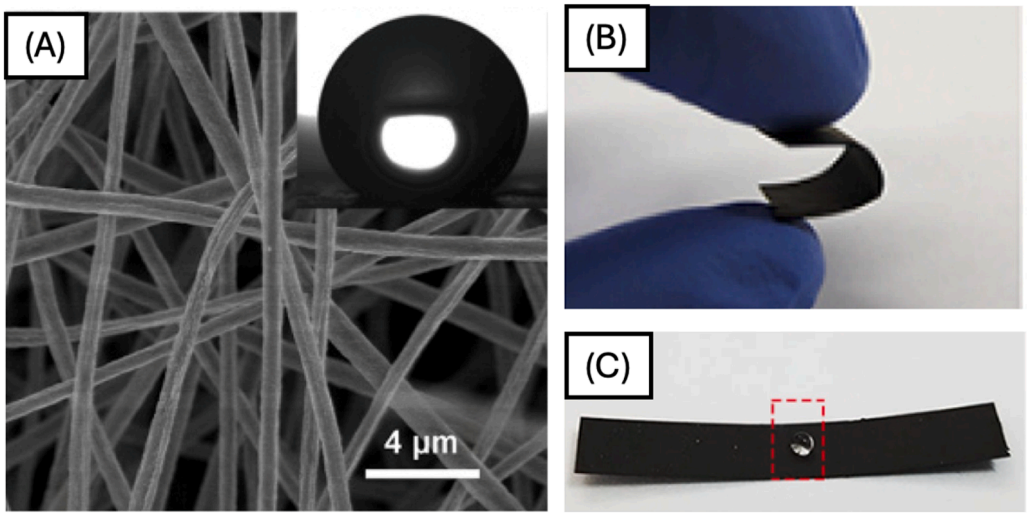


Fig. 10. **(A)** SEM images and the corresponding wetting behavior of SiOC-palladium ceramic nanofiber membrane, **(B)** The flexibility of SiOC-palladium ceramic membrane, and **(C)** Digital photo of the SiOC-palladium ceramic membrane after bending 300 times. (Reproduced from [248], with permission Elsevier, Copyright 2017).

layers by dip-coating tubular asymmetric porous Al_2O_3 ceramic substrates with intermediate layers of γ-Al_2O_3 or ZrO_2. At room temperature, the SiOC membrane had an H_2 permeance of 0.56 $m^3/(m^2.h.bar)$. When the temperature increased to 300°C, the permeance improved to 49.8 LMH, with ~10 perm selectivity for H_2/CO_2 and ~100 for hydrogen/propane (C_3H_8). In contrast, the SiCN membrane displayed a very low H_2/CO_2 ideal perm selectivity of 4.6. Interestingly, both systems hold high H_2/Sulfur hexafluoride (SF_6) perm selectivity, with values of 320 for SiOC and 103 for SiCN, indicating the absence of defects, suggesting that separation is primarily based on molecular sieving.

Prasad et al. [240] explored the hydrogen separation performance at high temperatures of a microporous SiOC membrane. Diluted vinyl-functionalized polysiloxane in anhydrous toluene (40 vol%) was a precursor. Monochannel α-Al_2O_3 tubes (with a pore size of 3 mm) served as supports with an intermediate γ-Al_2O_3 layer (pore size of 5 nm) located on the inner wall of the tube for the deposition of SiOC membrane. The SiOC ceramic layer was deposited as a thin membrane (~300 nm thick after three gradient precursor coatings and pyrolysis at 700 °C for 1 h in Ar) on a tubular porous γ-Al_2O_3/α-Al_2O_3 substrate. The resulting SiOC membranes ($Si_1O_{1.06}C_{1.15}$) had an SSA of ~400 $m^2.g^{-1}$. Photograph and SEM image of SiOC coated on the Al_2O_3 substrate can be seen in Fig. 11.

Single gas permeance characterization for H_2, CO_2, CH_4, and SF_6 yielded permeance values of 1.8×10^{-8} (for H_2) to 5.6×10^{-11} (for SF_6) $mol.m^{-2}.s^{-1}.Pa^{-1}$, with ideal permselectivities of H_2/CO_2 (9.1), H_2/N_2 (22.4), H_2/CH_4 (22.9), and H_2/SF_6 (320) at 300 °C. The ideal permselectivity for H_2/SF_6 due to the very low permeance of SF_6 is explained by the defect-free SiOC membrane. Additionally, the calculated activation energies of H_2 permeation for the SiOC membrane were lower than those for SiO_2 membranes. This lower activation energy indicates that the SiOC membrane possesses a different pore structure compared to SiO_2, allowing easier passage of H_2 molecules.

Similar to the previous work, SiOC membranes were fabricated using porous α-Al_2O_3 tubes with a total porosity of 50 % and an average pore size of 1 μm, incorporating a SiO_2−ZrO_2 intermediate layer for gas separation applications [249]. The SiOC membrane solution was prepared via the sol-gel method using silicon precursors such as vinyltrimethoxysilane, triethoxysilane, and 1,1,3,3-tetramethyldisiloxane. The top layer was formed by coating with the SiOC sol, followed by pyrolysis at 500−800 °C for 30 min under N_2. The influence of pyrolysis temperatures on the SiOC network structure and gas permeation properties was examined. Oxidative stability was assessed by measuring gas permeance over time during air treatment at 500 °C. The SiOC membrane pyrolyzed at 700 °C retained high selectivities for larger molecule separation (H_2/Carbon tetrafluoride (CF_4): 640, H_2/SF_6: 2900, N_2/CF_4: 98) and lower permeances for CH_4, CF_4, and SF_6 compared to the membrane pyrolyzed at 500 °C, got a high H_2 permeance of 9×10^{-7} $mol.m^{-2}.s^{-1}.Pa^{-1}$ and selectivities of H_2/N_2: 6, H_2/CF_4: 240, and H_2/SF_6: 1400. A membrane pyrolyzed at 800 °C had an H_2/N_2 selectivity of 62, approximately 10 times higher than that the sample pyrolyzed at 700 °C, due probably to the densification of SiOC networks via cleavage and redistribution reactions of Si−C and Si−O groups.

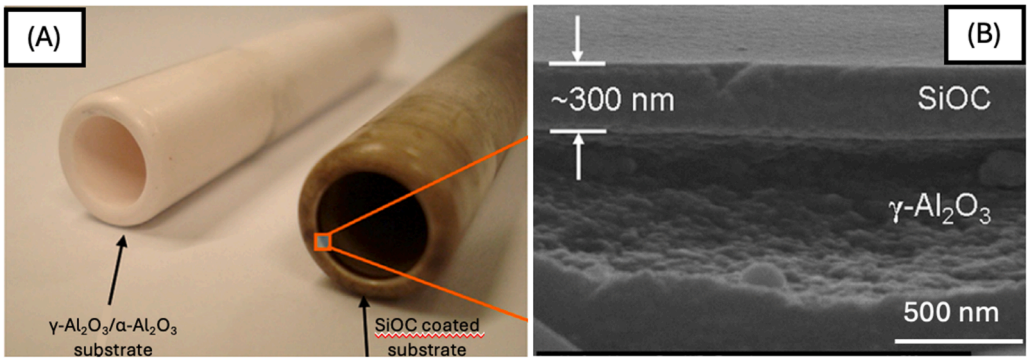


Fig. 11. **(A)** Photographs of the porous Al_2O_3 and SiOC-coated Al_2O_3 substrates **(B)** SEM image of the cross-section of SiOC-coated Al_2O_3 membrane. (Reproduced from [240], with permission John Wiley and Sons, Copyright 2015).

A novel selective laser printing process was used to create high-flux ceramic membranes for water and gas filtration [239]. The method began with crosslinked and ground polysiloxane powder prepared with a peroxide catalyst at 180 °C for 4 h. After pyrolysis at different temperatures (1000–1600 °C), this polymeric powder transformed into SiOC ceramics containing oxygen (3-21 wt%). The phenolic resin was added to the powder mixture and ball-milled for 4 h. The mixture was then laser-printed to form green bodies extracted from the mold. These green bodies underwent pyrolysis at 900 °C in an Ar atmosphere to convert the phenolic resin into pyrolytic carbon. The debonded bodies were then vacuum-impregnated with a polysiloxane precursor solution and further pyrolyzed. The study explored how sintering temperature affects the microstructure, mechanical properties, and filtration performance of SiOC ceramic membranes. It was found that water flux increased with rising porosity and pressure. Membranes pyrolyzed at 1600 °C exposed the highest porosity (42 vol%) and water flux (24.4 LMH) compared to other samples, achieving a gas flux of 2769 LMH. As sintering temperatures increased from 1000 to 1600 °C, both porosity (35 % to 42 %) and permeability rose, but flexural strength declined from 27 MPa to 18 MPa.

A SiOC membrane was fabricated on a Si_3N_4 substrate using multiple spin-coating steps [243]. The preparation involved mixing the precursor polymer (PHMS), with the crosslinking agent (TMTVS) in a 1:1 mass ratio, and a platinum catalyst. This mixture was then spin-coated onto the Si_3N_4 membrane and cured at 80-120 °C for 12 h. The cured gel was subsequently pyrolyzed at temperatures ranging from 500-1000 °C in an Ar atmosphere for 3 h. The resulting amorphous SiOC ceramic membrane, approximately 1.8 μm thick, yielded strong adhesion to the Si_3N_4 substrate. The membrane had stable H_2 permeation of 3.26×10^{-8} mol.m^{-2}.Pa^{-1}.s^{-1}, significantly higher than CO_2 permeation of 1.61×10^{-9} mol.m^{-2}.Pa^{-1}.s^{-1}. Single gas permeation tests revealed an ideal H_2/CO_2 selectivity of up to 20 at 25 °C and 5 bar, outperforming the Knudsen diffusion selectivity of 4.69, indicating that the SiOC membrane had good molecular sieving ability. These results indicate strong molecular sieving ability, because of the compatibility between SiOC and Si_3N_4, as well as the formation of robust chemical bonds at the interface. This performance, combined with good long-term stability, emphasizes the potential use of the membrane in hydrogen purification applications.

SiC-based membranes possess significant promise in separation processes due to their superior structural stability, mechanical strength, corrosion resistance, and durability at high temperatures [251, 258–262].

Studies by Wang et al. explored SiC membranes fabricated using different preceramic polymers, such as PCS, allyl-hydrido-PCS, and poly-titano-carbosilane, applied onto porous Al_2O_3 substrates [259,261, 262].

The preparation involved coating the Al_2O_3 tube surface, creating an intermediate layer to reduce defects, and applying a preceramic polymer solution, followed by curing and pyrolysis.

The relationship between single-gas permeance and pyrolysis temperature for SiC membranes was investigated [261]. For example, a polymeric membrane with a pore size of 0.61 nm, pyrolyzed at 350 °C, exhibited H_2 permeance of 5.87×10^{-7} mol.m^{-2}.Pa^{-1}.s^{-1} and an H_2/N_2 selectivity of 9.5. The dense polymer network, rich in organic groups, was responsible for the high selectivity but limited gas permeance due to increased steric hindrance. For ceramic membranes (750 °C, pore size 0.50 nm), the structure became denser with narrower pores due to rearrangement reactions during densification. Increasing the pyrolysis temperature from 350 °C to 750 °C improved gas permeance but reduced selectivity, with H_2 permeance rising to 1.95×10^{-6} mol.m^{-2}.Pa^{-1}.s^{-1} and H_2/N_2 selectivity decreasing to around 7. These membranes also had superior selectivity for N_2 over larger molecules like SF_6 or CF_4, indicating fewer defects. On the other hand, the separation of methyl acetate and CH_3OH via membranes presents a challenging task, as the membrane must withstand harsh solvents while maintaining good flux and selectivity. The study also examined SiC membranes for pervaporation, particularly for CH_3OH removal from organic solvents. The membrane displayed higher permeance during pervaporation than in single-gas permeation due to network swelling, which increased the membrane's free volume and pore size. However, this swelling negatively impacted selectivity. While the CH_3OH/toluene selectivity for the polymeric membrane was 0.72, the ceramic SiC membrane with a 0.50 nm pore size achieved a selectivity of 189. In pervaporation, the permeance of SiC ceramic membranes decreased as the solvent molecular size increased, paralleling the trend in single-gas permeation. This similarity suggests that the separation mechanism in pervaporation through these membranes is primarily driven by molecular sieving, much like single-gas permeation.

Allyl hydrido PCS-derived ceramic SiC membranes prepared at temperatures ranging from 300 to 800 °C with different pore structures displayed excellent gas permeation properties and good oxidation resistance at 500 °C under air [259]. SEM images of membranes pyrolyzed at 700 °C revealed a thin, crack-free, continuous separation layer of about 200 nm, deposited onto an intermediate layer (given in Fig. 12A**-B)**. Ceramic SiC membranes prepared at 700 °C had promising H_2 permeance, ranging from 2 to 4×10^{-6} mol.m^{-2}.Pa^{-1}.s^{-1} at 200 °C, with H_2/N_2 selectivity between 16 and 22, and H_2/SF_6 selectivity exceeding 10,000.

The permeation properties of H_2, N_2, and SF_6, as well as the H_2/N_2 and H_2/SF_6 selectivities, were influenced by pyrolysis temperature, see Fig. 12C. As the temperature increased from 300 to 800 °C, both H_2 and N_2 permeance initially increased and then decreased, whereas H_2/N_2 selectivity indicated an inverse trend. This suggests that the effective permeable pore structure expanded and then shrank as the temperature rose.

The development of Ti-incorporated porous SiC-based membranes for pervaporation separation was reported by Wang et al. [262]. The membranes, prepared at 750 °C pyrolysis, proved good selectivity for separating water or CH_3OH from liquid mixtures. The addition of titanium increased the molecular weight and prevented the collapse and densification of micropores during the pyrolysis process. The Ti-incorporated porous SiC membranes were tested at 50 °C for dehydrating water and separating CH_3OH in mixtures of CH_3OH, C_2H_6O, acetone (C_3H_6O), isopropyl alcohol (IPA), and methyl acetate (with a 10 wt% concentration of H_2O or CH_3OH). As the molecular size of the solvents increased (H_2O: 0.29 nm, CH_3OH: 0.38 nm, C_2H_6O: 0.43 nm, C_3H_6O: 0.47 nm, IPA: 0.47 nm, and methyl acetate: 0.48 nm), their permeance decreased, resulting in a significant rise in the separation factors for each system. For example, the separation factors were approximately 2.3 for H_2O/ CH_3OH, 48 for H_2O/C_2H_6O, 109 for H_2O/C_3H_6O, and 216 for H_2O/IPA. A similar trend was observed for CH_3OH removal, with CH_3OH permeance remaining consistent across all mixtures, while the permeance of other solvents decreased as their molecular size increased. The separation factors for CH_3OH/C_2H_6O and CH_3OH/IPA were 4 and 14.6, respectively.

2.2.3. *Metal filtration*

Impurities in metals and alloys weaken mechanical properties, damage surfaces, increase porosity, and elevate corrosion risk. Nonmetallic impurities, serving as stress points, may affect early failure. The size, shape, type, and distribution of these inclusions impact the quality of the finished product. Accordingly, metal melt filtration is employed in the casting industry to separate impurities such as slag residues, foundry sands, and trapped gas bubbles from the molten material to obtain uniform and quality products [263]. Three filtration mechanisms are seen in the process of filtering molten metals: *i)* macro filtration or sieving where particles larger than filter openings are trapped, *ii)* filtration through a layer formed by trapped inclusions at the filter entrance capturing more minor inclusions than the pores, and *iii)* filtration throughout the entire filter volume via its openings and channels [264]. Moreover, the molten metal flow types can typically be categorized as follows during the filtering: *Turbulent Flow*: characterized

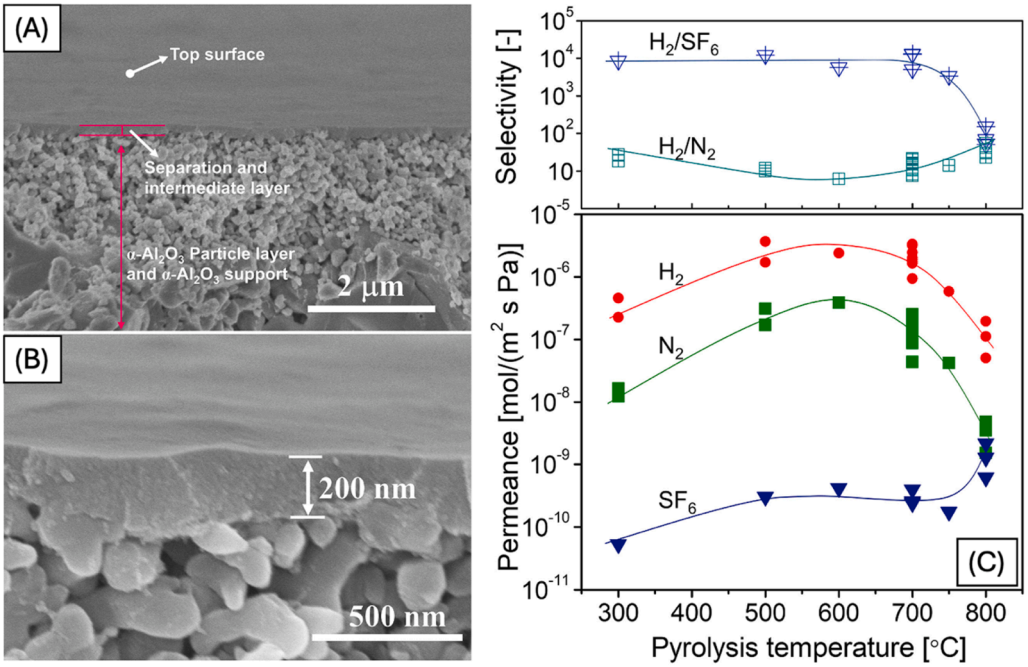


Fig. 12. **(A-B)** SEM image of cross-section of SiC coated Al_2O_3 membrane, and **(C)** Relationship between the gas permeation performance at 200°C of SiC membranes and the pyrolysis temperature (Reproduced from [259], with permission Elsevier, Copyright 2020).

by chaotic changes in pressure and velocity, causing irregular movement and potential defects in cast components due to turbulence and impurity mixing. *Laminar Flow:* involves smooth, orderly movement of molten metal in parallel layers with minimal disruption, ideal for reducing turbulence and defects in casting. *Transitional Flow:* An intermediate state between laminar and turbulent flow, featuring characteristics of both. It occurs under conditions where neither flow type can be exclusively maintained, influenced by factors like velocity and viscosity. Foam filters promote laminar flow, thereby enhancing casting quality and strength while reducing defects by converting turbulent flow to laminar flow [265].

Numerous companies globally produce molten metal filters in large volumes and various shapes and compositions. The filter material must be non-reactive with the metal, highly resistant to thermal shock, have high open porosity, and be mechanically stable. Cellular ceramics are preferred materials in metal casting processes. These filters are available in several forms (pressed, extruded, and foam) [266] and are extensively used, particularly in aluminum casting, cast iron, and other metals.

While detailed information on types and production methods of cellular ceramics is available in various publications [267–270], here we briefly mention pressed, extruded, and foam processing. Sieves and pressed filters are created by compacting damp ceramic powder. Paste composed of ceramic powder and water is applied for filters made through extrusion. Pore formers such as PVA beads are mixed into the paste to introduce porosity. The paste is then extruded into rods, where the pore-forming beads elongate within. On the other hand, ceramic foams are manufactured using the replica technique in which ceramic slurry is impregnated onto an organic scaffold, which is subsequently eliminated via firing, resulting in a porous ceramic structure. Utilizing open-cell PU foam as the scaffold in cellular filters grants good filtration capability due to its distinct, tailorable pore structure, which enables an indirect flow of metal melt. By adjusting the pore size and relative density of PU foam, ceramic replica filters can be customized to eliminate diverse contaminants, making them a preferred choice [271]. These foams are commercially found with typical cell sizes ranging from 10 to 60 PPI, being a significant utility in molten metal filtration applications, such as Al_2O_3, SiC, Carbon, and Mullite for cast iron, Al_2O_3, and mullite for a, and ZrO_2 and mullite for molten steel [263,272]. For instance, photographs of the ceramic foam filters (10 PPI) made of different materials (Al_2O_3, ZrO_2, SiC, and Al_2O_3–C) are shown in Fig. 13. A key advantage of PDC foams is that in some cases, the struts are not hollow. In contrast, foams obtained through slip powder processing have hollow structures, as the region where the parent PU foam was present leaves a void after decomposition. The processing technique results in foam with both hollow and dense struts [225], depending on the manufacturing step, rather than primarily having reticulated hollow struts.

Cellular ceramics, particularly ceramic foams, are widely exploited in industries for metal filtration. Ceramic foams produced via the PDCs route have been tested for molten metal filtration in only one publication. However, using ceramic foams produced via the PDC route for molten metal filtration is relatively unexplored, with only one documented work. This indicates a promising area for future research to develop further and optimize these materials for industrial use. The study reported [265] the synthesis and performance of PDC filters for molten metal filtration. SiOC and SiOC(N) foam filters were produced using flexible PU foam and 3D-printed PU templates, respectively. Both types of filters used a urethane-based polymeric template impregnated with a preceramic solution, followed by pyrolysis (1000-1200 °C). SiOC and SiOC(N) ceramics were then used to filter a molten Al alloy (A357). The casting system and tested ceramic filter with SEM images are given in Fig. 14.

The filtered Al samples were then mechanically tested. According to the results, filters improved the reproducibility and reliability of mechanical properties such as yield strength (190-205 MPa), ultimate tensile strength, and elongation at fracture. SiOC foam filters (with 4039 ± 313 μm cell size and ~ 35,000–37,000 $m^2.m^{-3}$ volumetric surface area) outperformed 3D-printed-SiOC(N) ceramic filters (having uniaxial channels of 1040 ± 66 μm and ~ 14,000–18,000 $m^2.m^{-3}$), likely due to their three-dimensional interconnected porosity and higher volumetric SSA. The foam structure is known to facilitate laminar flow. This means that the critical velocity of the molten metal increases by reducing turbulence, which helps prevent surface defects during casting and results in cast metal components with improved strength.

2.2.3.1. Panel: membranes. Inorganic non-metallic solid membranes are thin filters, commonly below 5 mm, typically made using oxides such as

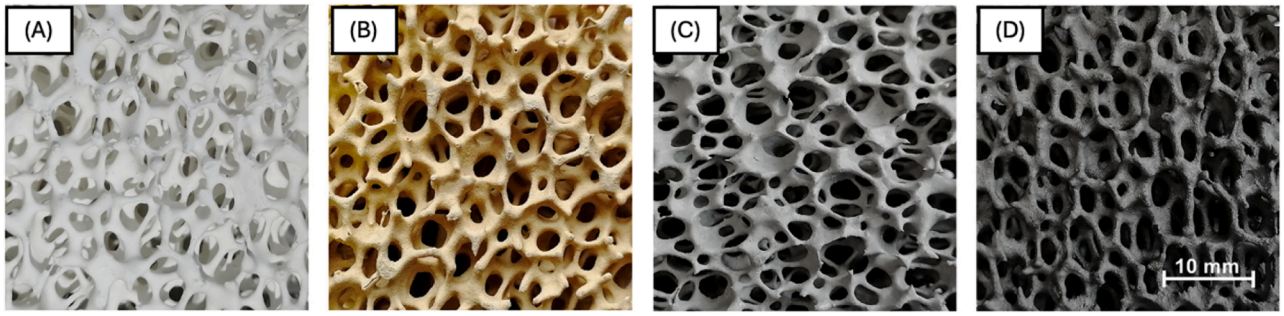


Fig. 13. Photographs of the ceramic foam filters (10 PPI) fabricated from different materials **(A)** Al_2O_3, **(B)** ZrO_2, **(C)** SiC, and **(D)** Al_2O_3–C. (Reproduced from [273], with permission John Wiley and Sons, Copyright 2021).

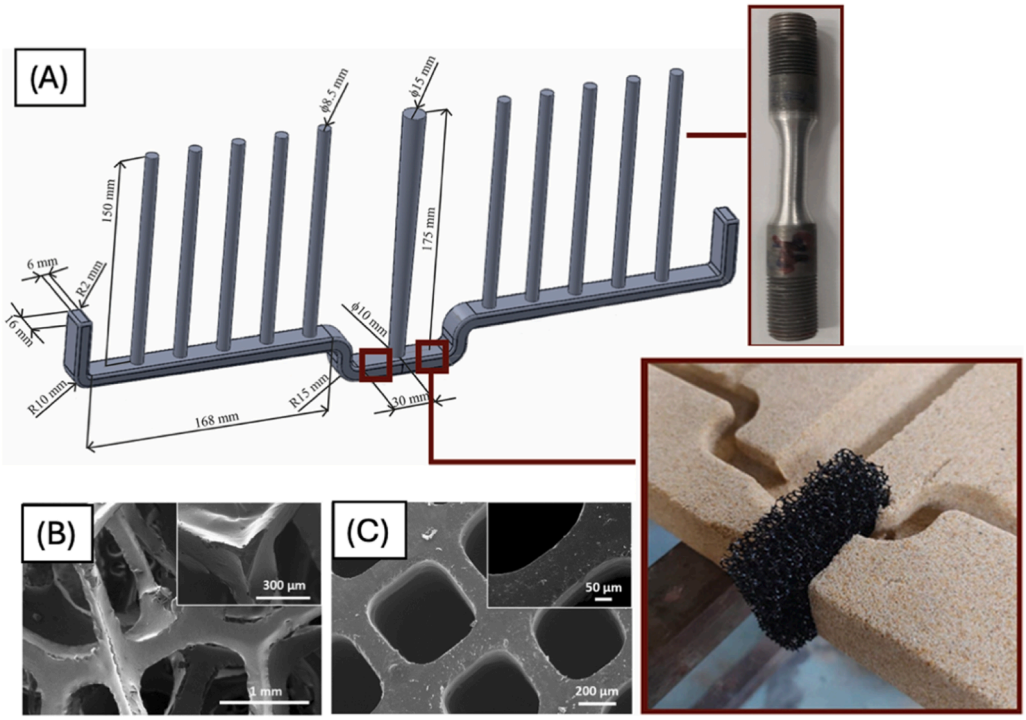


Fig. 14. **(A)** SolidWorks drawing of casting system including digital photos demonstrating the real position of the tested ceramic filter (bottom right) and example sample prepared after casting for the mechanical test (top right), SEM images of **(B)** SiOC foam ceramic filter produced via replica technique, and **(C)** 3D printed SiOC (N) cellular structure. (Reproduced from [265], with permission Springer Nature, Copyright 2022).

Al_2O_3, Zr_2O_4, or TiO_2, as well as carbides like SiC. A ceramic membrane usually has a total porosity between 30–50 vol% with a pore size (microfiltration membrane if the pore size is 0.1 to 10 µm, ultrafiltration membrane if it is between 1 to 100 nm, and nanofiltration if pores are below 2 nm), and topology allowing selective filtration of particles, molecules, or ions based on size or charge, commonly used in industries requiring high stability and resistance to harsh operating conditions.

Apart from many other characteristics, membrane mechanical strength and wear resistance depend heavily on the application. For example, high abrasion resistance is particularly required in applications where membranes are exposed to particulates, which may wear down the membrane surface, as in the case of wastewater treatment. High compressive strength is required when a membrane is to be used for high-pressure applications such as the ones in high-pressure membrane bioreactors, gas separation in petrochemical and natural gas processing, and reverse osmosis for water desalination. However, in most other applications, other properties became important instead of mechanical strength, such as for biomedical and pharmaceutical, where sterility and chemical resistance are crucial, and for the food and beverage industry, where purity and flavor preservation are important.

PDC membranes have already been produced and tested for several different applications. For example, the SiOC membrane was prepared using the phase inversion technique. The resulting samples had a total porosity from 30 to 50 %, with SSA ranging widely from 4 to 473 $m^2.g^{-1}$ and pore sizes between 1 and 10 µm [246]. In terms of mechanical performance, these membranes exhibited flexural strength reaching ~50 MPa. The authors claimed that the produced samples can be promising candidates for water purification applications.

SiOC composite nanofiltration membranes were manufactured using a dip-coating method, forming thin SiOC separation layers with thicknesses ranging from 1.05 to 2.38 µm [242]. Although porosity characteristics were not explicitly reported, these membranes had a compressive strength of ~30 MPa, i.e., a reasonable level of structural integrity. Water flux rates ranging from 3 to 22 LMH/bar and a dye rejection efficiency of up to 96 % were presented, they make the membranes highly effective at removing dye molecules from wastewater. Moreover, the membranes could maintain stable flux for over 24 h, underlining their potential for long-term use. In another work, SiOC

fibrous membranes, formed using electrospinning, yielded a tensile strength of 6.5 MPa and a modulus of 300 MPa [248]. Flexural testing (up to 300 bending cycles) indicated their flexibility and durability. The authors suggested that these membranes were well-suited for flexible filtration systems, especially where mechanical resilience and repeated stress endurance are essential.

Sponge-like SiOC membranes with spheroidal pores were developed, featuring total porosity levels between 30 % and 40 % and pore sizes ranging from 0.7 to 1.4 μm [241]. The mechanical strength of these membranes ranged from 28 MPa to 38 MPa. For microfiltration applications, the PDC membranes had sufficient flexural strength, comparable to various ceramic membranes for microfiltration reported in the literature, despite being sintered at lower temperatures (see Fig. 16). Filtration tests results expressed that water permeation rates reaching 370 LMH at 2 bar, along with oil-in-water emulsion filtration efficiencies of 98 %. The distinctive sponge-like structure and high water flux performance make these membranes especially suitable for oily wastewater treatment, combining high permeability with effective oil removal.

In the other work, neat and Pd-doped SiOC fibrous membranes were created through a combination of electrospinning and heat treatment, as shown in Fig. 15A-**B** [274]. The mechanical properties of the membranes were significantly enhanced by the in situ incorporation of palladium nanoparticles into the SiOC fibers (detailed in Fig. 15C). Increasing the palladium content reduced the pore diameter from 18.1 to 11.2 nm and increased the SSA from 30 to 52 $m^2.g^{-1}$. The neat and Pd-doped SiOC fibrous membranes entailed a flexural modulus of 2.23–7.79 kPa, tensile strength of 0.5–33.2 MPa, and an elastic modulus of 289–618 MPa. The filtration performance was measured with an airborne particle counter, marking 99.6 % efficiency for smaller particles and achieving 100 % efficiency for particles larger than 5 μm, with excellent corrosion resistance. These results suggest that durable PDC-SiOC fibrous membranes are well-suited for filtration applications in corrosive environments.

Selective laser printing was used to fabricate SiOC ceramic membranes with total porosities up to 42 % [239]. By tuning the microstructure and altering the total porosities, they achieved flexural strengths ranging up to 27 MPa. Additionally, water flux rates increased with higher porosity and applied pressure, indicating an adaptable approach to improve filtration performance as required. The work marks the potential of 3D-printed membranes for water and gas filtration applications, where high flux can be prioritized alongside moderate mechanical strength.

SiOC ceramic membranes [195] with total porosities reaching 65 vol % and an average pore size of 0.59 μm effectively removed oil droplets from water, and had a 95 % rejection rate. However, no mechanical properties were given.

Hydrophobic-oleophilic Si_3N_4 nanobelts with interconnected porosity (> 95 %) were obtained by impregnating preceramic siloxane resin into polyurethane foam and performing pyrolysis at 1500°C in an N_2 atmosphere [275]. The produced nanobelts selectively absorb pump oil and effectively separate it from water. Oil impregnation led to a weight increase of up to 2500 %, with over 90 % of the theoretical oil capacity filled. The oil can be easily removed from Si_3N_4 by heating to 600°C.

The relationship between microstructural (pore size and total porosity) and mechanical properties for different types of inorganic non-metallic solid membranes was analyzed and plotted in Fig. 16. Fig. 16A provides an overview indicating that membranes generally have total porosities between 20–60 vol%, with PDC-derived membranes displaying similar characteristics. Also, the pore distribution plot (Fig. 16B) indicates that membrane pore sizes range from the micron scale (suitable for microfiltration) down to the nanometer scale (ultrafiltration and nanofiltration). Fig. 16B also marks that PDCs offer the broadest range of pore sizes compared to the other materials.

The versatility in processing routes enables the design of PDC membranes with targeted porosity, mechanical strength, and surface properties. These materials show clear advantages in chemical resistance, flow stability, and application-specific tunability, particularly in oily wastewater treatment, dye removal, and desalination. The membranes exhibit strong mechanical performance, with flexural strength up to 50 MPa and stable operation under harsh conditions. Their application in water treatment has shown high efficiency, including up to 99.9 % salt rejection, 98 % oil removal, and 96 % dye rejection [156,241,242]. In gas separation, PDC membranes demonstrated high selectivity (e.g., $H_2/SF_6 > 2900$) and stable performance at elevated temperatures. Overall, PDC membranes stand out as multifunctional, durable, and scalable materials for next-generation filtration technologies, though greener production processes and long-term validation remain key future challenges. Future work should focus on scale-up, emission reduction in production, and long-term field performance validation.

2.3. Catalytic activity

Reactions facilitated by catalysts can be categorized as homogeneous or heterogeneous. In homogeneous catalysis, all reactants and the catalyst are in the same phase. In contrast, in heterogeneous catalysis, the catalyst is typically in the solid phase, while the reactants are in the liquid or gas phase. Accordingly, PDC catalysts can be considered an example of heterogeneous catalysis [145], where the reactants are in different phases. Although heterogeneous catalysts offer the advantage of easy separation and reuse due to phase differences, their activities may be low. The structure of the material plays the most significant role in heterogeneous catalysis [276].

In a broad classification, catalytic activity can be classified into thermocatalytic, photocatalytic, and electrocatalytic reactions based on the energy source used: heat, ultraviolet (UV) or visible light, and electrical energy, respectively. All these processes, in fact, are frequently employed in environmental applications to increase reaction rates. It is also commonly used to remediate organic pollutants and gases from water or air, converting them CO_2 and H_2O through oxidation. Several other examples can be found in comprehensive reviews focusing

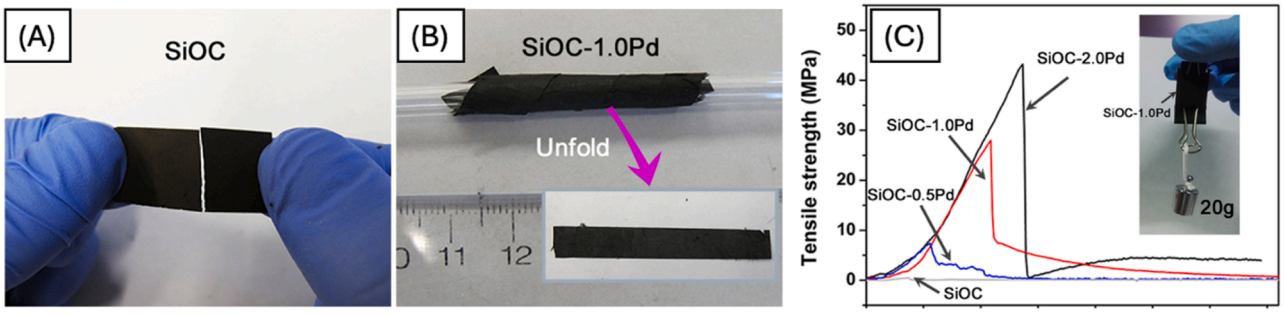


Fig. 15. (A) Digital pictures of bending performance for SiOC membrane and **(B)** Pd-doped SiOC membrane **(C)** Stress-strain curves of SiOC and Pd-doped SiOC membranes. (Inset shows the digital picture of the mechanical property of the Pd-doped SiOC membrane. (Reproduced from [274], with permission John Wiley and Sons, Copyright 2018).

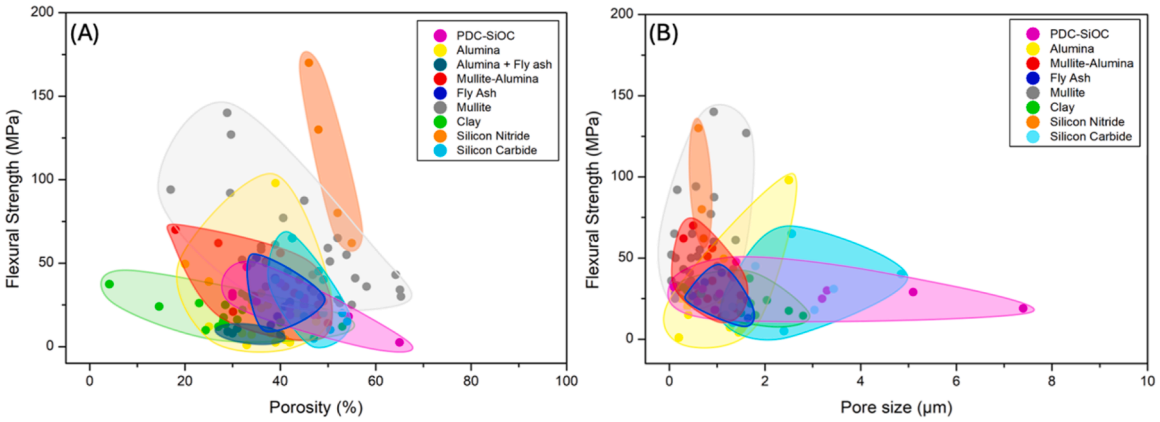


Fig. 16. **(A)** Flexural Strength (MPa) versus Porosity (%) chart, and **(B)** Flexural Strength (MPa) versus Pore size (μm) chart, (the data collected from the published papers).

explicitly on the topic [277–280].

Physical methods like adsorption are employed to remove contaminants from water, but these methods merely transfer chemical pollutants from water to other media, leading to secondary contamination. In contrast, photocatalytic oxidation technology is widely used in wastewater treatment due to its high efficiency and lack of secondary pollution [281].

The mechanism of photocatalytic degradation is as follows: When a semiconductor photocatalyst is exposed to a light source with energy higher than its bandgap, electron-hole pairs (e' as the reducing agent and $h^{\cdot}$ as the oxidizing agent) are generated. These pairs initiate chemical reactions that mineralize contaminants through oxidation and reduction reactions. Holes ($h^{\cdot}$) in the valence band migrate to the photocatalyst surface and react with water to produce hydroxyl radicals (•OH), known as oxidation reactions. Electrons (e') in the conduction band react with oxygen to form superoxide anion radicals, which undergo further reactions to generate hydroxyl radicals, known as reduction reactions. Ultimately, these hydroxyl radicals react with organic pollutants, yielding H_2O and CO_2 as end products [282]. An effective photocatalyst should be biologically and chemically inert, photo-stable, cost-effective, and non-toxic [283].

There are several different photocatalytic materials, including TiO_2, ZnO, iron oxide, tungsten trioxide, copper oxide, cadmium sulfide, bismuth vanadate, ceria (CeO_2), silver halides, and their composites. Such materials are extensively utilized in environmental applications and can be engineered for diverse purposes, including developing self-cleaning surfaces [284], mitigating air pollution [285], and hydrogen or oxygen evolution. In addition, a prevalent application lies in the removal of pollutants, such as phenolic compounds [286] and dyes, from wastewater, facilitating purification processes [287].

Although many research groups have employed photocatalytic degradation to dispose of organic substances, it has rarely been tested for PDCs (given in Table 3). SiOC/TiO_2 and SiOC/N-doped TiO_2 ceramic composites were made via a template-free method, and the samples were tested for MB degradation [203]. SiOC/N-doped TiO_2 ceramic composite, produced by pyrolysis at 700°C for 2h in Ar, displays superior photocatalytic performance (the highest photodegradation rate constant, k, 3.4×10^{-3}.min^{-1}) in comparison to both pure SiOC ceramic and the SiOC/TiO_2 ceramic composite, see Fig. 17.

N-doped TiO_2 was embedded within an amorphous SiOCN matrix to obtain a composite structure. The MB dye and the formed material were kept in dark for 12 h to reach equilibrium, followed by applying visible light. The photodegradation rate constant was calculated to be 8.3×10^{-3} min^{-1}. Additionally, it was observed that the SSA decreased from 186 to 130 $m^2.g^{-1}$ after the adsorption/catalyst experiment [216]. SiOCN/TiN nanocomposite, another novel material obtained by pyrolysis under an ammonia atmosphere and used as a precursor for PHMS, has been investigated for MB degradation [288]. Photodegradation efficiency and its rate constant were calculated 64 % and 4.2×10^{-3} min^{-1}, respectively.

Table 3
PDC-based photocatalyst and catalyst utilization for wastewater treatment and electrocatalytic reactions.

Photocatalysts	*SSA ($m^2.g^{-1}$)*	*Particle/ Pore size (nm)*	*Application*	*Efficiency (%)*	*Refs.*
SiOC/ TiO_2	~300			97	[154]
SiOC/ TiO_2	129	~7	MB Dye	N.A.	[202]
SiOC/TiO_2	254	4	Degradation	N.A.	[203]
SiOC/N-doped TiO_2	336	4		N.A.	[203]
SiOC/ZnO	~400	~4		100	[177]
SiOCN/TiO_2	186	11		N.A.	[216]
SiOCN /TiN	~1	N.A.		64	[288]
SiOCN / ZrO_2	N.A.	4-20			[290]
SiC/ Bi_2WO_6	0.00274	N.A.	RB Dye Degradation	90	[289]
SiOC/ Ni	85-410 1-20	3.0-3.2 6.2-6.4	CO_2 methanation	25	[291]
SiOC/ Ce	15	13-28	CO_2 decomposition	N.A.	[292]
SiOC/VC	239	N.A.	Oxygen reduction	Onset pot: 0.8V	[293]
SiOC ceramers	333–588	1-2	CO conversion	98	[294]
SiC	55-363	N.A.	CO conversion	90	[295]
SiC/W	170–277	N.A.	HER	N.A.	[296]
SiCO	N.A.	N.A.	IPA conversion	N.A.	[297]
SiBCN/rGO	N.A.	N.A.	H_2 evolution	Onset pot: -0.3V	[298]
SiOCN / Ni	232	N.A.	DRM	N.A.	[299]

HER = hydrogen evolution reaction, and DRM = dry reforming of methane.

SiOC/TiO_2 nanocomposite was obtained using the template-assisted method, and its photocatalytic activity against MB degradation was analyzed [202]. The photodegradation rate constant was calculated to be 4.8×10^{-3} min^{-1}. It has been stated that the synthesized nanocomposite reduces the band gap compared to pure titania and enhances the photocatalytic effect by forming Ti-O-C/Ti-C bonds.

The MB removal efficiencies of SiOC nanobeads produced via the emulsion method and their composites coated with TiO_2 were investigated by Icin et al. [154]. Produced materials were pyrolyzed at different temperatures (600, 1200 °C), and it was stated that their MB photodegradation efficiencies under UV light reached up to 97 %. The study documented that even after 3 repetitions of reusability tests, the degradation efficiency values of the produced composites remained above 90 %, see Fig. 18.

Mesoporous SiOC/ZnO nanocomposites with high SSA (up to 400

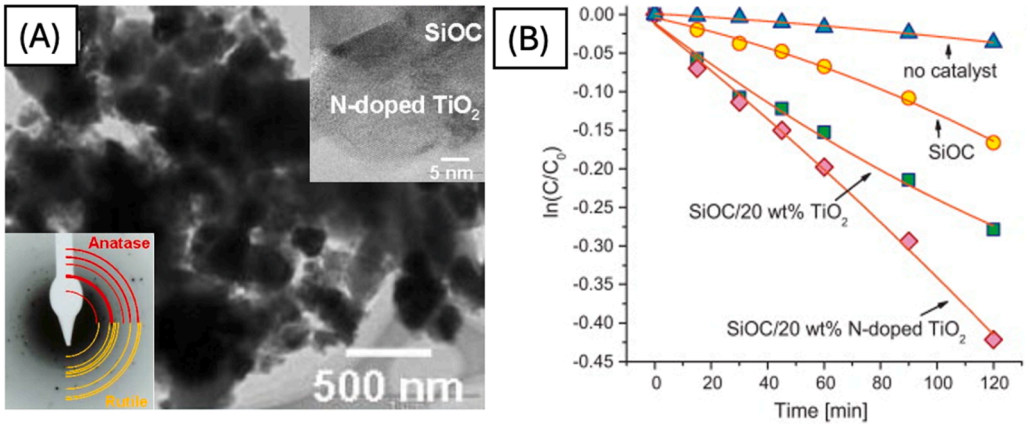


Fig. 17. **(A)** TEM micrograph (insets: SAED pattern and HRTEM micrograph) of SiOC/20 wt.% N-doped TiO_2 ceramic composite and **(B)** photocatalytic activity of SiOC ceramic and SiOC/20 wt.% TiO_2 and SiOC/20 wt.% N-doped TiO_2 ceramic composites pyrolyzed at 700 °C for 2 h in Ar atmosphere. (Reproduced from [203], with permission Elsevier, Copyright 2012).

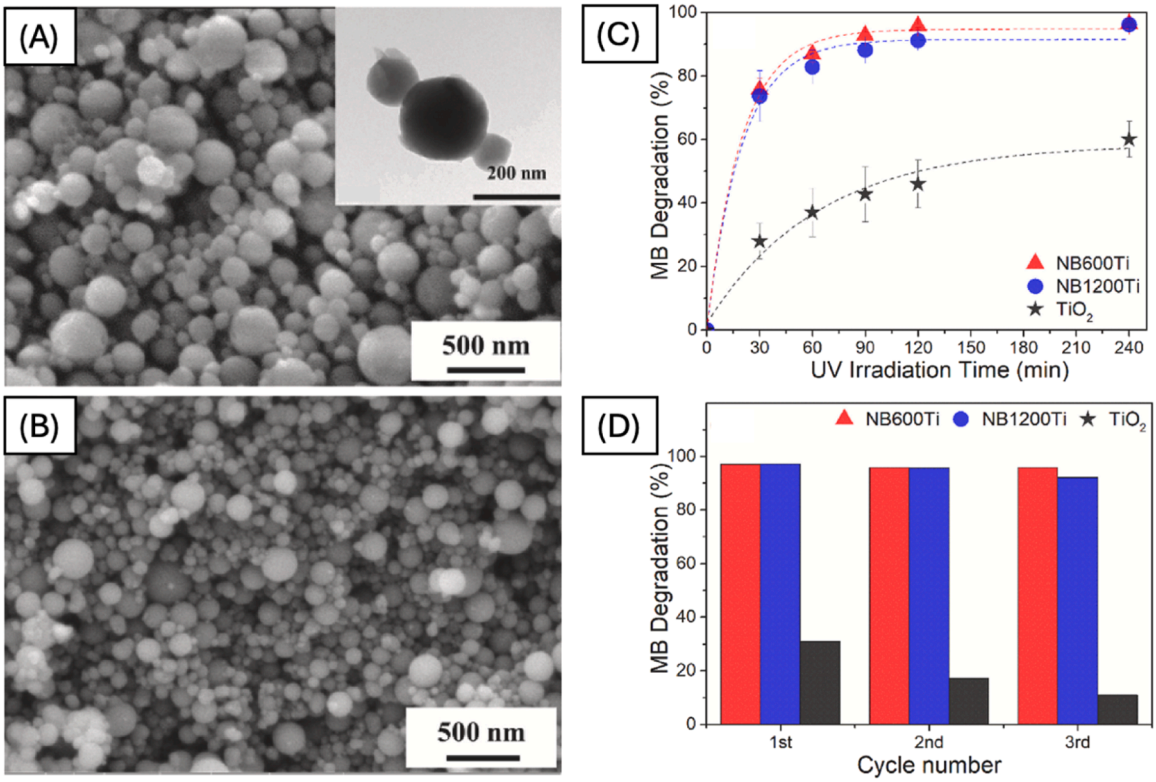


Fig. 18. SEM images of the emulsion-derived nanobeads **(A)** pyrolyzed at 600 °C (the inset are the TEM images), **(B)** pyrolyzed at 1200 °C, and **(C)** MB degradation efficiency under UV light irradiation for NB600Ti, NB1200Ti, and TiO_2 powder (the dashed lines represent the exponential non-linear fitting resulting with $R^2 > 0.737$), and (d) reusability of the photocatalyst (Reproduced from [154], with permission Elsevier, Copyright 2021).

$m^2.g^{-1}$) were synthesized for the degradation of MB in water. The impact of varying pyrolysis temperatures (700 and 900 °C) and the amount of ZnO (0-20 wt.%) on photocatalytic activities was investigated [177]. Higher pyrolysis temperatures and increased ZnO content were found to decrease the SSA. However, the enhancement in UV-induced photodegradation of MB was positively associated with higher ZnO content in the SiOC matrix. The synthesized nanocomposites containing higher ZnO content demonstrated rapid decolorization of the MB solution within 30 min under UV light exposure. While SiOC had approximately 50 % MB degradation efficiency, it reached 100 % with an increase in the ZnO ratio to 15 % in the composites.

Using the template-free PDC route, mesoporous SiC(O) ceramic nanocomposites were produced using bismuth tungstate (Bi_2WO_6) nanopowder and tested for RB photodegradation [289]. The resulting ceramic nanocomposites yield significantly higher photocatalytic activity than pure Bi_2WO_6 nanoparticles. Such an enhanced activity was due to the SiC in PDC, which provides an efficient transport pathway for dye molecules into the interior. In samples with high Bi_2WO_6 content (40 wt%), the photocatalytic degradation efficiency reached ~90 %, suggesting superb effectiveness for removing organic dyes from water.

In-situ formation of ZrO_2 crystals was observed when PHMS was used to produce SiOCN/ZrO_2 nanocomposites by Bhaskar et al. [290]. Nanocomposite foams were made with 10, 30, and 50 % zirconium (IV) butoxide (ZB), and detailed structural characterizations were employed.

Among the synthesized materials, the sample containing 50 % ZB and pyrolyzed at 1400 °C generated a hierarchical pore structure and stabilized t-ZrO_2, smaller than 15 nm. This sample's photocatalytic activity was evaluated for MB degradation. After 4h of visible light exposure, the nanocomposite manifested a photocatalytic efficiency of 72 % with a rate constant of 3.2×10^{-3} min^{-1}.

Reactions facilitated by catalysts can be categorized as homogeneous or heterogeneous. In homogeneous catalysis, all reactants and the catalyst are in the same phase. In contrast, in heterogeneous catalysis, the catalyst is typically in the solid phase, while the reactants are in the liquid or gas phase. Accordingly, PDC catalysts can be considered an example of heterogeneous catalysis [145], where the reactants are in different phases. Although heterogeneous catalysts offer the advantage of easy separation and reuse due to phase differences, their activities may be low. The structure of the material plays the most significant role in heterogeneous catalysis [276].

PDCs have been tested for thermocatalytic [292,300] and photocatalytic activities [202,216,288], whereas their application in electrocatalysis is less prevalent. In electrochemical reactions, resistance to high temperatures, particularly harsh acidic environments, is crucial for the stability of the catalyst. Therefore, it may be possible to employ PDCs in electrocatalytic reactions, even if they are not frequently studied (see Table 3) [293,296]. Functionalizing SiOC and SiCN components with metallic nanoparticles can allow for the creation of diverse supported catalysts used, for example, in hydrogen production [291,296,301–303] and pollution control.

Ni-modified polysiloxane-derived ceramics were produced by stereolithography, and their catalytic activities for CO_2 methanation were investigated [291]. The effects of different pyrolysis temperatures (600–800 °C) on the morphology and catalytic activity of the produced 3D-printed ceramic lattices have been studied. As the pyrolysis temperature increased, a decrease in SSA and a reduction in catalytic activity were observed. The SSA of these printed monoliths ceramics (pyrolyzed at 600 °C) increased from 84.5 to 410.4 $m^2.g^{-1}$ when it was ground into a powder, which corresponds with the improvement in their catalytic activity, as the CO_2 conversion value rose from 3.5 % to 25.6 %.

The catalytic effects of Ni/SiOCN nanomaterials produced using two PSZ polymers with different molecular structures were investigated through dry reforming of methane [299]. The sample pyrolyzed at 900 °C using a perhydropolysilazane-Ni precursor had ~ 230 $m^2.g^{-1}$ SSA and a microporous structure, exhibiting high activity.

Ce/SiOC nanocomposites produced by mixing different ratios of urea (0.1-0.75M), CeO_2 (6-10 mmol), and polymethyl-silsesquioxane and pyrolyzing under N_2 were investigated for their use as catalyst support materials in thermochemical CO_2 decomposition. The catalytic activity of the produced materials was evaluated based on the CO generated. While the thermocatalytic activity of catalysts consisting of pure phases can be measured by weight loss in dynamic scanning gravimetry thermogram through the release of O_2, different methods may be required for composites, as in this research. The activity of the produced catalyst nanocomposite was determined by detecting the intensity of the CO band at 2170 cm^{-1} using FTIR. It was observed that the material with a high Ce content yielded higher CO production results [292].

A new procedure was proposed for preparing metallic platinum dispersed in polysiloxane matrices for catalytic applications. Pyrolysis of polyvinylsiloxane with platinum at 1000 °C in Ar forms metallic platinum particles embedded in SiOC ceramics. The catalytic activities of the produced materials were monitored by analyzing different products in alcohol decomposition reactions using gas chromatography and calculating the decrease of activation energy. These platinum-containing systems disclose catalytic activity in IPA conversion [297].

A study evaluated the catalytic activity through CO oxidation using hybrid ceramic materials produced from poly-methyl-phenyl-silsesquioxane [294]. The platinum-containing materials, pyrolyzed at 500 °C, were investigated regarding the effect of varying amounts of the complexing agent (3-aminopropyltriethoxysilane, APTE). Although increasing the complexing agent led to a decrease in SSA values, the samples with 16 times the amount of APTE compared to platinum achieved up to 98 % CO conversion. The pyrolytic behavior of the produced materials showed that the thermal stability decreases with increasing APTE content. Samples containing the aminopropyl group are, therefore, suitable for applications below 300 °C due to the potential for carbon decomposition following pyrolytic conversion. Even though the produced materials may not be ideal for reactions at high temperatures, they could still be proposed as catalysts.

Similarly, macroporous ceramics were produced using Pt-containing polysiloxane precursors by direct foaming for testing as a catalyst in CO oxidation reactions [295]. The catalytic properties of samples pyrolyzed at 600 °C and 1400 °C were compared. The samples pyrolyzed at 600 °C had increased CO conversion with the increasing temperature, with smaller platinum particles (Fig. 19B) that affected their catalytic performance. In contrast, the samples pyrolyzed at 1400 °C displayed a high conversion rate (over 90 %) and reaction behavior typical of catalyst support systems, see Fig. 19C. The formation of nanowires on the cell walls of the foams (see Fig. 19A) enhanced the effective utilization of the catalyst material by exposing the Pt particles.

Further environmental applications of a catalyst employed is the hydrogen evolution reaction. Notably, a study has produced porous PDC/reduced-GO composites as electrocatalysts for hydrogen production [298]. Suggests that PDC composites can also be used in electrochemical catalysis due to their thermo-mechanical properties, chemical stability, and tailorable microstructure. It was noted that oxygen-enriched O-SiBCN/rGO composites had high electrocatalytic activity, with an onset potential of −340 mV and a Tafel slope of ~120 $mV.dec^{-1}$, making them effective catalysts in electrochemical reactions. The results indicated the exceptional long-term stability of O-SiBCN/rGO, and the potential of these materials for practical applications (Fig. 20C).

2.4. Energy and other applications

The broad applicability of PDCs in areas such as thermal insulation, electrical as well as dielectric and electromagnetic wave absorption, and electrochemical energy storage is due to their highly tunable properties. By adjusting the choice of pre-ceramic polymers and processing methods, these properties can be tailored to specific needs. This adaptability makes PDCs promising materials for use in industries like aerospace, defense, and energy, where high-temperature and extreme conditions are prevalent. There are already reviews about the energy-related applications, for more details, the interested reader is referred to recent reviews on PDCs [304–310].

3. Conclusions and outlook

This review joins the scientific and technological advancements in PDCs for environmental remediation, with a particular focus on sorption, filtration, and catalysis. Thanks to their tunable microstructure, high chemical and thermal stability, and surface functionalities, PDCs have shown strong potential in addressing water purification, gas separation, catalytic processes, and energy storage applications.

Specific issues are discussed in two separate panels: *(i)* In the context of sorption, experimental findings underline the pivotal influence of SSA and porosity on the adsorption efficiency of PDCs, particularly for removing dyes, pharmaceuticals, and metal ions. Adsorption performance extends beyond SSA optimization, with surface functionalities, such as Si-OH groups and sp^2 carbon domains, playing a critical role in facilitating specific bonding interactions and adsorption mechanisms. The robustness of PDC adsorbents under variable pH, temperature, and chemical conditions, combined with their cost-effectiveness and reusability, further establishes their suitability for diverse water treatment applications, and *(ii)* regarding membranes filtration, PDC membranes manifest high potential, characterized by porosities spanning from 30 %

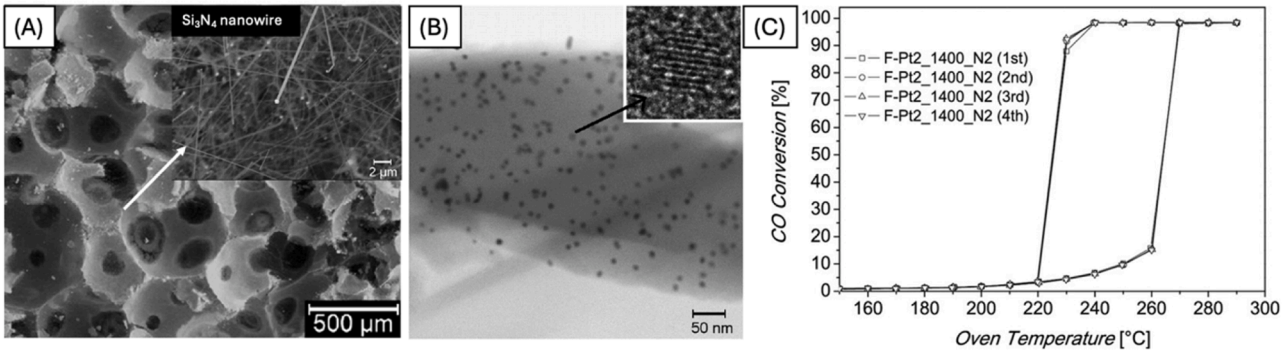


Fig. 19. **(A)** High-resolution SEM (inset: Si_3N_4 nanowire) image of the Pt-containing ceramic foam pyrolyzed at 1400 °C under N_2, **(B)** TEM image (inset: lattice structure of the Pt particles), and **(C)** CO conversion during four heat heating and cooling cycles of the samples. (Reproduced from [295], with permission John Wiley and Sons, Copyright 2013).

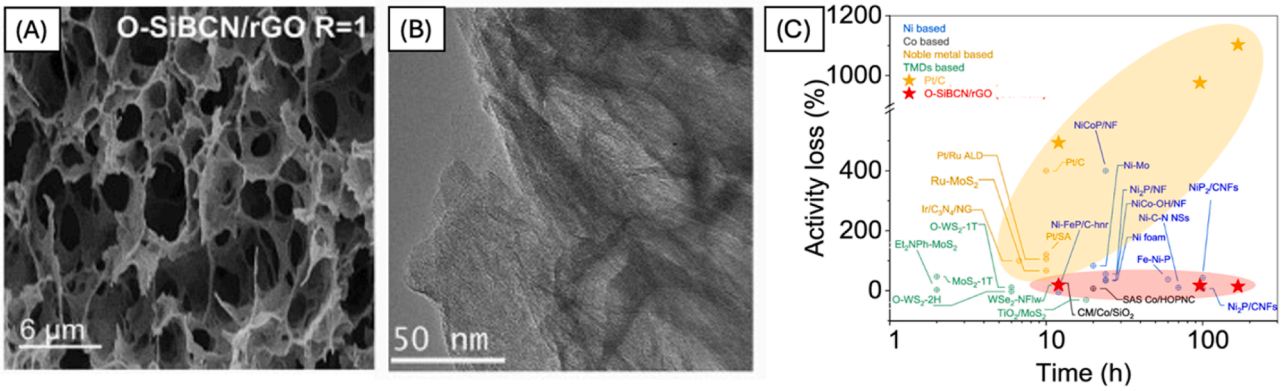


Fig. 20. **(A)** SEM, **(B)** TEM images of O-SiBCN/rGO composite ($R_{O\text{-}SiBCN/rGO} = 1$), and **(C)** Change in overpotential (%) for O-SiBCN/rGO and other electrocatalysts in the literature. (Reproduced from [298], with permission Springer Nature, Copyright 2020).

to 65 % and pore sizes covering nm to micron range with mechanical strengths reaching 50 MPa. Compared to other commonly used ceramic membranes, PDC membranes prove high efficiency through precise microstructural control and tailored surface characteristics, enabling their application across various industries, including wastewater treatment and gas separation. It was documented that advanced fabrication techniques such as phase inversion, dip-coating, electrospinning, and selective laser printing may improve structural and functional versatility. The adaptability of PDC membranes in terms of both mechanical integrity and filtration performance features their applicability for diverse and demanding filtration scenarios. Future progress in manufacturing techniques and material engineering will likely enhance their performance and broaden their industrial and environmental utility.

Since the microstructure of PDCs can be customized through the choice of precursors and production techniques, they can be designed to provide specific solutions to environmental issues. However, despite the significant potential, challenges still need to be addressed. One primary concern is the environmental impact of the PDC production process, particularly during synthesis and pyrolysis stage, where gases such as CH_4, C_6H_6, and CO may be released. Future research should focus on developing greener synthesis and methods that minimize these emissions and align with the principles of eco-friendly chemistry.

It is essential to focus on developing sustainable synthesis methods. To reduce the environmental footprint of PDC processing, novel synthesis methods should be designed using renewable resources and waste.

CRediT authorship contribution statement

Oyku Icin: Writing – original draft, Visualization, Investigation, Conceptualization. **Damla Zeydanlı:** Writing – review & editing, Investigation. **Mattia Biesuz:** Writing – review & editing. **Gian Domenico Sorarù:** Writing – review & editing. **Cekdar Vakifahmetoglu:** Writing – review & editing, Supervision, Conceptualization.

Declaration of competing interest

The authors declare that they have no known competing financial interests or personal relationships that could have appeared to influence the work reported in this paper.

The author is an Editorial Board Member/Editor-in-Chief/Associate Editor/Guest Editor for this journal and was not involved in the editorial review or the decision to publish this article.

Acknowledgments

In memory of dear friend and brilliant scientist, Dr. Caner Simsir. MB and GDS acknowledge the financial support of the European Office of Aerospace Research and Development (US Air Force Office of Scientific Research) within the project “From polymers to covalent glasses (Pol-Gla),” Award Nr. FA8655-23-1-724.

References

[1] F. Dong, R.T. Koodali, H. Wang, W. Ho, Nanomaterials for environmental applications, J. Nanomater. 2014 (2014) 276467, https://doi.org/10.1155/2014/276467.
[2] F. Perreault, A.F. De Faria, M. Elimelech, Environmental applications of graphene-based nanomaterials, Chem. Soc. Rev. 44 (2015) 5861–5896.
[3] S.M. Khopkar, Environmental pollution monitoring and control, New Age International, 2007.

[4] D. Pimentel, B. Berger, D. Filiberto, M. Newton, B. Wolfe, E. Karabinakis, S. Clark, E. Poon, E. Abbett, S. Nandagopal, Water resources: agricultural and environmental issues, Bioscience 54 (2004) 909–918.

[5] J. Jjagwe, P.W. Olupot, E. Menya, H.M. Kalibbala, Synthesis and application of granular activated carbon from biomass waste materials for water treatment: a review, J. Bioresour. Bioprod. 6 (2021) 292–322, https://doi.org/10.1016/j.jobab.2021.03.003.

[6] W. Ho, Efficient photocatalytic degradation of NO by ceramic foam air filters coated with mesoporous TiO2 thin films, Chinese J. Catal. 36 (2015) 2109–2118, https://doi.org/10.1016/S1872-2067(15)61003-8.

[7] L.M. Henning, A. Abdullayev, C. Vakifahmetoglu, U. Simon, H. Bensalah, A. Gurlo, M.F. Bekheet, Review on polymeric, inorganic, and composite materials for air filters: from processing to properties, Adv. Energy Sustain. Res. 2 (2021) 2100005, https://doi.org/10.1002/aesr.202100005.

[8] G.M. Nair, T. Sajini, B. Mathew, Advanced green approaches for metal and metal oxide nanoparticles synthesis and their environmental applications, Talanta Open 5 (2022) 100080, https://doi.org/10.1016/j.talo.2021.100080.

[9] X. Xing, R. Zhou, H. Liu, G. Han, Fabrication of metallic micro-/nano-composite materials for environmental applications, Coatings 12 (2022), https://doi.org/10.3390/coatings12121946.

[10] A. García, B. Rodríguez, H. Giraldo, Y. Quintero, R. Quezada, N. Hassan, H. Estay, Copper-modified polymeric membranes for water treatment: a comprehensive review, Membranes 11 (2021), https://doi.org/10.3390/membranes11020093 (Basel).

[11] S.-K. Ryi, J.-S. Park, S.-J. Park, D.-G. Lee, S.-H. Kim, Fabrication of nickel filter made by uniaxial pressing process for gas purification: Fabrication pressure effect, J. Memb. Sci. 299 (2007) 174–180, https://doi.org/10.1016/j.memsci.2007.04.042.

[12] S. Mallakpour, E. Azadi, C.M. Hussain, Fabrication of air filters with advanced filtration performance for removal of viral aerosols and control the spread of COVID-19, Adv. Colloid Interface Sci. 303 (2022) 102653, https://doi.org/10.1016/j.cis.2022.102653.

[13] M.-W. Kim, Y.-I. Kim, C. Park, A. Aldalbahi, H.S. Alanazi, S. An, A.L. Yarin, S. S. Yoon, Reusable and durable electrostatic air filter based on hybrid metallized microfibers decorated with metal–organic–framework nanocrystals, J. Mater. Sci. Technol. 85 (2021) 44–55, https://doi.org/10.1016/j.jmst.2020.12.065.

[14] J.L.C. Rowsell, O.M. Yaghi, Effects of functionalization, catenation, and variation of the metal oxide and organic linking units on the low-pressure hydrogen adsorption properties of metal−organic frameworks, J. Am. Chem. Soc. 128 (2006) 1304–1315, https://doi.org/10.1021/ja056639q.

[15] S. Li, Y. Chen, X. Pei, S. Zhang, X. Feng, J. Zhou, B. Wang, Water purification: adsorption over metal-organic frameworks, Chin. J. Chem. 34 (2016) 175–185, https://doi.org/10.1002/cjoc.201500761.

[16] A. Huang, Y. He, Y. Zhou, Y. Zhou, Y. Yang, J. Zhang, L. Luo, Q. Mao, D. Hou, J. Yang, A review of recent applications of porous metals and metal oxide in energy storage, sensing and catalysis, J. Mater. Sci. 54 (2019) 949–973, https://doi.org/10.1007/s10853-018-2961-5.

[17] E. Matei, A.M. Predescu, M. Râpă, A.A. Țurcanu, I. Mateș, N. Constantin, C. Predescu, Natural polymers and their nanocomposites used for environmental applications, Nanomaterials 12 (2022), https://doi.org/10.3390/nano12101707.

[18] L. Cumbal, J. Greenleaf, D. Leun, A.K. SenGupta, Polymer supported inorganic nanoparticles: characterization and environmental applications, React. Funct. Polym. 54 (2003) 167–180, https://doi.org/10.1016/S1381-5148(02)00192-X.

[19] X. Zhao, L. Lv, B. Pan, W. Zhang, S. Zhang, Q. Zhang, Polymer-supported nanocomposites for environmental application: a review, Chem. Eng. J. 170 (2011) 381–394, https://doi.org/10.1016/j.cej.2011.02.071.

[20] R. Vinodh, R. Padmavathi, D. Sangeetha, Separation of heavy metals from water samples using anion exchange polymers by adsorption process, Desalination 267 (2011) 267–276, https://doi.org/10.1016/j.desal.2010.09.039.

[21] L. Huang, R. Liu, J. Yang, Q. Shuai, B. Yuliarto, Y.V. Kaneti, Y. Yamauchi, Nanoarchitectured porous organic polymers and their environmental applications for removal of toxic metal ions, Chem. Eng. J. 408 (2021) 127991, https://doi.org/10.1016/j.cej.2020.127991.

[22] W.J. Orts, R.-E. Aicardo, R.E. Sojka, G.M. Glenn, S.H. Imam, K. Erlacher, J. S. Pedersen, Use of synthetic polymers and biopolymers for soil stabilization in agricultural, construction, and military applications, J. Mater. Civ. Eng. 19 (2007) 58–66, https://doi.org/10.1061/(ASCE)0899-1561(2007)19:1(58).

[23] J. Huang, R.B. Kogbara, N. Hariharan, E.A. Masad, D.N. Little, A state-of-the-art review of polymers used in soil stabilization, Constr. Build. Mater. 305 (2021) 124685, https://doi.org/10.1016/j.conbuildmat.2021.124685.

[24] T. Jaroszczyk, B.A. Pardue, C.E. Holm, Recent advances in engine air cleaners design and evaluation, J. KONES Powertrain Transp. 11 (2004) 259–275.

[25] A.F. Montefusco, The use of Nonwovens in air filtration, Filtr. Sep. 42 (2005) 30–31, https://doi.org/10.1016/S0015-1882(05)00446-5.

[26] M. Taylor, B. McCollister, D. Park, Highly bactericidal polyurethane effective against both normal and drug-resistant bacteria: potential use as an air filter coating, Appl. Biochem. Biotechnol. 178 (2016) 1053–1067, https://doi.org/10.1007/s12010-015-1928-0.

[27] X. Zhu, Z. Dai, K. Xu, Y. Zhao, Q. Ke, Fabrication of multifunctional filters via online incorporating nano-TiO2 into spun-bonded/melt-blown nonwovens for air filtration and toluene degradation, Macromol. Mater. Eng. 304 (2019) 1900350, https://doi.org/10.1002/mame.201900350.

[28] N. Deng, H. He, J. Yan, Y. Zhao, E. Ben Ticha, Y. Liu, W. Kang, B. Cheng, One-step melt-blowing of multi-scale micro/nano fabric membrane for advanced air-filtration, Polymer (Guildf) 165 (2019) 174–179, https://doi.org/10.1016/j.polymer.2019.01.035.

[29] M. Cao, F. Gu, C. Rao, J. Fu, P. Zhao, Improving the electrospinning process of fabricating nanofibrous membranes to filter PM2.5, Sci. Total Environ. 666 (2019) 1011–1021, https://doi.org/10.1016/j.scitotenv.2019.02.207.

[30] P. Zhang, S. Zhang, D. Wan, P. Zhang, Z. Zhang, G. Shao, Multilevel polarization-fields enhanced capture and photocatalytic conversion of particulate matter over flexible schottky-junction nanofiber membranes, J. Hazard. Mater. 395 (2020) 122639, https://doi.org/10.1016/j.jhazmat.2020.122639.

[31] F. Deuber, S. Mousavi, L. Federer, M. Hofer, C. Adlhart, Exploration of ultralight nanofiber aerogels as particle filters: capacity and efficiency, ACS Appl. Mater. Interfaces 10 (2018) 9069–9076, https://doi.org/10.1021/acsami.8b00455.

[32] M. Zhu, D. Hua, H. Pan, F. Wang, B. Manshian, S.J. Soenen, R. Xiong, C. Huang, Green electrospun and crosslinked poly(vinyl alcohol)/poly(acrylic acid) composite membranes for antibacterial effective air filtration, J. Colloid Interface Sci. 511 (2018) 411–423, https://doi.org/10.1016/j.jcis.2017.09.101.

[33] Y. Guo, W. He, J. Liu, Electrospinning polyethylene terephthalate/SiO2 nanofiber composite needle felt for enhanced filtration performance, J. Appl. Polym. Sci. 137 (2020) 48282, https://doi.org/10.1002/app.48282.

[34] H. Liu, S. Zhang, L. Liu, J. Yu, B. Ding, High-performance PM0.3 air filters using self-polarized electret nanofiber/nets, Adv. Funct. Mater. 30 (2020) 1909554, https://doi.org/10.1002/adfm.201909554.

[35] J. Zhang, G. Chen, G.S. Bhat, H. Azari, H. Pen, Electret characteristics of melt-blown polylactic acid fabrics for air filtration application, J. Appl. Polym. Sci. 137 (2020) 48309, https://doi.org/10.1002/app.48309.

[36] L. Shi, X. Zhuang, X. Tao, B. Cheng, W. Kang, Solution blowing nylon 6 nanofiber mats for air filtration, Fibers Polym. 14 (2013) 1485–1490, https://doi.org/10.1007/s12221-013-1485-5.

[37] M. Zhu, Q. Cao, B. Liu, H. Guo, X. Wang, Y. Han, G. Sun, Y. Li, J. Zhou, A novel cellulose acetate/poly (ionic liquid) composite air filter, Cellulose 27 (2020) 3889–3902, https://doi.org/10.1007/s10570-020-03034-8.

[38] K. Xu, J. Deng, R. Lin, H. Zhang, Q. Ke, C. Huang, Surface fibrillation of para-aramid nonwoven as a multi-functional air filter with ultralow pressure drop, J. Mater. Chem. A 8 (2020) 22269–22279, https://doi.org/10.1039/D0TA07886G.

[39] X. Wu, X. Chen, Q.M. Zhang, D.Q. Tan, Advanced dielectric polymers for energy storage, Energy Storage Mater. 44 (2022) 29–47, https://doi.org/10.1016/j.ensm.2021.10.010.

[40] S. Liu, J. Duvigneau, G.J. Vancso, Nanocellular polymer foams as promising high performance thermal insulation materials, Eur. Polym. J. 65 (2015) 33–45, https://doi.org/10.1016/j.eurpolymj.2015.01.039.

[41] S. Schiavoni, F. D'Alessandro, F. Bianchi, F. Asdrubali, Insulation materials for the building sector: a review and comparative analysis, Renew. Sustain. Energy Rev. 62 (2016) 988–1011, https://doi.org/10.1016/j.rser.2016.05.045.

[42] B. Mohammadi, A. Ershad-Langroudi, G. Moradi, A. Safaiyan, F.H. Kahnamuei, Foam for sound insulation. Polymeric Foams: Applications of Polymeric Foamsolym (Volume 2), American Chemical Society, 2023, pp. 12–253, https://doi.org/10.1021/bk-2023-1440.ch012.

[43] W.A. Abbas, B.S. Shaheen, L.G. Ghanem, I.M. Badawy, M.M. Abodouh, S. M. Abdou, S. Zada, N.K. Allam, Cost-effective face mask filter based on hybrid composite nanofibrous layers with high filtration efficiency, Langmuir 37 (2021) 7492–7502, https://doi.org/10.1021/acs.langmuir.1c00926.

[44] K. Min, S. Kim, S. Kim, Silk protein nanofibers for highly efficient, eco-friendly, optically translucent, and multifunctional air filters, Sci. Rep. 8 (2018) 9598, https://doi.org/10.1038/s41598-018-27917-w.

[45] M. Monier, D.M. Ayad, A.A. Sarhan, Adsorption of Cu(II), Hg(II), and Ni(II) ions by modified natural wool chelating fibers, J. Hazard. Mater. 176 (2010) 348–355, https://doi.org/10.1016/j.jhazmat.2009.11.034.

[46] L. Pang, S. Lin, J. Krakowiak, S. Yu, J. Hewitt, Performance analysis of sheep wool fibres as a water filter medium for human enteric virus removal, J. Water Process Eng. 47 (2022) 102800, https://doi.org/10.1016/j.jwpe.2022.102800.

[47] X. Huang, Y.-J. Wang, Y.-H. Di, Experimental study of wool fiber on purification of indoor air, Text. Res. J. 77 (2007) 946–950.

[48] N.A. Negm, M.G. Abd El Wahed, A.R.A. Hassan, M.T.H. Abou Kana, Feasibility of metal adsorption using brown algae and fungi: effect of biosorbents structure on adsorption isotherm and kinetics, J. Mol. Liq. 264 (2018) 292–305, https://doi.org/10.1016/j.molliq.2018.05.027.

[49] X. Li, D. Zhang, F. Sheng, H. Qing, Adsorption characteristics of copper (II), Zinc (II) and mercury (II) by four kinds of immobilized fungi residues, Ecotoxicol. Environ. Saf. 147 (2018) 357–366, https://doi.org/10.1016/j.ecoenv.2017.08.058.

[50] A. Al Bsoul, L. Zeatoun, A. Abdelhay, M. Chiha, Adsorption of copper ions from water by different types of natural seed materials, Desalin. Water Treat. 52 (2014) 5876–5882, https://doi.org/10.1080/19443994.2013.808593.

[51] L.M. Henning, U. Simon, A. Abdullayev, B. Schmidt, C. Pohl, T. Nunez Guitar, C. Vakifahmetoglu, V. Meyer, M.F. Bekheet, A. Gurlo, Effect of fomes fomentarius cultivation conditions on its adsorption performance for anionic and cationic dyes, ACS Omega 7 (2022) 4158–4169, https://doi.org/10.1021/acsomega.1c05748.

[52] Y.I. Tarasevich, Application of natural adsorbents and adsorption-active materials based thereon in the processes of water purification, in: A.B.T. S, S. S, C. Dąbrowski (Eds.), Adsorpt Its Appl Ind Environ Prot, Elsevier, 1999, pp. 659–722, https://doi.org/10.1016/S0167-2991(99)80375-9.

[53] A.M. Dziubek, A.L. Kowal, Water treatment by coagulation-adsorption with dolomite, in: L. Pawlowski, A.J. Verdier, W.J.B.T. S, E.S. Lacy (Eds.), Chem Prot Environ, Elsevier, 1984, pp. 205–211, https://doi.org/10.1016/S0166-1116(08)71229-9.

[54] A.K. Singh, D.P. Singh, K.K. Panday, V.N. Singh, Wollastonite as adsorbent for removal of Fe(II) from water, J. Chem. Technol. Biotechnol. 42 (1988) 39–49, https://doi.org/10.1002/jctb.280420106.

[55] A.S. Brooks, M.N. Rozenwald, L.D. Geohring, L.W. Lion, T.S. Steenhuis, Phosphorus removal by wollastonite: a constructed wetland substrate, Ecol. Eng. 15 (2000) 121–132, https://doi.org/10.1016/S0925-8574(99)00056-7.

[56] C.-F. Lin, S.-S. Lo, H.-Y. Lin, Y. Lee, Stabilization of cadmium contaminated soils using synthesized zeolite, J. Hazard. Mater. 60 (1998) 217–226, https://doi.org/10.1016/S0304-3894(98)00092-2.

[57] G.O. Ihekweme, J.N. Shondo, K.I. Orisekeh, G.M. Kalu-Uka, I.C. Nwuzor, A. P. Onwualu, Characterization of certain Nigerian clay minerals for water purification and other industrial applications, Heliyon 6 (2020) e03783, https://doi.org/10.1016/j.heliyon.2020.e03783.

[58] G.S. Simate, N. Maledi, A. Ochieng, S. Ndlovu, J. Zhang, L.F. Walubita, Coal-based adsorbents for water and wastewater treatment, J. Environ. Chem. Eng. 4 (2016) 2291–2312, https://doi.org/10.1016/j.jece.2016.03.051.

[59] A. Azdarpour, O. Rahmani, R. Junin, M.A. Yeop, Use of olivine for carbon dioxide mineral sequestration, 2013 IEEE Bus. Eng. Ind. Appl. Colloq. (2013) 561–564, https://doi.org/10.1109/BEIAC.2013.6560191.

[60] K. Rausis, A.R. Stubbs, I.M. Power, C. Paulo, Rates of atmospheric CO2 capture using magnesium oxide powder, Int. J. Greenh. Gas Control. 119 (2022) 103701, https://doi.org/10.1016/j.ijggc.2022.103701.

[61] N. McQueen, P. Kelemen, G. Dipple, P. Renforth, J. Wilcox, Ambient weathering of magnesium oxide for CO2 removal from air, Nat. Commun. 11 (2020) 3299, https://doi.org/10.1038/s41467-020-16510-3.

[62] E. Eyo, S. Abbey, J. Oti, S. Ng'ambi, E. Ganjian, E. Coakley, Microstructure and physical-mechanical characteristics of treated kaolin-bentonite mixture for application in compacted liner systems, Sustainability 13 (2021), https://doi.org/10.3390/su13041617.

[63] Y. Wang, Y. Qi, Y. Li, J. Wu, X. Ma, C. Yu, L. Ji, Preparation and characterization of a novel nano-absorbent based on multi-cyanoguanidine modified magnetic chitosan and its highly effective recovery for Hg(II) in aqueous phase, J. Hazard. Mater. 260 (2013) 9–15, https://doi.org/10.1016/j.jhazmat.2013.05.001.

[64] W. Wei, Y. Han, J. Chen, F. Han, D. Zou, F. Zhang, Z. Zhong, W. Xing, Fabrication of robust SiC ceramic membrane filter with optimized flap for industrial coal-fired flue gas filtration, Sep. Purif. Technol. 302 (2022) 122075, https://doi.org/10.1016/j.seppur.2022.122075.

[65] Z. Zhong, W. Xing, X. Li, F. Zhang, Removal of organic aerosols from furnace flue gas by ceramic filters, Ind. Eng. Chem. Res. 52 (2013) 5455–5461, https://doi.org/10.1021/ie400046z.

[66] G. Saracco, L. Montanaro, Catalytic ceramic filters for flue gas cleaning. 1. Preparation and characterization, Ind. Eng. Chem. Res. 34 (1995) 1471–1479.

[67] N. Labhsetwar, P. Doggali, S. Rayalu, R. Yadav, T. Mistuhashi, H. Haneda, Ceramics in environmental catalysis: applications and possibilities, Chin. J. Catal. 33 (2012) 1611–1621, https://doi.org/10.1016/S1872-2067(11)60440-3.

[68] Y. Dai, W. Liu, E. Formo, Y. Sun, Y. Xia, Ceramic nanofibers fabricated by electrospinning and their applications in catalysis, environmental science, and energy technology, Polym. Adv. Technol. 22 (2011) 326–338, https://doi.org/10.1002/pat.1839.

[69] T. Arumugham, N.J. Kaleekkal, S. Gopal, J. Nambikkattu, K. R, A.M. Aboulella, S. Ranil Wickramasinghe, F. Banat, Recent developments in porous ceramic membranes for wastewater treatment and desalination: a review, J. Environ. Manage. 293 (2021) 112925, https://doi.org/10.1016/j.jenvman.2021.112925.

[70] K. Suresh, N. Katara, Design and development of circular ceramic membrane for wastewater treatment, Mater. Today Proc. 43 (2021) 2176–2181, https://doi.org/10.1016/j.matpr.2020.12.109.

[71] Z. He, Z. Lyu, Q. Gu, L. Zhang, J. Wang, Ceramic-based membranes for water and wastewater treatment, Colloids Surf. A Physicochem. Eng. Asp. 578 (2019) 123513, https://doi.org/10.1016/j.colsurfa.2019.05.074.

[72] R. Baby, B. Saifullah, M.Z. Hussein, Carbon nanomaterials for the treatment of heavy metal-contaminated water and environmental remediation, Nanoscale Res. Lett. 14 (2019) 341, https://doi.org/10.1186/s11671-019-3167-8.

[73] K.P. Shejale, D. Yadav, H. Patil, S. Saxena, S. Shukla, Evaluation of techniques for the remediation of antibiotic-contaminated water using activated carbon, Mol. Syst. Des. Eng. 5 (2020) 743–756.

[74] J. Rivera-Utrilla, M. Sánchez-Polo, V. Gómez-Serrano, P.M. Álvarez, M.C. M. Alvim-Ferraz, J.M. Dias, Activated carbon modifications to enhance its water treatment applications. An overview, J. Hazard. Mater. 187 (2011) 1–23, https://doi.org/10.1016/j.jhazmat.2011.01.033.

[75] Z. Gong, K. Alef, B.-M. Wilke, P. Li, Activated carbon adsorption of PAHs from vegetable oil used in soil remediation, J. Hazard. Mater. 143 (2007) 372–378, https://doi.org/10.1016/j.jhazmat.2006.09.037.

[76] M. Lewoyehu, Comprehensive review on synthesis and application of activated carbon from agricultural residues for the remediation of venomous pollutants in wastewater, J. Anal. Appl. Pyrolysis 159 (2021) 105279, https://doi.org/10.1016/j.jaap.2021.105279.

[77] F. Wang, S. Hao, B. Dong, N. Ke, N.Z. Khan, L. Hao, L. Yin, X. Xu, S. Agathopoulos, Porous-foam mullite-bonded SiC-ceramic membranes for high-efficiency high-temperature particulate matter capture, J. Alloys Compd. 893 (2022) 162231, https://doi.org/10.1016/j.jallcom.2021.162231.

[78] J.C.-T. Lin, T.-C. Hsiao, S.-S. Hsiau, D.-R. Chen, Y.-K. Chen, S.-H. Huang, C.-C. Chen, M.-B. Chang, Effects of temperature, dust concentration, and filtration superficial velocity on the loading behavior and dust cakes of ceramic candle filters during hot gas filtration, Sep. Purif. Technol. 198 (2018) 146–154, https://doi.org/10.1016/j.seppur.2017.06.014.

[79] I. Voigt, J. Adler, M. Weyd, R. Kriegel, Ceramic filters and membranes, Ceram. Sci. Technol. (2013) 117–167, https://doi.org/10.1002/9783527631971.ch03.

[80] R. Xiong, G. Sun, K. Si, Q. Liu, K. Liu, Pressure drop prediction of ceramic membrane filters at high temperature, Powder Technol. 364 (2020) 647–653, https://doi.org/10.1016/j.powtec.2020.01.085.

[81] B. Bishop, J. Cardin, R. Goldsmith, E. Altwicker, D. Griffith, Advanced regenerable HEPA filters based on ceramic honeycomb materials. Proceedings of the WM 2004 Conference, Febr., n.d., 2004.

[82] D. Das, N. Kayal, Permeability and dust filtration behaviour of porous SiC ceramic candle filter, Mater. Today Proc. 39 (2021) 1235–1240, https://doi.org/10.1016/j.matpr.2020.04.090.

[83] N. Hooftman, M. Messagie, J. Van Mierlo, T. Coosemans, A review of the European passenger car regulations – real driving emissions vs local air quality, Renew. Sustain. Energy Rev. 86 (2018) 1–21, https://doi.org/10.1016/j.rser.2018.01.012.

[84] J. Adler, Ceramic diesel particulate filters, Int. J. Appl. Ceram. Technol. 2 (2005) 429–439, https://doi.org/10.1111/j.1744-7402.2005.02044.x.

[85] W.A. Cutler, Overview of ceramic materials for diesel particulate filter applications, in: Proceedings of the 28th International Conference on Advanced Ceramics and Composites A: Ceramic Engineering and Science Proceedings, 2004, pp. 421–430, https://doi.org/10.1002/9780470291184.ch61.

[86] H.-W. Li, C.-Y. Wu, F. Tepper, J.-H. Lee, C.N. Lee, Removal and retention of viral aerosols by a novel alumina nanofiber filter, J. Aerosol Sci. 40 (2009) 65–71, https://doi.org/10.1016/j.jaerosci.2008.09.003.

[87] X. Mao, Y. Bai, J. Yu, B. Ding, Flexible and highly temperature resistant polynanocrystalline zirconia nanofibrous membranes designed for air filtration, J. Am. Ceram. Soc. 99 (2016) 2760–2768, https://doi.org/10.1111/jace.14278.

[88] M.D. de, M. Innocentini, J.R. Coury, M. Fukushima, P. Colombo, High-efficiency aerosol filters based on silicon carbide foams coated with ceramic nanowires, Sep. Purif. Technol. 152 (2015) 180–191, https://doi.org/10.1016/j.seppur.2015.08.027.

[89] J.C. Ruiz, P. Blanc, E. Prouzet, P. Coryn, P. Laffont, A. Larbot, Solid aerosol removal using ceramic filters, Sep. Purif. Technol. 19 (2000) 221–227, https://doi.org/10.1016/S1383-5866(00)00056-3.

[90] A. Larbot, M. Bertrand, S. Marre, E. Prouzet, Performances of ceramic filters for air purification, Sep. Purif. Technol. 32 (2003) 81–85, https://doi.org/10.1016/S1383-5866(03)00062-5.

[91] X. Li, M.J. Patel, I.S. Cole, Portable air purifiers' predicted efficacy in mitigating airborne pathogen transmission in an office room featuring mixing ventilation, Fluids 8 (2023), https://doi.org/10.3390/fluids8120307.

[92] B. Shimekit, H. Mukhtar, F. Ahmad, S. Maitra, Ceramic membranes for the separation of carbon dioxide—a review, Trans. Indian Ceram. Soc. 68 (2009) 115–138, https://doi.org/10.1080/0371750X.2009.11082166.

[93] M. Back, M. Bauer, H. Stanjek, S. Peiffer, Sequestration of CO2 after reaction with alkaline earth metal oxides CaO and MgO, Appl. Geochem. 26 (2011) 1097–1107, https://doi.org/10.1016/j.apgeochem.2011.03.125.

[94] H. Pfeiffer, Advances on alkaline ceramics as possible CO_2 captors, in: Proceedings of the Advances in CO2 Conversion and Utilization American Chemical Society, 2010, pp. 15–233, https://doi.org/10.1021/bk-2010-1056.ch015.

[95] C.R.V Morgado, V. Esteves, CO2 Sequestration And Valorization, BoD–Books on Demand, 2014.

[96] C.P. Kaushik, R.K. Mishra, P. Sengupta, A. Kumar, D. Das, G.B. Kale, K. Raj, Barium borosilicate glass – a potential matrix for immobilization of sulfate bearing high-level radioactive liquid waste, J. Nucl. Mater. 358 (2006) 129–138, https://doi.org/10.1016/j.jnucmat.2006.07.004.

[97] X. Zhang, P. Gu, Y. Liu, Decontamination of radioactive wastewater: state of the art and challenges forward, Chemosphere 215 (2019) 543–553, https://doi.org/10.1016/j.chemosphere.2018.10.029.

[98] H. Ma, M. Shen, Y. Tong, X. Wang, Radioactive wastewater treatment technologies: a review, Molecules 28 (2023), https://doi.org/10.3390/molecules28041935.

[99] W.E. Lee, M.I. Ojovan, M.C. Stennett, N.C. Hyatt, Immobilisation of radioactive waste in glasses, glass composite materials and ceramics, Adv. Appl. Ceram. 105 (2006) 3–12, https://doi.org/10.1179/174367606X81669.

[100] N.A. El-Alaily, W.M. Abdallah, B.A. Sabrah, A.I. Saad, Preparation and characterization of immobilizing radioactive waste glass from industrial wastes, Silicon 9 (2017) 117–130, https://doi.org/10.1007/s12633-015-9330-7.

[101] P.A. Tempest, A comparison of borosilicate glass and synthetic minerals as media for the immobilization of high-level radioactive waste, Nucl. Technol. 52 (1981) 415–425, https://doi.org/10.13182/NT81-A32715.

[102] J.E. Mendel, W.A. Ross, R.P. Turcotte, J.L. McElroy, Physical properties of glass for immobilization of high level radioactive waste, Nucl. Chem. Waste Manag. 1 (1980) 17–28, https://doi.org/10.1016/0191-815X(80)90025-X.

[103] J.H. Simmons, P.B. Macedo, A. Barkatt, T.A. Litovitz, Fixation of radioactive waste in high silica glasses, Nature 278 (1979) 729–731, https://doi.org/10.1038/278729a0.

[104] N.P. Laverov, B.I. Omel'yanenko, S.V Yudintsev, S.V Stefanovsky, B.S. Nikonov, Glasses for immobilization of low- and intermediate-level radioactive waste, Geol. Ore Depos. 55 (2013) 71–95, https://doi.org/10.1134/S1075701513020037.

[105] O.N. Koroleva, L.A. Nevolina, N.M. Korobatova, Glass-containing matrices based on borosilicate glasses for the immobilization of radioactive wastes, J. Compos. Sci. 7 (2023), https://doi.org/10.3390/jcs7120505.

[106] L. Wang, T. Liang, Ceramics for high level radioactive waste solidification, J. Adv. Ceram. 1 (2012) 194–203, https://doi.org/10.1007/s40145-012-0019-8.

[107] O. Terra, N. Clavier, N. Dacheux, R. Podor, Preparation and characterization of lanthanum–gadolinium monazites as ceramics for radioactive waste storage, New J. Chem. 27 (2003) 957–967, https://doi.org/10.1039/B212805P.
[108] L. Zhou, F. Li, J.-X. Liu, S.-K. Sun, Y. Liang, G.-J. Zhang, High-entropy A2B2O7-type oxide ceramics: a potential immobilising matrix for high-level radioactive waste, J. Hazard. Mater. 415 (2021) 125596, https://doi.org/10.1016/j.jhazmat.2021.125596.
[109] D. Li, X. Zeng, Z. Li, Z.-Y. Shen, H. Hao, W. Luo, X. Wang, F. Song, Z. Wang, Y. Li, Progress and perspectives in dielectric energy storage ceramics, J. Adv. Ceram. 10 (2021) 675–703, https://doi.org/10.1007/s40145-021-0500-3.
[110] Z. Yang, H. Du, L. Jin, D. Poelman, High-performance lead-free bulk ceramics for electrical energy storage applications: design strategies and challenges, J. Mater. Chem. A 9 (2021) 18026–18085.
[111] R. Kolb, C. Fasel, V. Liebau-Kunzmann, R. Riedel, SiCN/C-ceramic composite as anode material for lithium ion batteries, J. Eur. Ceram. Soc. 26 (2006) 3903–3908, https://doi.org/10.1016/j.jeurceramsoc.2006.01.009.
[112] E.J. Cheng, T. Kimura, M. Shoji, H. Ueda, H. Munakata, K. Kanamura, Ceramic-based flexible sheet electrolyte for Li batteries, ACS Appl. Mater. Interfaces 12 (2020) 10382–10388, https://doi.org/10.1021/acsami.9b21251.
[113] Y. Ren, K. Chen, R. Chen, T. Liu, Y. Zhang, C.-W. Nan, Oxide electrolytes for lithium batteries, J. Am. Ceram. Soc. 98 (2015) 3603–3623, https://doi.org/10.1111/jace.13844.
[114] L. Han, F. Li, X. Deng, J. Wang, H. Zhang, S. Zhang, Foam-gelcasting preparation, microstructure and thermal insulation performance of porous diatomite ceramics with hierarchical pore structures, J. Eur. Ceram. Soc. 37 (2017) 2717–2725, https://doi.org/10.1016/j.jeurceramsoc.2017.02.032.
[115] K. Zhao, F. Ye, L. Cheng, J. Yang, X. Chen, An overview of ultra-high temperature ceramic for thermal insulation: structure and composition design with thermal conductivity regulation, J. Eur. Ceram. Soc. 43 (2023) 7241–7262, https://doi.org/10.1016/j.jeurceramsoc.2023.07.046.
[116] E.C. Hammel, O.L.-R. Ighodaro, O.I. Okoli, Processing and properties of advanced porous ceramics: an application based review, Ceram. Int. 40 (2014) 15351–15370, https://doi.org/10.1016/j.ceramint.2014.06.095.
[117] Z. Wei, S. Li, Y. Li, X. Li, R. Xiang, N. Xu, Porous alumina ceramics with enhanced mechanical and thermal insulation properties based on sol-treated rice husk, Ceram. Int. 44 (2018) 22616–22621, https://doi.org/10.1016/j.ceramint.2018.09.036.
[118] M. Zhu, R. Ji, Z. Li, H. Wang, L. Liu, Z. Zhang, Preparation of glass ceramic foams for thermal insulation applications from coal fly ash and waste glass, Constr. Build. Mater. 112 (2016) 398–405, https://doi.org/10.1016/j.conbuildmat.2016.02.183.
[119] W. Zhou, W. Yan, N. Li, Y. Li, S. Schafföner, Y. Dai, Z. Zhang, L. Yuan, Fabrication, characterization and thermal-insulation modeling of foamed mullite-SiC ceramics, J. Alloys Compd. 829 (2020) 154523, https://doi.org/10.1016/j.jallcom.2020.154523.
[120] X. Zeng, E. Li, G. Xia, N. Xie, Z.-Y. Shen, M. Moskovits, R. Yu, Silica-based ceramics toward electromagnetic microwave absorption, J. Eur. Ceram. Soc. 41 (2021) 7381–7403, https://doi.org/10.1016/j.jeurceramsoc.2021.08.009.
[121] H. Wei, X. Yin, F. Jiang, Z. Hou, L. Cheng, L. Zhang, Optimized design of high-temperature microwave absorption properties of CNTs/Sc2Si2O7 ceramics, J. Alloys Compd. 823 (2020) 153864, https://doi.org/10.1016/j.jallcom.2020.153864.
[122] L. Gao, W. Zhou, F. Luo, D. Zhu, J. Wang, Dielectric and microwave absorption properties of KNN/Al2O3 composite ceramics, Ceram. Int. 43 (2017) 12731–12735, https://doi.org/10.1016/j.ceramint.2017.06.158.
[123] C. Jia, L. Li, Y. Liu, B. Fang, H. Ding, J. Song, Y. Liu, K. Xiang, S. Lin, Z. Li, W. Si, B. Li, X. Sheng, D. Wang, X. Wei, H. Wu, Highly compressible and anisotropic lamellar ceramic sponges with superior thermal insulation and acoustic absorption performances, Nat. Commun. 11 (2020) 3732, https://doi.org/10.1038/s41467-020-17533-6.
[124] M. Carlesso, R. Giacomelli, S. Günther, D. Koch, S. Kroll, S. Odenbach, K. Rezwan, Near-net-shaped porous ceramics for potential sound absorption applications at high temperatures, J. Am. Ceram. Soc. 96 (2013) 710–718, https://doi.org/10.1111/jace.12160.
[125] D. Cuiyun, C. Guang, X. Xinbang, L. Peisheng, Sound absorption characteristics of a high-temperature sintering porous ceramic material, Appl. Acoust. 73 (2012) 865–871, https://doi.org/10.1016/j.apacoust.2012.01.004.
[126] T.S. da N. Guenka, M.R. Machado, A.M.A. Silva, M.A.A. Nunes, Freeze-cast porous Al_2O_3/MgO ceramics as potential acoustic sound absorption, Appl. Acoust. 220 (2024) 109964, https://doi.org/10.1016/j.apacoust.2024.109964.
[127] N. Yan, Q. Fu, Y. Zhang, K. Li, W. Xie, J. Zhang, L. Zhuang, X. Shi, Preparation of pore-controllable zirconium carbide ceramics with tunable mechanical strength, thermal conductivity and sound absorption coefficient, Ceram. Int. 46 (2020) 19609–19616, https://doi.org/10.1016/j.ceramint.2020.05.023.
[128] F. Yang, S. Zhao, W. Sun, K. Li, J. Chen, Z. Fei, Z. Yang, Fibrous porous mullite ceramics modified by mullite whiskers for thermal insulation and sound absorption, J. Eur. Ceram. Soc. 43 (2023) 521–529, https://doi.org/10.1016/j.jeurceramsoc.2022.10.025.
[129] M. Yang, L. Yang, Z. Chen, Y. Ding, L. Liu, W. Qiong, T. Liu, M. Li, Multifunctional flexible SiO_2/BNNBs nanofibrous aerogel for thermal insulation, infrared stealth and sound-absorption, Ceram. Int. 49 (2023) 22393–22399, https://doi.org/10.1016/j.ceramint.2023.04.069.
[130] L. Cai, J. Tian, K. Feng, Y. Liu, Q. Jiang, Sound absorption model of foam glass-ceramics based on microstructure, J. Non Cryst. Solids 604 (2023) 122136, https://doi.org/10.1016/j.jnoncrysol.2023.122136.
[131] E. Rambaldi, F. Prete, M.C. Bignozzi, Acoustic and thermal performances of ceramic tiles and tiling systems, Ceram. Int. 41 (2015) 7252–7260, https://doi.org/10.1016/j.ceramint.2015.03.032.
[132] L. Cao, H. Shan, D. Zong, X. Yu, X. Yin, Y. Si, J. Yu, B. Ding, Fire-resistant and hierarchically structured elastic ceramic nanofibrous aerogels for efficient low-frequency noise reduction, Nano Lett. 22 (2022) 1609–1617, https://doi.org/10.1021/acs.nanolett.1c04532.
[133] L. Zhu, S. Li, Y. Li, N. Xu, Novel applications of waste ceramics on the fabrication of foamed materials for exterior building walls insulation, Constr. Build. Mater. 180 (2018) 291–297, https://doi.org/10.1016/j.conbuildmat.2018.05.290.
[134] Q. Yu, [Retracted] application of foam glass-ceramic composite thermal insulation material in traditional buildings, J. Chem. 2022 (2022) 9662805, https://doi.org/10.1155/2022/9662805.
[135] T. Aydin, The development of porcelain foams lighter than water for heat isolation application, J. Therm. Anal. Calorim. 136 (2019) 535–539, https://doi.org/10.1007/s10973-018-7691-z.
[136] M. Marangoni, B. Nait-Ali, D.S. Smith, M. Binhussain, P. Colombo, E. Bernardo, White sintered glass-ceramic tiles with improved thermal insulation properties for building applications, J. Eur. Ceram. Soc. 37 (2017) 1117–1125, https://doi.org/10.1016/j.jeurceramsoc.2016.10.019.
[137] A. Lamy-Mendes, A.D.R. Pontinha, P. Alves, P. Santos, L. Durães, Progress in silica aerogel-containing materials for buildings' thermal insulation, Constr. Build. Mater. 286 (2021) 122815, https://doi.org/10.1016/j.conbuildmat.2021.122815.
[138] M. Reim, W. Körner, J. Manara, S. Korder, M. Arduini-Schuster, H.-P. Ebert, J. Fricke, Silica aerogel granulate material for thermal insulation and daylighting, Sol. Energy 79 (2005) 131–139, https://doi.org/10.1016/j.solener.2004.08.032.
[139] C. Buratti, E. Moretti, Glazing systems with silica aerogel for energy savings in buildings, Appl. Energy 98 (2012) 396–403, https://doi.org/10.1016/j.apenergy.2012.03.062.
[140] X.Q. Cao, R. Vassen, D. Stoever, Ceramic materials for thermal barrier coatings, J. Eur. Ceram. Soc. 24 (2004) 1–10, https://doi.org/10.1016/S0955-2219(03)00129-8.
[141] I. Belyaev, A. Dean, H. Eger, G. Hubmann, R. Jandrisovits, M. Kern, M. Kundi, H. Moshammer, P. Lercher, K. Müller, G. Oberfeld, P. Ohnsorge, P. Pelzmann, C. Scheingraber, R. Thill, EUROPAEM EMF guideline 2016 for the prevention, diagnosis and treatment of EMF-related health problems and illnesses, 31 (2016) 363–397. 10.1515/reveh-2016-0011.
[142] W. Li, Z. Yu, Q. Wen, Y. Feng, B. Fan, R. Zhang, R. Riedel, Ceramic-based electromagnetic wave absorbing materials and concepts towards lightweight, flexibility and thermal resistance, Int. Mater. Rev. 68 (2023) 487–520, https://doi.org/10.1080/09506608.2022.2077028.
[143] C. Ma, W. Yu, G. Ma, W. Haidou, Recent progress on high temperature radar absorbing coatings (RACs): a review, Crit. Rev. Solid State Mater. Sci. 48 (2023) 726–753, https://doi.org/10.1080/10408436.2022.2118663.
[144] P. Wang, L. Cheng, Y. Zhang, H. Wu, Y. Hou, W. Yuan, L. Zheng, Flexible, hydrophobic SiC ceramic nanofibers used as high frequency electromagnetic wave absorbers, Ceram. Int. 43 (2017) 7424–7435, https://doi.org/10.1016/j.ceramint.2017.03.001.
[145] B. Araldi Silva, L.F. Belchior Ribeiro, S.Y. Gómez González, D. Hotza, R. de Fátima Peralta Muniz Moreira, A. De Noni Junior, SiOC and SiCN-based ceramic supports for catalysts and photocatalysts, Microporous Mesoporous Mater. 327 (2021) 111435, https://doi.org/10.1016/j.micromeso.2021.111435.
[146] C. Vakifahmetoglu, D. Zeydanli, P. Colombo, Porous polymer derived ceramics, Mater. Sci. Eng. R Rep.. 106 (2016) 1–30.
[147] P. Greil, Polymer derived engineering ceramics, Adv. Eng. Mater. 2 (2000) 339–348.
[148] P. Colombo, G. Mera, R. Riedel, G.D. Soraru, Polymer-derived ceramics: 40 years of research and innovation in advanced ceramics, J. Am. Ceram. Soc. 93 (2010) 1805–1837.
[149] S. Fu, M. Zhu, Y. Zhu, Organosilicon polymer-derived ceramics: an overview, J. Adv. Ceram. 8 (2019) 457–478, https://doi.org/10.1007/s40145-019-0335-3.
[150] Q. Wen, Z. Yu, R. Riedel, The fate and role of in situ formed carbon in polymer-derived ceramics, Prog. Mater. Sci. 109 (2020) 100623, https://doi.org/10.1016/j.pmatsci.2019.100623.
[151] V. Belot, R.J.P. Corriu, D. Leclercq, P.H. Mutin, A. Vioux, Silicon oxycarbide glasses with low O/Si ratio from organosilicon precursors, J. Non Cryst. Solids 176 (1994) 33–44, https://doi.org/10.1016/0022-3093(94)90208-9.
[152] S. Liemersdorf, R. Riedel, J. Oberle, Influence of the gas atmosphere on the composition and phase development of polymer-derived SiOC-ceramics, J. Am. Ceram. Soc. 91 (2008) 325–328, https://doi.org/10.1111/j.1551-2916.2007.02112.x.
[153] J. Pan, J. Ren, Y. Xie, X. Wei, Y. Guan, X. Yan, H. Tang, X. Cheng, Porous SiOC composites fabricated from preceramic polymers and wood powders for efficient dye adsorption and removal, Res. Chem. Intermed. 43 (2017) 3813–3832, https://doi.org/10.1007/s11164-016-2850-y.
[154] O. Icin, C. Vakifahmetoglu, Dye removal by polymer derived ceramic nanobeads, Ceram. Int. 47 (2021) 27050–27057, https://doi.org/10.1016/j.ceramint.2021.06.118.
[155] D. Zeydanli, S. Akman, C. Vakifahmetoglu, Polymer-derived ceramic adsorbent for pollutant removal from water, J. Am. Ceram. Soc. 101 (2018) 2258–2265.
[156] B.-B. Dong, F.-H. Wang, M.-Y. Yang, J.-L. Yu, L.-Y. Hao, X. Xu, G. Wang, S. Agathopoulos, Polymer-derived porous SiOC ceramic membranes for efficient oil-water separation and membrane distillation, J. Memb. Sci. 579 (2019) 111–119, https://doi.org/10.1016/j.memsci.2019.02.066.

[157] Y. Jüttke, H. Richtera, I. Voigta, R.M. Prasadb, M.S. Bazarjanib, A. Gurlob, R. Riedelb, Polymer derived ceramic membranes for gas separation, Chem. Eng. 32 (2013).
[158] Y. Iwamoto, Precursors-derived ceramic membranes for high-temperature separation of hydrogen, J. Ceram. Soc. Jpn. 115 (2007) 947–954.
[159] G.S. Barroso, W. Krenkel, G. Motz, Low thermal conductivity coating system for application up to 1000°C by simple PDC processing with active and passive fillers, J. Eur. Ceram. Soc. 35 (2015) 3339–3348, https://doi.org/10.1016/j.jeurceramsoc.2015.02.006.
[160] Y. Wang, X. Li, X. Pei, L. He, Z. Huang, Q. Huang, Preparation of highly porous SiC via ceramic precursor conversion and evaluation of its thermal insulation performance, Adv. Appl. Ceram. 119 (2020) 398–406, https://doi.org/10.1080/17436753.2020.1789940.
[161] M. Biesuz, E. Zera, M. Tomasi, P. Jana, O. Ersen, W. Baaziz, A. Lindemann, G. D. Sorarù, Polymer-derived Si3N4 nanofelts for flexible, high temperature, lightweight and easy-manufacturable super-thermal insulators, Appl. Mater. Today 20 (2020) 100648, https://doi.org/10.1016/j.apmt.2020.100648.
[162] W. Wang, L. Pang, M. Jiang, Y. Zhu, F. Wang, J. Sun, H. Qi, Enhancing the thermal insulation properties of polymer-derived SiCN(O) ceramic aerogels with a polysilazane-precursor design, Ceram. Int. 49 (2023) 15829–15841, https://doi.org/10.1016/j.ceramint.2023.01.178.
[163] O. Icin, T. Semerci, G.D. Soraru, C. Vakifahmetoglu, Design and performance comparison of polymer-derived ceramic ambigels and aerogels, ACS Omega (2023), https://doi.org/10.1021/acsomega.3c04607.
[164] L. Qiu, Y. Du, Y. Bai, Y. Feng, X. Zhang, J. Wu, X. Wang, C. Xu, Experimental characterization and model verification of thermal conductivity from mesoporous to macroporous SiOC ceramics, J. Therm. Sci. 30 (2021) 465–476, https://doi.org/10.1007/s11630-021-1422-7.
[165] G. Liu, J. Kaspar, L.M. Reinold, M. Graczyk-Zajac, R. Riedel, Electrochemical performance of DVB-modified SiOC and SiCN polymer-derived negative electrodes for lithium-ion batteries, Electrochim. Acta. 106 (2013) 101–108.
[166] P. Vallachira Warriam Sasikumar, E. Zera, M. Graczyk-Zajac, R. Riedel, G. D. Soraru, Structural design of polymer-derived SiOC ceramic aerogels for high-rate Li ion storage applications, J. Am. Ceram. Soc. 99 (2016) 2977–2983, https://doi.org/10.1111/jace.14323.
[167] M. Graczyk-Zajac, C. Fasel, R. Riedel, Polymer-derived-SiCN ceramic/graphite composite as anode material with enhanced rate capability for lithium ion batteries, J. Power Sources 196 (2011) 6412–6418, https://doi.org/10.1016/j.jpowsour.2011.03.076.
[168] M. Graczyk-Zajac, G. Mera, J. Kaspar, R. Riedel, Electrochemical studies of carbon-rich polymer-derived SiCN ceramics as anode materials for lithium-ion batteries, J. Eur. Ceram. Soc. 30 (2010) 3235–3243, https://doi.org/10.1016/j.jeurceramsoc.2010.07.010.
[169] L.M. Reinold, Y. Yamada, M. Graczyk-Zajac, H. Munakata, K. Kanamura, R. Riedel, The influence of the pyrolysis temperature on the electrochemical behavior of carbon-rich SiCN polymer-derived ceramics as anode materials in lithium-ion batteries, J. Power Sources 282 (2015) 409–415, https://doi.org/10.1016/j.jpowsour.2015.02.074.
[170] X. Guo, Y. Feng, X. Lin, Y. Liu, H. Gong, Y. Zhang, The dielectric and microwave absorption properties of polymer-derived SiCN ceramics, J. Eur. Ceram. Soc. 38 (2018) 1327–1333, https://doi.org/10.1016/j.jeurceramsoc.2017.10.031.
[171] Q. Li, X. Yin, W. Duan, L. Kong, B. Hao, F. Ye, Electrical, dielectric and microwave-absorption properties of polymer derived SiC ceramics in X band, J. Alloys Compd. 565 (2013) 66–72, https://doi.org/10.1016/j.jallcom.2013.02.176.
[172] D. Malwal, P. Gopinath, Fabrication and applications of ceramic nanofibers in water remediation: a review, Crit. Rev. Environ. Sci. Technol. 46 (2016) 500–534, https://doi.org/10.1080/10643389.2015.1109913.
[173] K.P. Gopinath, D.-V.N. Vo, D. Gnana Prakash, A. Adithya Joseph, S. Viswanathan, J. Arun, Environmental applications of carbon-based materials: a review, Environ. Chem. Lett. 19 (2021) 557–582, https://doi.org/10.1007/s10311-020-01084-9.
[174] M.M.B.T.-P. N. for E P. Arunachalam, 6 - Polymer-based nanocomposites for energy and environmental applications, in: M. Jawaid, E.A. Khan (Eds.), Woodhead Publishing Series in Composites Science and Engineering, Woodhead Publishing, 2018, pp. 185–203, https://doi.org/10.1016/B978-0-08-102262-7.00006-4.
[175] A. Kumar, Advanced Ceramics for Energy and Environmental Applications, CRC Press, Boca Raton, 2021.
[176] D. Jiang, Y. Zeng, M. Singh, J. Heinrich, Ceramic Materials and Components For Energy And Environmental Applications, John Wiley & Sons, 2010.
[177] M. Hojamberdiev, R.M. Prasad, K. Morita, M.A. Schiavon, R. Riedel, Polymer-derived mesoporous SiOC/ZnO nanocomposite for the purification of water contaminated with organic dyes, Microporous Mesoporous Mater. 151 (2012) 330–338, https://doi.org/10.1016/j.micromeso.2011.10.015.
[178] A. Lale, M. Schmidt, M.D. Mallmann, A.V.A. Bezerra, E.D. Acosta, R.A. F. Machado, U.B. Demirci, S. Bernard, Polymer-derived ceramics with engineered mesoporosity: from design to application in catalysis, Surf. Coat. Technol. 350 (2018) 569–586, https://doi.org/10.1016/j.surfcoat.2018.07.061.
[179] Q. Wen, F. Qu, Z. Yu, M. Graczyk-Zajac, X. Xiong, R. RIEDEL, Erratum to: Si-based polymer-derived ceramics for energy conversion and storage, J. Adv. Ceram. 11 (2022) 984, https://doi.org/10.1007/s40145-022-0600-8 M4 - Citavi.
[180] P. Colombo, Engineering porosity in polymer-derived ceramics, J. Eur. Ceram. Soc. 28 (2008) 1389–1395, https://doi.org/10.1016/j.jeurceramsoc.2007.12.002.
[181] W.S. Chai, J.Y. Cheun, P.S. Kumar, M. Mubashir, Z. Majeed, F. Banat, S.-H. Ho, P. L. Show, A review on conventional and novel materials towards heavy metal adsorption in wastewater treatment application, J. Clean. Prod. 296 (2021) 126589, https://doi.org/10.1016/j.jclepro.2021.126589.
[182] K.B. Tan, M. Vakili, B.A. Horri, P.E. Poh, A.Z. Abdullah, B. Salamatinia, Adsorption of dyes by nanomaterials: recent developments and adsorption mechanisms, Sep. Purif. Technol. 150 (2015) 229–242, https://doi.org/10.1016/j.seppur.2015.07.009.
[183] A. Stafiej, K. Pyrzynska, Adsorption of heavy metal ions with carbon nanotubes, Sep. Purif. Technol. 58 (2007) 49–52, https://doi.org/10.1016/j.seppur.2007.07.008.
[184] S.Sen Gupta, K.G. Bhattacharyya, Kinetics of adsorption of metal ions on inorganic materials: a review, Adv. Colloid Interface Sci. 162 (2011) 39–58, https://doi.org/10.1016/j.cis.2010.12.004.
[185] F. Su, C. Lu, S. Hu, Adsorption of benzene, toluene, ethylbenzene and p-xylene by NaOCl-oxidized carbon nanotubes, Colloids Surf. A Physicochem. Eng. Asp. 353 (2010) 83–91, https://doi.org/10.1016/j.colsurfa.2009.10.025.
[186] M.Mozaffari Majd, V. Kordzadeh-Kermani, V. Ghalandari, A. Askari, M. Sillanpää, Adsorption isotherm models: a comprehensive and systematic review (2010−2020), Sci. Total Environ. 812 (2022) 151334, https://doi.org/10.1016/j.scitotenv.2021.151334.
[187] J. Wang, X. Guo, Adsorption kinetic models: physical meanings, applications, and solving methods, J. Hazard. Mater. 390 (2020) 122156, https://doi.org/10.1016/j.jhazmat.2020.122156.
[188] A.M. Awad, S.M.R. Shaikh, R. Jalab, M.H. Gulied, M.S. Nasser, A. Benamor, S. Adham, Adsorption of organic pollutants by natural and modified clays: a comprehensive review, Sep. Purif. Technol. 228 (2019) 115719, https://doi.org/10.1016/j.seppur.2019.115719.
[189] D. Ewis, M.M. Ba-Abbad, A. Benamor, M.H. El-Naas, Adsorption of organic water pollutants by clays and clay minerals composites: a comprehensive review, Appl. Clay Sci. 229 (2022) 106686, https://doi.org/10.1016/j.clay.2022.106686.
[190] V. Hernández-Montoya, M.A. Pérez-Cruz, D.I. Mendoza-Castillo, M.R. Moreno-Virgen, A. Bonilla-Petriciolet, Competitive adsorption of dyes and heavy metals on zeolitic structures, J. Environ. Manage. 116 (2013) 213–221, https://doi.org/10.1016/j.jenvman.2012.12.010.
[191] Z. Jeirani, C.H. Niu, J. Soltan, Adsorption of emerging pollutants on activated carbon, 33 (2017) 491–522. 10.1515/revce-2016-0027.
[192] D.D. Do, H.D. Do, A model for water adsorption in activated carbon, Carbon N. Y. 38 (2000) 767–773, https://doi.org/10.1016/S0008-6223(99)00159-1.
[193] L. Meng, X. Zhang, Y. Tang, K. Su, J. Kong, Hierarchically porous silicon–carbon–nitrogen hybrid materials towards highly efficient and selective adsorption of organic dyes, Sci. Rep. 5 (2015) 7910, https://doi.org/10.1038/srep07910.
[194] A. Zambotti, A. Bruni, M. Biesuz, G.D. Sorarù, L. Rivoira, M. Castiglioni, B. Onida, M.C. Bruzzoniti, Glyphosate adsorption performances of polymer-derived SiC/C aerogels, J. Environ. Chem. Eng. 11 (2023) 109771, https://doi.org/10.1016/j.jece.2023.109771.
[195] Z. Zhang, Y. Bao, X. Sun, K. Chen, M. Zhou, L. He, Q. Huang, Z. Huang, Z. Chai, Y. Song, Mesoporous polymer-derived ceramic membranes for water purification via a self-sacrificed template, ACS Omega (2020), https://doi.org/10.1021/acsomega.0c01021.
[196] S. Somma, E. Reverchon, L. Baldino, Water purification of classical and emerging organic pollutants: an extensive review, ChemEngineering 5 (2021), https://doi.org/10.3390/chemengineering5030047.
[197] S. Wang, Y. Peng, Natural zeolites as effective adsorbents in water and wastewater treatment, Chem. Eng. J. 156 (2010) 11–24, https://doi.org/10.1016/j.cej.2009.10.029.
[198] J. Mo, Q. Yang, N. Zhang, W. Zhang, Y. Zheng, Z. Zhang, A review on agro-industrial waste (AIW) derived adsorbents for water and wastewater treatment, J. Environ. Manage 227 (2018) 395–405, https://doi.org/10.1016/j.jenvman.2018.08.069.
[199] I. Ali, New generation adsorbents for water treatment, Chem. Rev. 112 (2012) 5073–5091, https://doi.org/10.1021/cr300133d.
[200] D. Mehta, S. Mazumdar, S.K. Singh, Magnetic adsorbents for the treatment of water/wastewater—A review, J. Water Process Eng. 7 (2015) 244–265, https://doi.org/10.1016/j.jwpe.2015.07.001.
[201] E. Barrios, L. Zhai, A review of the evolution of the nanostructure of SiCN and SiOC polymer derived ceramics and the impact on mechanical properties, Mol. Syst. Des. Eng. 5 (2020) 1606–1641.
[202] E. Wasan Awin, A. Lale, K.C.N.H. Kumar, U. Bilge Demirci, S. Bernard, R. Kumar, Novel precursor-derived meso-/macroporous TiO2/SiOC nanocomposites with highly stable anatase nanophase providing visible light photocatalytic activity and superior adsorption of organic dyes, Materials (Basel) 11 (2018) 362, https://doi.org/10.3390/ma11030362.
[203] M. Hojamberdiev, R.M. Prasad, K. Morita, Y. Zhu, M.A. Schiavon, A. Gurlo, R. Riedel, Template-free synthesis of polymer-derived mesoporous SiOC/TiO2 and SiOC/N-doped TiO2 ceramic composites for application in the removal of organic dyes from contaminated water, Appl. Catal. B Environ. 115 (2012) 303–313.
[204] Z. Yu, S. Li, P. Zhang, Y. Feng, X. Liu, Polymer-derived mesoporous Ni/SiOC(H) ceramic nanocomposites for efficient removal of acid fuchsin, Ceram. Int. 43 (2017) 4520–4526, https://doi.org/10.1016/j.ceramint.2016.12.104.
[205] M.C. Bruzzoniti, M. Appendini, B. Onida, M. Castiglioni, M. Del Bubba, L. Vanzetti, P. Jana, G.D. Sorarù, L. Rivoira, Regenerable, innovative porous silicon-based polymer-derived ceramics for removal of methylene blue and rhodamine B from textile and environmental waters, Environ. Sci. Pollut. Res. 25 (2018) 10619–10629, https://doi.org/10.1007/s11356-018-1367-x.

[206] M.C. Bruzzoniti, M. Appendini, L. Rivoira, B. Onida, M. Del Bubba, P. Jana, G. D. Soraru, Polymer-derived ceramic aerogels as sorbent materials for the removal of organic dyes from aqueous solutions, J. Am. Ceram. Soc. 101 (2018) 821–830, https://doi.org/10.1111/jace.15241.
[207] J. Yener, T. Kopac, G. Dogu, T. Dogu, Dynamic analysis of sorption of methylene blue dye on granular and powdered activated carbon, Chem. Eng. J. 144 (2008) 400–406, https://doi.org/10.1016/j.cej.2008.02.009.
[208] E. Zera, E. Brancaccio, L. Tognana, L. Rivoira, M.C. Bruzzoniti, G.D. Sorarù, Reactive atmosphere synthesis of polymer-derived Si–O–C–N aerogels and their Cr adsorption from aqueous solutions, Adv. Eng. Mater. 20 (2018) 1701130, https://doi.org/10.1002/adem.201701130.
[209] M.H. Al-Malack, A.A. Basaleh, Adsorption of heavy metals using activated carbon produced from municipal organic solid waste, Desalin. Water Treat. 57 (2016) 24519–24531, https://doi.org/10.1080/19443994.2016.1144536.
[210] J. Pan, W. Shen, Y. Zhao, H. Sun, T. Guo, Y. Cheng, N. Zhao, H. Tang, X. Yan, Difunctional hierarchical porous SiOC composites from silicone resin and rice husk for efficient adsorption and as a catalyst support, Colloids Surf. A Physicochem. Eng. Asp. 584 (2020) 124041, https://doi.org/10.1016/j.colsurfa.2019.124041.
[211] S.A.C. Carabineiro, T. Thavorn-Amornsri, M.F.R. Pereira, J.L. Figueiredo, Adsorption of ciprofloxacin on surface-modified carbon materials, Water Res. 45 (2011) 4583–4591, https://doi.org/10.1016/j.watres.2011.06.008.
[212] S. Shi, Y. Fan, Y. Huang, Facile low temperature hydrothermal synthesis of magnetic mesoporous carbon nanocomposite for adsorption removal of ciprofloxacin antibiotics, Ind. Eng. Chem. Res. 52 (2013) 2604–2612, https://doi.org/10.1021/ie303036e.
[213] J.G. Shang, X.R. Kong, L.L. He, W.H. Li, Q.J.H. Liao, Low-cost biochar derived from herbal residue: characterization and application for ciprofloxacin adsorption, Int. J. Environ. Sci. Technol. 13 (2016) 2449–2458, https://doi.org/10.1007/s13762-016-1075-3.
[214] P. Jana, M.C. Bruzzoniti, M. Appendini, L. Rivoira, M. Del Bubba, D. Rossini, L. Ciofi, G.D. Sorarù, Processing of polymer-derived silicon carbide foams and their adsorption capacity for non-steroidal anti-inflammatory drugs, Ceram. Int. 42 (2016) 18937–18943.
[215] Z. Yu, Y. Feng, S. Li, Y. Pei, Influence of the polymer–polymer miscibility on the formation of mesoporous SiC (O) ceramics for highly efficient adsorption of organic dyes, J. Eur. Ceram. Soc. 36 (2016) 3627–3635.
[216] E.W. Awin, A. Lale, K.C. Hari Kumar, S. Bernard, R. Kumar, Disordered mesoporous polymer derived N-doped TiO2/Si-O-C-N nanocomposites with nanoscaled heterojunctions towards enhanced adsorption and harnessing of visible light, Appl. Surf. Sci. 508 (2020) 144953, https://doi.org/10.1016/j.apsusc.2019.144953.
[217] G. Crini, E. Lichtfouse, L.D. Wilson, N. Morin-Crini, Conventional and non-conventional adsorbents for wastewater treatment, Environ. Chem. Lett. 17 (2019) 195–213, https://doi.org/10.1007/s10311-018-0786-8.
[218] D.M. Ruthven, Principles of Adsorption And Adsorption Processes, John Wiley & Sons, 1984.
[219] M.A.S.D. Barros, P.A. Arroyo, E.A. Silva, in: H. Nakajima (Ed.), General Aspects of Aqueous Sorption Process in Fixed Beds, IntechOpen, Rijeka, 2013, p. 14, https://doi.org/10.5772/51954. Ch.
[220] C. Stabler, E. Ionescu, M. Graczyk-Zajac, I. Gonzalo-Juan, R. Riedel, Silicon oxycarbide glasses and glass-ceramics: "All-Rounder" materials for advanced structural and functional applications, J. Am. Ceram. Soc. 101 (2018) 4817–4856, https://doi.org/10.1111/jace.15932.
[221] J. Koornneef, A. Ramirez, T. van Harmelen, A. van Horssen, W. Turkenburg, A. Faaij, The impact of CO2 capture in the power and heat sector on the emission of SO2, NOx, particulate matter, volatile organic compounds and NH3 in the European Union, Atmos. Environ. 44 (2010) 1369–1385, https://doi.org/10.1016/j.atmosenv.2010.01.022.
[222] B.V.S. Chauhan, K. Corada, C. Young, K.L. Smallbone, K.P. Wyche, Review on sampling methods and health impacts of fine (PM2.5, ≤2.5 μm) and ultrafine (UFP, PM0.1, ≤0.1 μm) particles, Atmosphere 15 (2024), https://doi.org/10.3390/atmos15050572 (Basel).
[223] D.E. Schraufnagel, J.R. Balmes, C.T. Cowl, S. De Matteis, S.-H. Jung, K. Mortimer, R. Perez-Padilla, M.B. Rice, H. Riojas-Rodriguez, A. Sood, G.D. Thurston, T. To, A. Vanker, D.J. Wuebbles, Air pollution and noncommunicable diseases: a review by the forum of international respiratory societies' environmental committee, part 2: air pollution and organ systems, Chest 155 (2019) 417–426, https://doi.org/10.1016/j.chest.2018.10.041.
[224] I. Manisalidis, E. Stavropoulou, A. Stavropoulos, E. Bezirtzoglou, Environmental and health impacts of air pollution: a review, Front. Public Heal. 8 (2020) 505570.
[225] T. Semerci, M.D. de Mello Innocentini, G.A. Marsola, P.R.O. Lasso, G.D. Soraru, C. Vakifahmetoglu, Hot air permeable preceramic polymer derived reticulated ceramic foams, ACS Appl. Polym. Mater. 2 (2020) 4118–4126.
[226] Y. Dong, H. Wu, F. Yang, S. Gray, Cost and efficiency perspectives of ceramic membranes for water treatment, Water Res. 220 (2022) 118629, https://doi.org/10.1016/j.watres.2022.118629.
[227] A.J. Pyzik, C.G. Li, New design of a ceramic filter for diesel emission control applications, Int. J. Appl. Ceram. Technol. 2 (2005) 440–451, https://doi.org/10.1111/j.1744-7402.2005.02045.x.
[228] J.W. Brockmeyer, L.S. Aubrey, Application of ceramic foam filters in molten metal filtration, Appl. Refract. Ceram. Eng. Sci. Proc. (1987) 63–74, https://doi.org/10.1002/9780470320372.ch8.
[229] K.P. Goswami, G. Pugazhenthi, Credibility of polymeric and ceramic membrane filtration in the removal of bacteria and virus from water: a review, J. Environ. Manage. 268 (2020) 110583, https://doi.org/10.1016/j.jenvman.2020.110583.
[230] S. Heidenreich, Hot gas filtration – a review, Fuel 104 (2013) 83–94, https://doi.org/10.1016/j.fuel.2012.07.059.
[231] L. Lang, H. Zhu, Y. Ding, X. Yin, C. Wu, X. Yu, A.V Bridgwater, Mini-review on hot gas filtration in biomass gasification: focusing on ceramic filter candles, Energy Fuels 35 (2021) 11800–11819, https://doi.org/10.1021/acs.energyfuels.1c01458.
[232] S. Schaafhausen, E. Yazhenskikh, S. Heidenreich, M. Müller, Corrosion of silicon carbide hot gas filter candles in gasification environment, J. Eur. Ceram. Soc. 34 (2014) 575–588, https://doi.org/10.1016/j.jeurceramsoc.2013.10.011.
[233] B. Alonso-Fariñas, M. Lupion, M. Rodriguez-Galan, J. Martinez-Fernandez, New candle prototype for hot gas filtration industrial applications, Fuel 114 (2013) 120–127, https://doi.org/10.1016/j.fuel.2012.12.054.
[234] F.C. Patcas, G.I. Garrido, B. Kraushaar-Czarnetzki, CO oxidation over structured carriers: a comparison of ceramic foams, honeycombs and beads, Chem. Eng. Sci. 62 (2007) 3984–3990, https://doi.org/10.1016/j.ces.2007.04.039.
[235] O. Santoliquido, G. Bianchi, P.D. Eggenschwiler, A. Ortona, Additive manufacturing of periodic ceramic substrates for automotive catalyst supports, Int. J. Appl. Ceram. Technol. 14 (2017) 1164–1173, https://doi.org/10.1111/ijac.12745.
[236] C. Li, L. Huangfu, J. Li, S. Gao, G. Xu, J. Yu, Recent advances in catalytic filters for integrated removal of dust and NOx from flue gas: fundamentals and applications, Resour. Chem. Mater. 1 (2022) 275–289, https://doi.org/10.1016/j.recm.2022.06.002.
[237] F. Sandra, A. Ballestero, V.L. NGuyen, M.N. Tsampas, P. Vernoux, C. Balan, Y. Iwamoto, U.B. Demirci, P. Miele, S. Bernard, Silicon carbide-based membranes with high soot particle filtration efficiency, durability and catalytic activity for CO/HC oxidation and soot combustion, J. Memb. Sci. 501 (2016) 79–92, https://doi.org/10.1016/j.memsci.2015.12.015.
[238] Q. Wang, L. Yu, H. Nagasawa, M. Kanezashi, T. Tsuru, High-performance molecular-separation ceramic membranes derived from oxidative cross-linked polytitanocarbosilane, J. Am. Ceram. Soc. 103 (2020) 4473–4488, https://doi.org/10.1111/jace.17108.
[239] K. Wang, H. Xiao, J. Yin, X. Chen, X. Liu, Z. Huang, Fabrication of precursor-derived high-flux SiOC ceramic membranes via selective laser printing, J. Am. Ceram. Soc. 107 (2024) 3637–3643, https://doi.org/10.1111/jace.19717.
[240] R.M. Prasad, Y. Jüttke, H. Richter, I. Voigt, R. Riedel, A. Gurlo, Mechanism of gas separation through amorphous silicon oxycarbide membranes, Adv. Eng. Mater. 18 (2016) 721–727, https://doi.org/10.1002/adem.201500380.
[241] N.C. Fontão, L.N. Ferrari, J.C. Sapatieri, K. Rezwan, M. Wilhelm, Influence of the pyrolysis temperature and TiO2-incorporation on the properties of SiOC/SiC composites for efficient wastewater treatment applications, Membranes 12 (2022), https://doi.org/10.3390/membranes12020175 (Basel).
[242] Z. Xu, J. Lu, G. Zhang, R. Liu, W. Zhang, Q. Meng, Compact SiOC ceramic composite nanofiltration membranes by slow dip coating for water purification, Ceram. Int. 50 (2024) 23115–23123, https://doi.org/10.1016/j.ceramint.2024.04.034.
[243] H. Jin, X. Xu, Preparation and gas separation of amorphous silicon oxycarbide membrane supported on silicon nitride membrane, Membranes 14 (2024), https://doi.org/10.3390/membranes14030063 (Basel).
[244] M.B. Asif, Z. Zhang, Ceramic membrane technology for water and wastewater treatment: a critical review of performance, full-scale applications, membrane fouling and prospects, Chem. Eng. J. 418 (2021) 129481, https://doi.org/10.1016/j.cej.2021.129481.
[245] Y. Wang, B. Ma, M. Ulbricht, Y. Dong, X. Zhao, Progress in alumina ceramic membranes for water purification: status and prospects, Water Res. 226 (2022) 119173, https://doi.org/10.1016/j.watres.2022.119173.
[246] N.C. Fontão, M. Wilhelm, K. Rezwan, Asymmetric polysiloxane-based SiOC membranes produced via phase inversion tape casting process, Mater. Des. 198 (2021) 109328, https://doi.org/10.1016/j.matdes.2020.109328.
[247] F. Guo, D. Su, Y. Liu, J. Wang, X. Yan, J. Chen, S. Chen, High acid resistant SiOC ceramic membranes for wastewater treatment, Ceram. Int. 44 (2018) 13444–13448, https://doi.org/10.1016/j.ceramint.2018.04.149.
[248] N. Wu, L.Y. Wan, Y. Wang, F. Ko, Conversion of hydrophilic SiOC nanofibrous membrane to robust hydrophobic materials by introducing palladium, Appl. Surf. Sci. 425 (2017) 750–757, https://doi.org/10.1016/j.apsusc.2017.07.098.
[249] H. Inde, M. Kanezashi, H. Nagasawa, T. Nakaya, T. Tsuru, Tailoring a thermally stable amorphous SiOC structure for the separation of large molecules: the effect of calcination temperature on sioc structures and gas permeation properties, ACS Omega 3 (2018) 6369–6377, https://doi.org/10.1021/acsomega.8b00632.
[250] T. Miyazaki, H. Nagasawa, T. Tsuru, M. Kanezashi, Design of a SiOC network structure with oxidation stability and application to hydrogen separation membranes at high temperatures, J. Memb. Sci. 625 (2021) 119147, https://doi.org/10.1016/j.memsci.2021.119147.
[251] T. Nagano, K. Sato, T. Saitoh, Y. Iwamoto, Gas permeation properties of amorphous SiC membranes synthesized from polycarbosilane without oxygen-curing process, J. Ceram. Soc. Jpn. 114 (2006) 533–538, https://doi.org/10.2109/jcersj.114.533.
[252] O. Icin, C. Vakifahmetoglu, Hybrid preceramic aerogels for oil and solvent cleanup, Adv. Eng. Mater. (2025) 2402182, https://doi.org/10.1002/adem.202402182 n/a.
[253] O. Icin, A.M. Abebe, G.D. Soraru, C. Vakifahmetoglu, SiOC foam-aerogel composites: optimal balance of lightness and excellent thermal insulation, J. Am. Ceram. Soc. 107 (2024) 6729–6740, https://doi.org/10.1111/jace.19967.

[254] T. Konegger, C.-C. Tsai, H. Peterlik, S.E. Creager, R.K. Bordia, Asymmetric polysilazane-derived ceramic structures with multiscalar porosity for membrane applications, Microporous Mesoporous Mater. 232 (2016) 196–204, https://doi.org/10.1016/j.micromeso.2016.06.027.
[255] N. Sazali, W.N.W. Salleh, A.F. Ismail, N.H. Ismail, N. Yusof, F. Aziz, J. Jaafar, K. Kadirgama, Influence of intermediate layers in tubular carbon membrane for gas separation performance, Int. J. Hydrog. Energy 44 (2019) 20914–20923, https://doi.org/10.1016/j.ijhydene.2018.06.148.
[256] Y. Dong, B. Lin, J. Zhou, X. Zhang, Y. Ling, X. Liu, G. Meng, S. Hampshire, Corrosion resistance characterization of porous alumina membrane supports, Mater. Charact. 62 (2011) 409–418, https://doi.org/10.1016/j.matchar.2011.01.012.
[257] Y. Dong, X. Feng, D. Dong, S. Wang, J. Yang, J. Gao, X. Liu, G. Meng, Elaboration and chemical corrosion resistance of tubular macro-porous cordierite ceramic membrane supports, J. Memb. Sci. 304 (2007) 65–75, https://doi.org/10.1016/j.memsci.2007.06.058.
[258] H. Suda, Y. Uchimaru, I. Fujiwara, K. Haraya, Preparation and characterization of SiC membranes for high temperature hydrogen separation, Trans. Res. Soc. Jpn. 29 (2004) 3255–3258.
[259] Q. Wang, M. Yokoji, H. Nagasawa, L. Yu, M. Kanezashi, T. Tsuru, Microstructure evolution and enhanced permeation of SiC membranes derived from allylhydridopolycarbosilane, J. Memb. Sci. 612 (2020) 118392, https://doi.org/10.1016/j.memsci.2020.118392.
[260] R.A. Wach, M. Sugimoto, A. Idesaki, M. Yoshikawa, Molecular sieve SiC-based membrane for hydrogen separation produced by radiation curing of preceramic polymers, Mater. Sci. Eng. B 140 (2007) 81–89, https://doi.org/10.1016/j.mseb.2007.04.008.
[261] Q. Wang, N. Xu, Q. Liu, Q. Dong, H. Nagasawa, M. Kanezashi, R. Zhou, T. Tsuru, Low-temperature cross-linking fabrication of sub-nanoporous SiC-based membranes for application to the pervaporation removal of methanol, J. Memb. Sci. 662 (2022) 121008, https://doi.org/10.1016/j.memsci.2022.121008.
[262] Q. Wang, Y. Kawano, L. Yu, H. Nagasawa, M. Kanezashi, T. Tsuru, Development of high-performance sub-nanoporous SiC-based membranes derived from polytitanocarbosilane, J. Memb. Sci. 598 (2020) 117688, https://doi.org/10.1016/j.memsci.2019.117688.
[263] N.V Buchilin, V.G. Maksimov, V.G. Babashov, Ceramic filters for aluminum melt (Review), Glas. Ceram. 72 (2015) 246–252, https://doi.org/10.1007/s10717-015-9766-7.
[264] L.J. Gauckler, M.M. Waeber, C. Conti, M. Jacob-Duliere, Ceramic foam for molten metal filtration, JOM 37 (1985) 47–50, https://doi.org/10.1007/BF03258640.
[265] T. Semerci, K.C. Dizdar, A. Kulkarni, D. Dispinar, G.D. Soraru, C. Vakifahmetoglu, Polymer-derived ceramic molten metal filters, J. Mater. Sci. 57 (2022) 14723–14734, https://doi.org/10.1007/s10853-022-07542-9.
[266] A.L. Matthews, Ceramic filters for the cast metal industry, Key Eng. Mater. 122–124 (1996) 293–304, https://doi.org/10.4028/www.scientific.net/KEM.122-124.293.
[267] R.A. Olson III, L.C.B. Martins, Cellular ceramics in metal filtration, Adv. Eng. Mater. 7 (2005) 187–192, https://doi.org/10.1002/adem.200500021.
[268] M. Scheffler, P. Colombo, Cellular Ceramics: Structure, Manufacturing, Properties And Applications, John Wiley & Sons, 2006.
[269] D.J. Green, P. Colombo, Cellular ceramics: intriguing structures, novel properties, and innovative applications, MRS Bull. 28 (2003) 296–300, https://doi.org/10.1557/mrs2003.84.
[270] P. Colombo, Conventional and novel processing methods for cellular ceramics, Philos. Trans. R. Soc. A Math. Phys. Eng. Sci. 364 (2005) 109–124, https://doi.org/10.1098/rsta.2005.1683.
[271] Z. Taslicukur, C. Balaban, N. Kuskonmaz, Production of ceramic foam filters for molten metal filtration using expanded polystyrene, J. Eur. Ceram. Soc. 27 (2007) 637–640, https://doi.org/10.1016/j.jeurceramsoc.2006.04.129.
[272] D. Haase, A. Füssel, J. Adler, U. Petasch, 60 Years of open-celled ceramics based on replica technique: applications, obstacles, and opportunities, Adv. Eng. Mater. (2024) 2301804, https://doi.org/10.1002/adem.202301804 n/a.
[273] L.-M. Heisig, K. Markuske, E. Werzner, R. Wulf, T.M. Fieback, Experimental and simplified predictive determination of extinction coefficients of ceramic open-cell foams used for metal melt filtration, Adv. Eng. Mater. 24 (2022) 2100723, https://doi.org/10.1002/adem.202100723.
[274] N. Wu, B. Wang, Y. Wang, Enhanced mechanical properties of amorphous SiOC nanofibrous membrane through in situ embedding nanoparticles, J. Am. Ceram. Soc. 101 (2018) 4763–4772, https://doi.org/10.1111/jace.15732.
[275] M. Biesuz, M. Tomasi, B. Santhosh, V.M. Sglavo, G.D. Sorarù, Polymer-derived Si3N4 nanofelts as a novel oil spills clean-up architecture, J. Environ. Chem. Eng. 8 (2020) 104134, https://doi.org/10.1016/j.jece.2020.104134.
[276] Y. Wang, H. Arandiyan, J. Scott, A. Bagheri, H. Dai, R. Amal, Recent advances in ordered meso/macroporous metal oxides for heterogeneous catalysis: a review, J. Mater. Chem. A 5 (2017) 8825–8846.
[277] L.F. Liotta, M. Gruttadauria, G. Di Carlo, G. Perrini, V. Librando, Heterogeneous catalytic degradation of phenolic substrates: catalysts activity, J. Hazard. Mater. 162 (2009) 588–606, https://doi.org/10.1016/j.jhazmat.2008.05.115.
[278] A. Kulkarni, S. Siahrostami, A. Patel, J.K. Nørskov, Understanding catalytic activity trends in the oxygen reduction reaction, Chem. Rev. 118 (2018) 2302–2312, https://doi.org/10.1021/acs.chemrev.7b00488.
[279] K. Pirkanniemi, M. Sillanpää, Heterogeneous water phase catalysis as an environmental application: a review, Chemosphere 48 (2002) 1047–1060, https://doi.org/10.1016/S0045-6535(02)00168-6.
[280] P. Frontera, A. Macario, M. Ferraro, P. Antonucci, Supported catalysts for CO2 methanation: a review, Catalysts 7 (2017), https://doi.org/10.3390/catal7020059.
[281] U.G. Akpan, B.H. Hameed, Parameters affecting the photocatalytic degradation of dyes using TiO2-based photocatalysts: a review, J. Hazard. Mater. 170 (2009) 520–529, https://doi.org/10.1016/j.jhazmat.2009.05.039.
[282] M. Umar, H.A. Aziz, Photocatalytic degradation of organic pollutants in water, Org. Pollut. Risk Treat. 8 (2013) 196–197, https://doi.org/10.5772/53699.
[283] R. Wang, K. Shi, D. Huang, J. Zhang, S. An, Synthesis and degradation kinetics of TiO2/GO composites with highly efficient activity for adsorption and photocatalytic degradation of MB, Sci. Rep. 9 (2019) 1–9, https://doi.org/10.1038/s41598-019-54320-w.
[284] S. Banerjee, D.D. Dionysiou, S.C. Pillai, Self-cleaning applications of TiO2 by photo-induced hydrophilicity and photocatalysis, Appl. Catal. B Environ. 176–177 (2015) 396–428, https://doi.org/10.1016/j.apcatb.2015.03.058.
[285] A. Talaiekhozani, S. Rezania, K.-H. Kim, R. Sanaye, A.M. Amani, Recent advances in photocatalytic removal of organic and inorganic pollutants in air, J. Clean. Prod. 278 (2021) 123895, https://doi.org/10.1016/j.jclepro.2020.123895.
[286] V. Vaiano, M. Matarangolo, J.J. Murcia, H. Rojas, J.A. Navío, M.C. Hidalgo, Enhanced photocatalytic removal of phenol from aqueous solutions using ZnO modified with Ag, Appl. Catal. B Environ. 225 (2018) 197–206, https://doi.org/10.1016/j.apcatb.2017.11.075.
[287] T. Ishikawa, in: M. Singh, T. Ohji, R.B.T.- G, S.M.of A.M. Asthana (Eds.), Chapter 16 - Green Manufacturing of Photocatalytic Materials for Environmental Applications, Elsevier, Oxford, 2016, pp. 459–474, https://doi.org/10.1016/B978-0-12-411497-5.00016-3.
[288] E.W. Awin, A. Lale, K.C. Hari Kumar, U.B. Demirci, S. Bernard, R. Kumar, Plasmon enhanced visible light photocatalytic activity in polymer-derived TiN/Si-O-C-N nanocomposites, Mater. Des. 157 (2018) 87–96, https://doi.org/10.1016/j.matdes.2018.06.060.
[289] Y. Feng, S. Lai, L. Yang, R. Riedel, Z. Yu, Polymer-derived porous Bi2WO6/SiC(O) ceramic nanocomposites with high photodegradation efficiency towards Rhodamine B, Ceram. Int. 44 (2018) 8562–8569, https://doi.org/10.1016/j.ceramint.2018.02.061.
[290] S. Bhaskar, E.W. Awin, K.C.H. Kumar, A. Lale, S. Bernard, R. Kumar, Design of nanoscaled heterojunctions in precursor-derived t-ZrO2/SiOC(N) nanocomposites: Transgressing the boundaries of catalytic activity from UV to visible light, Sci. Rep. 10 (2020) 430, https://doi.org/10.1038/s41598-019-57394-8.
[291] J. Essmeister, L. Schachtner, E. Szoldatits, S. Schwarz, A. Lichtenegger, B. Baumann, K. Föttinger, T. Konegger, Polymer-derived Ni/SiOC materials structured by vat-based photopolymerization with catalytic activity in CO2 methanation, Open Ceram. 14 (2023) 100350, https://doi.org/10.1016/j.oceram.2023.100350.
[292] B. García, E. Casado, A. Tamayo, Synthesis and characterization of Ce/SiOC nanocomposites through the polymer derived ceramic method and evaluation of their catalytic activity, Ceram. Int. 46 (2020) 1362–1373, https://doi.org/10.1016/j.ceramint.2019.09.099.
[293] K. Papakollu, A. Bhardwaj, E. Ionescu, S. Mathur, R. Kumar, Effect of structural changes at various length scales in SiVOC ceramic nanocomposites on electrocatalytic performance for the oxygen reduction reaction, ACS Appl. Mater. Interfaces 15 (2023) 34895–34908, https://doi.org/10.1021/acsami.3c05449.
[294] M. Adam, M. Wilhelm, G. Grathwohl, Polysiloxane derived hybrid ceramics with nanodispersed Pt, Microporous Mesoporous Mater. 151 (2012) 195–200, https://doi.org/10.1016/j.micromeso.2011.10.037.
[295] M. Adam, C. Vakifahmetoglu, P. Colombo, M. Wilhelm, G. Grathwohl, Polysiloxane-derived ceramics containing nanowires with catalytically active tips, J. Am. Ceram. Soc. 97 (2014) 959–966, https://doi.org/10.1111/jace.12708.
[296] Z. Yu, K. Mao, Y. Feng, Single-source-precursor synthesis of porous W-containing SiC-based nanocomposites as hydrogen evolution reaction electrocatalysts, J. Adv. Ceram. 10 (2021) 1338–1349, https://doi.org/10.1007/s40145-021-0508-8.
[297] M. Wójcik-Bania, A. Krowiak, J. Strzezik, M. Hasik, Pt supported on cross-linked poly(vinylsiloxanes) and SiCO ceramics — new materials for catalytic applications, Mater. Des. 96 (2016) 171–179, https://doi.org/10.1016/j.matdes.2016.02.013.
[298] Q. Hanniet, M. Boussmen, J. Barés, V. Huon, I. Iatsunskyi, E. Coy, M. Bechelany, C. Gervais, D. Voiry, P. Miele, C. Salameh, Investigation of polymer-derived Si–(B)–C–N ceramic/reduced graphene oxide composite systems as active catalysts towards the hydrogen evolution reaction, Sci. Rep. 10 (2020) 22003, https://doi.org/10.1038/s41598-020-78558-x.
[299] J. Wang, A. Gili, M. Grünbacher, S. Praetz, J.D. Epping, O. Görke, G. Schuck, S. Penner, C. Schlesiger, R. Schomäcker, A. Gurlo, M.F. Bekheet, Silicon oxycarbonitride ceramic containing nickel nanoparticles: from design to catalytic application, Mater. Adv. 2 (2021) 1715–1730, https://doi.org/10.1039/d0ma00917b.
[300] U.P.M. Ashik, W.M.A. Wan Daud, H.F. Abbas, Production of greenhouse gas free hydrogen by thermocatalytic decomposition of methane – a review, Renew. Sustain. Energy Rev. 44 (2015) 221–256, https://doi.org/10.1016/j.rser.2014.12.025.
[301] E. Szoldatits, J. Essmeister, L. Schachtner, T. Konegger, K. Föttinger, Polymer-derived SiOC as support material for Ni-based catalysts: CO2 methanation performance and effect of support modification with La2O3, Front. Chem. 11 (2023). https://www.frontiersin.org/journals/chemistry/articles/10.3389/fchem.2023.1163503.

[302] E.M. Cepollaro, S. Cimino, L. Lisi, M. Biesuz, B. Santhosh, G.D. Sorarù, Ru/Al2O3 on polymer-derived SiC foams as structured catalysts for CO2 methanation, Catalysts 12 (2022), https://doi.org/10.3390/catal12090956.
[303] P. Mikšovsky, K. Rauchenwald, S. Naghdi, H. Rabl, D. Eder, T. Konegger, K. Bica-Schröder, Silicon oxycarbide (SiOC)-supported ionic liquids: heterogeneous catalysts for cyclic carbonate formation, ACS Sustain. Chem. Eng. 12 (2024) 1455–1467, https://doi.org/10.1021/acssuschemeng.3c05569.
[304] W. Duan, X. Yin, Q. Li, L. Schlier, P. Greil, N. Travitzky, A review of absorption properties in silicon-based polymer derived ceramics, J. Eur. Ceram. Soc. 36 (2016) 3681–3689, https://doi.org/10.1016/j.jeurceramsoc.2016.02.002.
[305] A. Xia, J. Yin, X. Chen, X. Liu, Z. Huang, Polymer-derived Si-based ceramics: recent developments and perspectives, Crystals 10 (2020) 824.
[306] S. Packirisamy, K.J. Sreejith, D. Devapal, B. Swaminathan, in: Y.R. Mahajan, R. Johnson (Eds.), Polymer-Derived Ceramics and Their Space Applications BT - Handbook of Advanced Ceramics and Composites: Defense, Security, Aerospace and Energy Applications, Springer International Publishing, Cham, 2020, pp. 975–1080, https://doi.org/10.1007/978-3-030-16347-1_31.
[307] P. Miele†, S. Bernard, D. Cornu, B. Toury, Recent developments in polymer-derived ceramic fibers (PDCFs): preparation, properties and applications – a review, Soft Mater. 4 (2007) 249–286, https://doi.org/10.1080/15394450701310228.
[308] R.P. Chaudhary, C. Parameswaran, M. Idrees, A.S. Rasaki, C. Liu, Z. Chen, P. Colombo, Additive manufacturing of polymer-derived ceramics: materials, technologies, properties and potential applications, Prog. Mater. Sci. 128 (2022) 100969, https://doi.org/10.1016/j.pmatsci.2022.100969.
[309] S. Mukherjee, Z. Ren, G. Singh, Molecular polymer-derived ceramics for applications in electrochemical energy storage devices, J. Phys. D Appl. Phys. 51 (2018) 463001, https://doi.org/10.1088/1361-6463/aadb18.
[310] R. Bhandavat, Z. Pei, G. Singh, Polymer-derived ceramics as anode material for rechargeable Li-ion batteries: a review, Nanomater. Energy 1 (2012) 324–337, https://doi.org/10.1680/nme.12.00030.